ISSN 0387-6144

BULLETIN OF THE
RESEARCH LABORATORY FOR NUCLEAR REACTORS

VOL. 37 2013

RESEARCH LABORATORY FOR NUCLEAR REACTORS
TOKYO INSTITUTE OF TECHNOLOGY

BULLETIN OF THE RESEARCH LABORATORY FOR NUCLEAR REACTORS

BULL. RES. LAB. NUCL. REACTOR, Vol.37, 2013

CONTENTS

I. Celebration of Professor Saito’s 65th Birthdays

II. Research Reports

A. Energy Engineering

B. Mass Transmutation Engineering

C. System and Safety Engineering

III. Co-operative Researches

Research staffs of RESEARCH LABORATORY FOR NUCLEAR REACTORS, TOKYO INSTITUTE OF TECHONOGY

Director

Toyohiko YANO	Professor

Energy Engineering Division

Masayuki IGASHIRA	Professor
Satoshi CHIBA	Professor
Minoru TAKAHASHI	Professor
Hiroshi AKATSUKA	Associate Professor
Yukitaka KATO	Associate Professor
Hiroaki TSUTSUI	Associate Professor
Tetsuo SAWADA	Assistant Professor
Junichi RYU	Assistant Professor
Kotaro KONDO	Assistant Professor

Mass Transmutation Engineering Division

Toyohiko YANO	Professor
Kenji TAKESHITA	Professor
Yoshiyuki OGURI	Professor
Toru OBARA	Professor
Yoshihisa MATSUMOTO	Associate Professor
Jun ONOE	Associate Professor
Noriyosu HAYASHIZAKI	Associate Professor
Takehiko TSUKAHARA	Associate Professor
Katsumi YOSHIDA	Assistant Professor
Jun NISHIYAMA	Assistant Professor
Tatsuya KATABUCHI	Assistant Professor
Haruaki MATSUURA	Assistant Professor
Masao NOMURA	Assistant Professor
Masayuki HARADA	Assistant Professor
Koichiro TAKAO	Assistant Professor

System and Safety Engineering Division

Masaki SAITO	Distinguished Professor
Yasuhisa IKEDA	Professor
Shunji IIO	Associate Professor
Hiroshige KIKURA	Associate Professor
Hiroshi SAGARA	Assistant Professor
Etsuko KOIZUMI	Assistant Professor

International Nuclear Research Cooperation Center

Masaki OZAWA	Professor

Common Staffs

Tadashi YOSHIDA	Visiting Professor
Ivaniuk FEDIR	Visiting Professor
Fumiaki KAWAKAMI	Visiting Professor
Eiichi ASANO	Visiting Professor
Takatoshi TAKEMOTO	Visiting Associate Professor

Technical Staffs

Ken-ichi TOSAKA	Senior Technical Specialist
Atsushi NEZU	Senior Technical Specialist
Keizo MATSUMURA	Senior Technical Specialist
Masamitsu IMAI	Senior Technical Specialist
Hitoshi FUKUDA	Senior Technical Specialist
Mitsuo MATSUZAKI	Senior Technical Specialist

Research Program on Protected Plutonium Production (P^3)
and
Academy for 3S (Safety, Security, Safeguards)

Masaki SAITO

Abstract

Nuclear engineering education has been initiated in 1957 at the graduate school of Tokyo Institute of Technology. Higher Educational activities have been conducted for more than half century. More than 1000 Master students and 200 Doctoral students graduated from the Department of Nuclear Engineering in Tokyo Institute of Technology. Many of them are working in nuclear industries and institutes. International course of nuclear engineering was initiated in 1994, and 130 students from 20 overseas countries have graduated from Master and Doctoral Programs.

The research program, **"Protected Plutonium Production (P^3)"** has been performed to enhance the proliferation resistance of plutonium by the transmutation of Minor Actinides (MAs). In 2011, **Academy for "Global Nuclear Safety and Security Agent"** was initiated with the unique features of a full boarding system and a curriculum that combines education in liberal arts and science/engineering. Both educational and research programs have been supported by the Ministry of Education, Culture, Sports, Science and Technology in Japan.

1. PROTECTED PLUTONIUM PRODECTION (P^3)

"Protected Plutonium Production (P^3)" has been proposed to enhance the proliferation resistance of plutonium by the transmutation of Minor Actinides (MAs). Doping the small amount of MAs such as ^{237}Np or ^{241}Am with large neutron capture cross-section into the uranium fuel to enhance the production of ^{238}Pu or ^{242}Pu, which have high spontaneous fission neutron source or also high decay heat to makes the process of the nuclear weapon manufacture and maintenance technologically difficult, can be effective for improving the isotopic barrier of proliferation resistance of the plutonium in thermal reactors. Super weapon grade plutonium could be produced in the blanket of a conventional FBR. However, by increasing the ^{238}Pu or ^{242}Pu ratio in the total plutonium by MAs doping into the fresh blanket, the protected plutonium with high proliferation-resistance can be bred.

A new evaluation function, "***attractiveness***", defined as a ratio of potential of fission yield to the technological difficulties of nuclear explosive device, has been proposed to evaluate the proliferation resistance of Pu based on the nuclear material property for Plutonium Categorization.

Instead of the geological disposal or just their burning of MAs by the fission reaction, they should be treated as valuable fertile materials to enhance the proliferation resistance of plutonium produced in the thermal and fast breeder reactors for peace and sustainable prosperity in future.

2. ACADEMY FOR 3S (SAFETY, SECURITY, SAFEGUARDS)

(1) BACKGROUND

While the coming of peak oil is projected, energy consumption in emerging countries is skyrocketing. Securing a stable and long-term energy supply is an urgent task for all of us, and many countries are seeking an increased share of nuclear and renewable energy sources. Japan has been on the cutting edge of world-class research, development and utilization of nuclear energy.

Nevertheless, we face new challenges:

- On September 11, 2001, a large-scale disaster resulting from an international terrorist attack occurred in the United States. Nuclear power plants were among the intended targets.
- On March 11, 2011, the Great East Japan Earthquake and subsequent Tsunami triggered a severe and large-scale nuclear accident at the Fukushima Daiichi Nuclear Power Station.

Even given those challenges, the global community recognizes that nuclear energy must play an essential role in sustainable development. Further, Japan has a unique role to fulfill: recover from the Fukushima accident, learn from it, and contribute to the safe operation of the nuclear power plants in the world.

(2) MISSIONS AND PRPBLEMS TO BE SOLVED

The Tokyo Institute of Technology (Tokyo Tech) thinks Japan may suffer from a shortage of human resources to fulfill the above tasks, so it is an imperative for Tokyo Tech by fully utilizing its resources, to educate students so that they may take a leading role globally in public sectors, academia and industry in the use of nuclear energy.

Tokyo Tech recognizes the challenges before us that we need to tackle through human resource development in this educational program. The challenge is to control threats that may arise from the use of nuclear energy—such as nuclear proliferation, nuclear terrorism, large-scale nuclear disaster resulting radiation exposure to the public—primarily in the field of 3S(Safety, Security and Safeguard).

Tackling these challenges and finding solutions will contribute to the well-being of humankind by building a safer and more peaceful world. We will train students to serve global nuclear safety/security professionals with the communication skills and social literacy to become global leaders in the 3S field.

Those selected will join a full boarding program at the "DOJO for Global Nuclear Safety and Security," living and learning together with supervisors, who will also serve as their mentors. They will not only care about their students but also help them to become leading global professionals through stimulating discussions.

(3) OUTLINE OF THE ACADEMY

To train applicants to become world-class leaders in industry, the public sector and academia in the field of nuclear energy both domestically and internationally, we offer a balanced, systematic and high-level education in both coursework and research mentoring. The structure of the program is as follows:

1) Full Boarding System "DOJO for Global Nuclear Safety and Security "

Six months after enrollment in the master's degree program, each of students will be allowed to become member of a specific laboratory. At the same time, 10-15 students every year are selected and allowed to become members of the "DOJO for Global Nuclear Safety and Security" program.

At the DOJO students are expected to live in a dormitory with other students and their supervisors, and are given opportunities to discuss various issues related to but not limited to their coursework and learn from each other. Each of the students will also be responsible for writing a master's thesis under the supervision of their respective laboratory instructors. Students are expected to think about the implications and societal value of their research results.

2) Second-step selection for elevated education

Several students who have completed the master's program in the "DOJO for Global Nuclear Energy Safety and Security" are eligible for further study in the doctoral course. The selection of several students will be made at the end of the master's course.

In the doctoral course, students will continue study through coursework, do internships both in and outside of Japan, and carry out thesis research at the laboratory. Those who have completed the course and produced an acceptable doctoral thesis receive a doctoral degree, and are expected to follow the career path to become global leaders after graduation.

3) Credits from coursework

Students must earn **a total of 50 or more credits** from the compulsory subjects shown below during their master's and doctoral courses.

- **Dojo Subjects(New)**
- **Basic and Specific Subjects in Nuclear Science and Engineering**
- **Social/Communication Subjects**
- **Nuclear Safety/Security Practical Training (New)**
    - ➢ Fieldwork in measuring environmental radiation in Fukushima area
    - ➢ Simulations of severe nuclear reactor accidents
    - ➢ Numerical simulation of the behavior of radioactive material in the environment
    - ➢ Nuclear security training
- **High-Level International Liberal Arts (New)**
    - ➢ International politics, international law, economy, history, philosophy, art, culture, English, and French
- **Internship Subjects (New)**
    - ➢ Domestic internship (six months)
    - ➢ Overseas internship (one year)
- **Volunteer activities (New)**

In addition to the above, there will be "Science cafés", "Special Dojo lectures" by domestic and international experts, "International seminars on nuclear safety/ security".

In summary, This Educational Program

- ➢ Is intended to contribute to human resource development, ultimately for the well-being of humankind by building a safer and more peaceful world, and
- ➢ Offers students an educational program that will help them become global safety/security professionals having social literacy who can act globally to build a safe, more peaceful world. They are expected to find career paths not only domestically (such as in government, the police, the coast guard, and nuclear power facilities), but also internationally, such as in the IAEA.

A.1 Feasibility Study of an Accelerator-Based Brachytherapy System Using Proton-Induced Characteristic X-rays

Yoshiyuki OGURI and Kotaro KONDO

1. Introduction

Recently ion beam therapy has received much attention as a method of treating deep-seated cancers with low normal tissue damage, and remarkable treatment performances have been reported. However, this method is still not very common, since high-energy ion accelerators are generally large in size and very expensive.

On the other hand, as another method of deep-seated cancer treatment, brachytherapy has been widely utilized for many types of tumors, and significant therapeutic performances have already been established. One of the advantages of this method is its low cost. However, this method poses a potential risk of lost source accidents and inadvertent exposure in surgical personnel during the seed implantation.

To overcome the problems of conventional brachytherapy mentioned above, we have proposed an accelerator-driven on/off-switchable radiation source[1,2]. A thin evacuated stainless-steel syringe needle is inserted into a tumor deep inside the patient’s body. A MeV proton beam is transported through the needle to a small heavy-metal target attached at the end. Proton-induced characteristic X-rays with energies of ≈ 20-30 keV emitted from the target are used for irradiation of the cancer. Since prompt radiations driven by particle accelerators are used, lost source accidents cannot occur. Although X-rays are also produced by the collision of protons onto the needle’s inner wall on the way to the heavy-metal target at the end, they do not penetrate the needle wall and do not escape outside, because the energies of characteristic X-rays of stainless steel materials (Cr, Fe and Ni) are lower than 10 keV. In addition, high-energy protons delivered by a huge accelerator are not necessary, because protons are transported to the diseased portion through the vacuum in the syringe needle. A similar therapy using an electron beam, instead of a proton beam, has been proposed. However, in the case of an electron beam, X-rays are produced mainly by bremsstrahlung, which has a continuous energy spectrum with a maximum energy equal to the incident electron energy. Accordingly, the X-ray energy spectrum is not very well-defined. The X-rays can also be emitted from the wall along the whole needle length in addition to the needle end, unless a very careful focusing of the driver beam is provided.

In this note, we experimentally investigate the X-ray energy spectra measured at the needle end in the above setup. The intensity not only of the characteristic X-rays from the heavy-metal target, but also of background radiation from the needle wall is examined. We discuss the feasibility and problems of this method as a substitute of radioactive pins being used for conventional brachytherapy.

2. Experimental method

The experiment was performed at the tandem electrostatic accelerator facility at the Research Laboratory for Nuclear Reactors, Tokyo Tech. Details of the beam transport to the end of the syringe needle have been published elsewhere[1,2]. We used a commercially available stainless-steel syringe needle for research use (Hamilton 91022). The outer diameter, inner diameter, and the length of the needle were 0.7 mm, 0.4 mm, and 50 mm, respectively. 2.5-MeV protons were used as projectiles.

The structure of the needle tip, including a heavy-metal target is illustrated in Fig. 1. From the tip of the needle to a depth of 4 mm, the inner diameter was enlarged by drilling in order to reduce the wall thickness from 0.15 mm to 0.10 mm. This part of the needle wall worked as an X-ray window. A 0.5-mm-diameter Ag ($Z = 47$) wire was inserted into the bore. Epoxy glue was used to seal the vacuum. Since the end of the Ag wire facing the proton beam was cut at 45°, KX-rays of Ag (K_α: 22.1 keV, K_β: 24.9 keV) can be efficiently extracted perpendicularly through the X-ray window. On the other hand, the protons do not directly hit the X-ray window, owing to the enlargement of the inner diameter. If we use data of X-ray attenuation coefficient, the transmission of Ag K_αX-rays and Fe K_αX-rays through the 0.1-mm thick stainless steel wall are 20% and 0.3%, respectively. Therefore, even if a part of the proton beam hits the wall, only Ag KX-rays can be extracted.

The setup of the X-ray spectrometry is also shown in Fig. 1. We used a CdTe X-ray detector (AMPTEK XR-100T-CdTe, effective area = 3×3 mm^2) with a

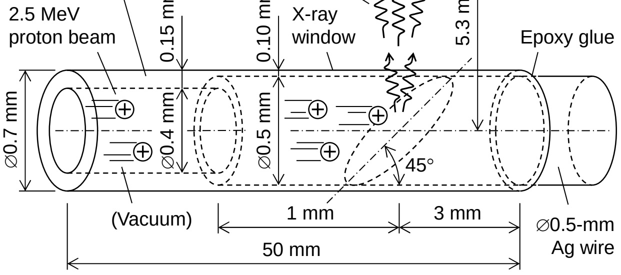

Fig. 1 Structure of the needle end including the Ag target and the X-ray window. The geometry of the X-ray spectrometry is also illustrated.

"side-on" geometry. The intrinsic detection efficiency for Fe K_α and for Ag K_αX-rays were 95% and $\approx$ 100%, respectively. The energy spectrum of the X-rays that passed through the 0.1-mm thick X-ray window was measured. The distance between the center of the proton beam spot and the detector element was 5.3 mm.

3. Results and discussion

Fig. 2 shows the measured X-ray energy spectrum. The measuring time was 15 minutes. We see that the spectrum consists mainly of line emissions, and the intensity of the continuous component is negligibly small. Except for the strong Ag KX-rays, K lines of Cr, Fe, and Ni originating from stainless steel are recognized. However, the intensity of these X-rays is $\approx 10^2$ times lower than those of the Ag KX-rays. Thus, as expected, we successfully extracted only Ag KX-rays by using the needle wall as a filter.

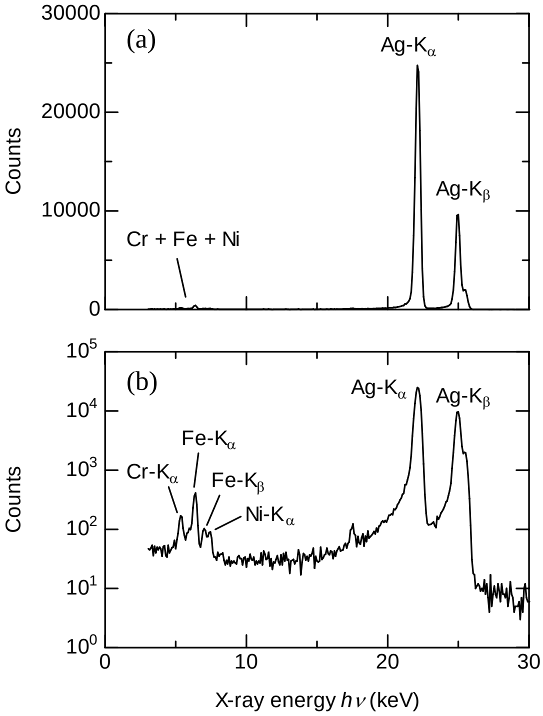

Fig. 2 Measured X-ray energy spectrum; (a) Linear plot. (b) Logarithmic plot. The measuring time was 15 minutes.

The measured count rate of the Ag K_α emission was 1.4×10^2 photons/s. Using this experimental result and the conversion factor from the photon fluence to the absorbed dose at 22 keV, the dose rate on the needle surface was calculated to be $\approx$ 2 mGy/h. If we assume that the practical irradiation time is less than $\approx$ 1 h, the total dose is only $\approx$ 1 mGy. On the other hand, total dose in conventional brachytherapy is typically $\approx 10^2$ Gy. Thus one sees that the X-ray intensity must be increased by a factor of $\approx 10^5$ for practical clinical use of this method.

4. Conclusions

We successfully extracted only the Ag KX-rays which can be compatibly used for the cancer treatment. A high monochromaticity of the extracted X-rays is convenient for tailoring individual treatment plans.

However, we found that an extensive improvement of the X-ray intensity is needed, if we employ this method as an alternative to the conventional brachytherapy. To achieve the required X-ray intensity, it is necessary to not only increase the incident proton beam energy/current, but to also pay a careful attention in designing the needle/target system in which the temperature rise of the tissue around the needle is minimized.

Acknowledgement

We thank H. Fukuda for skillful operation of the tandem accelerator. S. Matsui is gratefully acknowledged for preparation of the experimental devices. This work was supported by KAKENHI (Grant-in-Aid for Challenging Exploratory Research), No. 24650291, Japan Society for the Promotion of Science (JSPS).

References

[1] Y. Oguri and J. Hasegawa, "Development of a Proton-Induced Characteristic X-ray Source for Deep-Seated Tumor Treatment Using a Syringe Needle", *2011 Fall Meeting of the Atomic Energy Society of Japan,* September 19-22, 2011, Kitakyushu, Japan, I13.

[2] Y. Oguri and J. Hasegawa, "Proton-Beam-Transport Experiments through a Syringe Needle for the Development of a Cancer Therapy Using Proton-Induced X-rays", *Bull. Res. Lab. Nucl. Reactor.*, Vol. **35**, pp. 19-20, 2011.

A.2 Dependence on Vibrational Quantum Number of H_2 Rotational Temperature of a Low-Pressure Microwave Discharge Plasma

Hiroshi AKATSUKA, Atsuhi NEZU and Haruaki MATSUURA

1. Introduction

Atomic and molecular processes of hydrogen plasmas become essential in the divertor regions of magnetically-confined thermonuclear fusion plasmas. In these processes as well as other applications of the low-temperature hydrogen plasmas for material processing, it is essential to measure and control the plasma parameters, one of which is a gas temperature that is generally lower than electron temperature, since these plasmas are generally in a state of non-equilibrium. These days, rotational temperature measurement is often applied to monitor the approximate value of gas temperature in plasma processing. In the present study, we examine the rotational temperature of Fulcher-α band spectrum and report results of its dependence on the discharge condition.

2. Experiment

Hydrogen plasma is generated by using a rectangular waveguide with a cavity and a quartz tube, one end of which is inserted into a vacuum chamber. The discharge apparatus is basically the same as that described elsewhere [3].

3. Physical Principle to Determine Rotational Temperature

The Fulcher-α band spectrum is originated from the electronic transition of H_2 molecule from d $^3\Pi_u^-$ state to a $^3\Sigma_g^+$ state. If we denote the transition probability from the upper state (d, v', J') to the lower state (a, v'', J'') as $A_{av''J''}^{dv'J'}$, it can be described based upon the Franck-Condon principle:

$$A_{av''J''}^{dv'J'} = \frac{16\pi^3}{3h\varepsilon_0 \left(\lambda_{av''J''}^{dv'J'}\right)^3} \left(\overline{R_e}\right)^2 q_{v'v''} \frac{S_{J'J''}}{2J'+1}, \qquad (1)$$

where ε_0 is the vacuum permittivity, $\left(\overline{R_e}\right)^2$ is the transition moment, $q_{v'v''}$ is the Franck-Condon factor and $S_{J'J''}$ is the Hönl-London factor. It is already found that the assumption of the Franck-Condon principle causes little error for the transition probability of the vibrationally diagonal transition $\Delta v = v' - v'' = 0$. It must be also noted that both P and R-branches of the Fulcher-α band contain anomaly. We adopted Q-branch to determine the rotational temperature [5].

4. Results and Discussion

Figure 1 shows the rot-vibrational population density distribution of H_2 d state measured with the discharge pressure 1 Torr. The rotational temperature $T_d(v')$ can be determined for each rot vibrational state $v' = 0 - 4$ of the d state. It is found that the rotational temperature of each vibrational level $T_d(v')$ monotonically decreases with increasing vibrational quantum number v', which is found commonly to any discharge conditions. This is because the higher vibrational levels of H_2 molecule have the larger intermolecular distance, and consequently, larger inertia moment I. Near corona equilibrium holds for the present hydrogen plasma. Therefore, the H_2 d state must have the same angular momentum $I\omega$ with the original ground state, since the mass of electron is negligibly small. That is, the higher vibrational level of d state must have smaller ω. Then, the consequential rotational energy $I\omega^2/2$ becomes smaller for the higher vibrational level. Then, the rotational temperature as indication of rotational energy distribution shows monotonic decrease as the increasing vibrational quantum number [7].

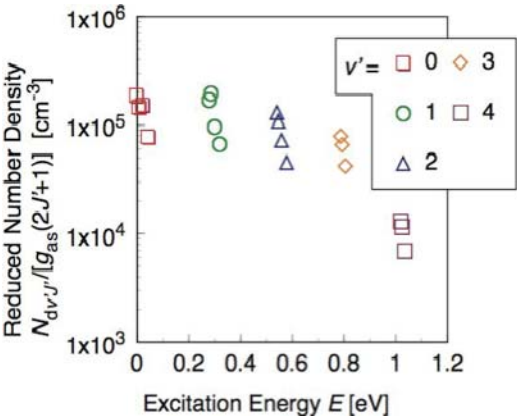

Fig. 1 Measured rot-vibrational population density distribution of H_2 d state at 1 Torr.

Reference

[1] T. Nozaki, Y. Unno, and K. Okazaki: Plasma Sources Sci. Technol. 11 (2002) 431.

[2] S. Nunomura, M. Kondo, and H. Akatsuka: Plasma Sources Sci. Technol. 15 (2006) 783.

[3] Y. Ichikawa, T. Sakamoto, A. Nezu, H. Matsuura, and H. Akatsuka: Jpn. J. Appl. Phys. 49 (2010) 106101.

[4] V. N. Ochkin: Spectroscopy of Low Temperature Plasma (Wiley-VCH, Weinheim, Germany, 2009).

[5] S. Kado, D. Yamasaki, Y. Iida, and B. Xiao: J. Plasma Fusion Res. 80 (2004) 783 [in Japanese].

[6] B. P. Lavrov, M. Osiac, A. V. Pipa, and J. Röpcke: Plasma Sources Sci. Technol. 12 (2003) 576.

[7] Y. Shimizu, A. Nezu, H. Matsuura and H. Akatsuka: *Proc. 30th Symp. on Plasma Processing (SPP)*, The Japan Society of Applied Physics, pp. 131-132 (2013).

A.3 A Study on Excitation Kinetics of Low-Pressure Discharge Oxygen Plasma

Hiroshi AKATSUKA, Atsushi NEZU and Haruaki MATSUURA

1. Introduction

It is needless to say that oxygen plasma is essential for various engineering fields even in nuclear engineering, in addition to electronic and astronautic engineering. In recent years, it is believed that metastable oxygen atom O ^{1}D can be the key species. We focus on the number densities of excited species, particularly of O ^{1}D state in the oxygen plasma. We examine the effects on the excitation kinetics of electron energy probabilistic function, which is abbreviated as EEPF hereafter in this research.

2. Numerical Procedure

In the present study, we treat low-pressure discharge oxygen plasma, about 1 Torr, and discuss excitation kinetics for several excited species in the oxygen plasma as one of main objectives. The pressure condition is chosen to simulate the process of FET gate oxidation. Therefore we chose eight species: O_2 X $^3\Sigma_g$, O_2 a $^1\Delta_g$, O_2 b $^1\Sigma_g$, O^-, O_3, O_2^+, O ^{3}P and O ^{1}D in the simulation of kinetic model. We can assume that other species have much smaller number densities, and consequently, they can be neglected in the present kinetic modeling. In this research, we mainly treat two sets of equations in the calculation to simulate the excitation kinetics. First, we have the following set of rate balance equations when we consider molecular processes in the plasma.

$$\frac{\mathrm{d}[\mathrm{A}]}{\mathrm{d}t} = -\nu_{\mathrm{W}}[\mathrm{A}] + G \qquad (1)$$

where [A] is the number density of the species considered, ν_{W} is the rate coefficient of wall loss process, which is determined by boundary conditions on discharge tube wall, G is source term of species A through population-depopulation processes. Second, we solve the following Boltzmann equation:

$$-\frac{\mathrm{d}}{\mathrm{d}u}\left[\frac{1}{3}\left(\frac{E}{N}\right)^2 \frac{u}{\sigma_{\mathrm{c}}(u)+\sum_j \sigma_j^{\mathrm{si}}(u)}\frac{\mathrm{d}f}{\mathrm{d}u}+\frac{2m_{\mathrm{e}}}{M}\sigma_{\mathrm{c}}(u)u^2\left(f+kT_{\mathrm{g}}\frac{\mathrm{d}f}{\mathrm{d}u}\right)\right]$$
$$+\sum_j u\sigma_j^{\mathrm{si}}(u)f(u)-\sum_j \left(u+u_j^{\mathrm{si}}\right)\sigma_j^{\mathrm{si}}\left(u+u_j^{\mathrm{si}}\right)f\left(u+u_j^{\mathrm{si}}\right)=0, \qquad (2)$$

where $f(u)$ is the EEPF normalized as $\int_0^\infty f(u)u^{1/2}\mathrm{d}u = 1$, u is electron energy in eV, m_{e} is the electron mass, M is the molecular mass, T_{g} is the gas temperature in K, σ_{c} is the momentum transfer cross section, and $\sigma^{\mathrm{si}}{}_i$ is the cross section for the i-th inelastic collision.

We calculated back and forth until self-consistent solution is obtained with respect to the excited-state populations and EEPF. After several times' iteration, the system becomes the steady-state as a self-consistent solution, where we can understand excitation kinetics of oxygen plasma [1].

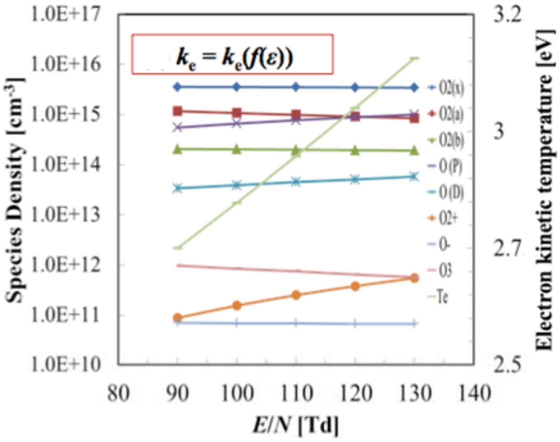

Fig. 1 Number densities of various species in oxygen plasma calculated as functions of reduced electric field, where the rate coefficients are calculated with the cross section and EEPF.

3. Results and Discussion

We calculated the rate coefficients of population and depopulation processes in the model with the rate coefficients given by [2, 3], which are given as functions of electron temperature T_{e}. When we adopted these rate coefficients, it is found that the number density ratio of O_2 a $^1\Delta_g$ to that of O_2 X $^3\Sigma_g$ becomes too large. Therefore, we treat the rate coefficients as function of the EEDF calculated as a solution to the Boltzmann equation (2) in the calculation with the corresponding cross-sections. As a result, Fig. 1 shows the numerical result under the same conditions but with non-Maxwellian EEPF. This result indicates that the number density of atomic oxygen increases with increasing reduced electric field E/N and, on the other hand, that of the molecular oxygen decreases. These results agree with previous study [1, 4]. As a result, it is concluded that the effect of EEPF is significant with respect to the excitation kinetics of low-temperature oxygen plasma [6].

Reference

[1] T. Sakamoto, H. Matsuura, and H. Akatsuka: *J. Adv. Oxid. Technol.* **10**, 247 (2007).

[2] M. Capitelli, C. M. Ferreira, B. F. Gordiets, and A. I. Osipov: "*Plasma Kinetics in Atmospheric Gases*", Springer Verlag, Berlin (2000).

[3] M. A. Lieberman and A. J. Lichtenberg: "*Principles of Plasma Discharges and Materials Processing*", 2nd ed., Wiley Interscience, Hoboken, NJ: Wiley, (2005).

[4] Y. Ichikawa, T. Sakamoto, A. Nezu, H. Matsuura, and H. Akatsuka: *Jpn. J. Appl. Phys.*, **49**, 106101 (2010).

[5] J. Konno, A. Nezu, H. Matsuura and H. Akatsuka: *Proc. 30th Symp. on Plasma Processing (SPP)*, The Japan Society of Applied Physics, pp. 151-152 (2013).

A.4 Nitrogen Arc-Jet as Atomic Radical Source - Dominance of Atomic N Lines in Comparison with Molecular N_2 Band Spectra

Hiroshi AKATSUKA, Atsushi NEZU and Haruaki MATSUURA

1. Introduction

We developed an arc-heated magnetically-trapped expanding plasma jet generator [1], and examined plasma parameters of various expanding plasma jets into a rarefied gas wind tunnel under weak magnetic field [2], including spectroscopic characteristics by optical emission spectroscopic (OES) measurement [3, 4]. In the present study, we examined characteristics of expanding nitrogen plasma, particularly of its spectroscopic characteristics, which gives essential fluid dynamic information of nitrogen plasma jet as a thruster for astronautic applications for artificial satellites.

2. Experiments

The plasma jet generator applied in the present study is the same with our previous studies. Its detailed account was already described elsewhere [1, 3, 4].

3. Results and Discussion

Figure 1 is a typical spectrum emitted from the expanding nitrogen plasma. We can find neither signal of first positive system (1PS) spectrum nor that of second positive system (2PS). Figure 2 shows three atomic nitrogen lines with considerable intensity. These characteristics are completely opposite to the nitrogen plasma in a cylindrical discharge tube as ionizing plasma [5]. Excited species in the expanding nitrogen plasma jet consist almost of atomic species, and scarce in molecular species, which was common to hydrogen arc jet plasma generated in the same discharge apparatus [3].

We consider that this is partly because the electron temperature T_e of the expanding nitrogen plasma is considerably low, which is measured by a Langmuir single probe to be about $0.2 \leq T_e$ [eV] ≤ 0.7, while the electron density N_e is considerably high, about $10^{10} \leq N_e$ [cm^{-3}] $\leq 10^{12}$ in the expanding region. The present nitrogen plasma is found to be a recombining plasma with low electron temperature, where the excited states are mostly generated by three-body recombination for monatomic discharge species like helium or argon. The arc-jet must pass through the arc-region, where the plasma is in the state of LTE and temperature becomes high up to 2 eV. The equilibrium composition of the arc plasma species (before expansion) can be estimated by the theoretical calculation based on chemical equilibrium, which shows the temperature dependence of number densities of essential species in the nitrogen arc plasma at the state of thermodynamic equilibrium ($\Delta G = 0$) with its total pressure $P = 1$ atm, which shows there exists neither neutral nor ionic molecular species of nitrogen when $T \sim 12000$ K, which is lower than typical temperature of arc plasma under atmospheric pressure [6]. Consequently, when the plasma passes here, molecular species are considered to be fully dissociated into atomic species. It is considered that this expanding nitrogen plasma has a potential to be applied as a source of atomic nitrogen [7].

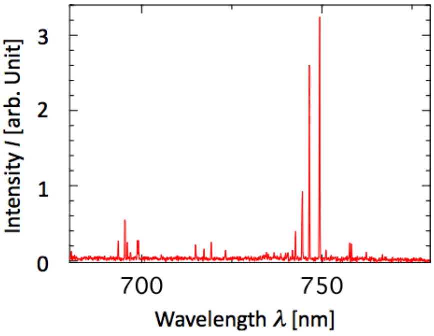

Fig. 1 Emission spectrum of the expanding nitrogen plasma.

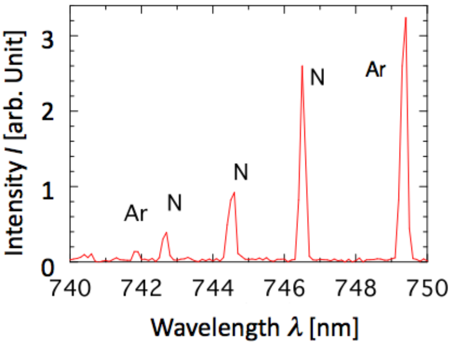

Fig. 2 Close-up view of Fig. 1 in the wavelength region 740 − 750 nm.

Reference

[1] H. Akatsuka and M. Suzuki: *Rev. Sci. Instrum.*, **64**, 1734 (1993).

[2] K. Yoshida, T. Shibata, A. Nezu, H. Matsuura, and H. Akatsuka: *IEEE Trans. Plasma Sci.*, **37**, 1414 (2009).

[3] H. Akatsuka and M. Suzuki: *Phys. Rev. E*, **49**, 1534 (1994).

[4] H. Akatsuka and M. Suzuki: *Plasma Sources Sci. Technol.*, **4**, 125 (1995).

[5] Y. Ichikawa, T. Sakamoto, A. Nezu, H. Matsuura, and H. Akatsuka: *Jpn. J. Appl. Phys.*, **49**, 106101 (2010).

[6] S. V. Dresvin, A. V. Donskoy, V. M. Gol'dfarb, and V. S. Klubnikin, "*Fisica i Tekhnika Nizikotemperaturnoy Plasmy (Physics and Techniques of Low-Temperature Plasma)*", Moscow Atomizdat, Moscow (1972) [in Russian].

[7] M. Hatcho, S. Watanabe, H. Matsuura and H. Akatsuka: *The Papers on Tech. Meeting on "Plasma Science and Technology"*, IEE Japan, PST-13, pp. 13-18 (2013) [in Japanese].

A.5 Reactivity Enhancement of Magnesium Oxide/Water Chemical Heat Storage for Nuclear Heat Recovery

Yukitaka KATO and Junichi RYU

1. INTRODUCTION

For safety design of nuclear reactors for preventing severe accident, thermal energy management of the reactors is important. Chemical heat pump (CHP) has potential to ease severe accident by temporal heat storage under lower pressure. A CHP using the chemical reaction between water (H_2O) and magnesium oxide (MgO) in Eq. 1 has been studied [1,2] for the purpose.

$$Mg(OH)_2(s) \Leftrightarrow MgO(s)+H_2O(g),\ \Delta H = -\ 81.0\ \text{kJ mol}^{-1} \quad (1)$$

CHPs based on a MgO/H_2O reaction system are expected to find applications in not only the purpose, but also waste heat utilization for nuclear reactors, cogeneration systems comprising gas and diesel engines, solar heat panels, and fuel cells.

The low thermal conductivity of magnesium hydroxide ($Mg(OH)_2$) is a problem for a MgO/H_2O chemical heat pump. Low reactant thermal conductivity can induce low performance of the chemical heat pump, such as prolongation of reaction time and reduction of heat output rate. Methods for enhancement of the thermal conductivity of reaction materials have been investigated for a packed bed reactor in a chemical heat pump. One promising method is the introduction of carbon based materials, that is, carbon nanofibers, carbon nanotubes, and expanded graphite into heat storage reactants [3,4].

Expanded graphite (EG) is introduced in this study among the carbon based materials because of its high mass productivity and cost performance. It was reported that the heat transfer and reactivity of reactants for solid-gas chemical heat pumps was greatly improved by the mixing of EG and solid reactants [5]. EG is durable at high temperatures and is chemically inert. EG also has been widely used as a kind of functional carbon material in sealing, catalyzing, mechanical parts for space flight, military affairs, and environmental protection [6,7].

A mixed composite of EG and $Mg(OH)_2$ was experimentally examined in a previous study. The mixture had a tendency for weak contact between EG and $Mg(OH)_2$, and easily separated into the two materials. Then, calcium chloride ($CaCl_2$) was employed for enhancement of the contact between EG and $Mg(OH)_2$. $CaCl_2$ is known as a water absorber and chemical heat pump material [8,9]. The potential of EG mixed with $Mg(OH)_2$ and calcium chloride ($CaCl_2$), referred to as EMC, was discussed [10]. $CaCl_2$ mixed with EG mixture showed an improvement in the degree of contact between EG and $Mg(OH)_2$, and also an enhancement of $Mg(OH)_2$ hydration and dehydration abilities as a result of its high hydrophilic ability. However, the measurement was only done for one set of mixing ratio between EG and $Mg(OH)_2$. Mixing ratio optimization between the raw materials was needed for commercializing EMC as a material for a chemical heat pump packed bed reactor. The high thermal conductivity of EG was expected to positively affect $Mg(OH)_2$ dehydration by enhancing the thermal conductivity of the mixture and the high porosity of EG increased the reaction surface area of the material. The mixing weight ratio optimization between EG and $Mg(OH)_2$ for dehydration was discussed kinetically to determine the effect of EG in EMC in this study.

2. Experiment

$Mg(OH)_2$ (99.9%, 0.07 μm, Wako Pure Chemical Industries, Ltd.), $CaCl_2$ (99.9%, Wako Pure Chemical Industries, Ltd.), and EG were mixed for EMC production. A mixing weight ratio, n, between the $Mg(OH)_2$ content of EMC and EMC itself, and the mixing molar ratio, α, between $Mg(OH)_2$ and $CaCl_2$ in EMC are defined as Eqs.2 and 3, respectively.

$$\text{Mixing weight ratio } (n) = \frac{w_{\mathrm{Mg(OH)_2}}}{w_{\mathrm{EG}} + w_{\mathrm{Mg(OH)_2}}} \quad (2)$$

$$\text{Mixing molar ratio } (\alpha) = \frac{\text{mole number of CaCl}_2\text{ in EMC [mole]}}{\text{mole number of Mg(OH)}_2\text{ in EMC [mole]}} \quad (3)$$

EMC was prepared using the following process:

(1) The weights of $Mg(OH)_2$ and $CaCl_2$ were measured using a digital balance.

(2) These materials were charged into a flask with 100 mL of ethanol.

(3) The $Mg(OH)_2$ and $CaCl_2$ were dispersed in ethanol using an ultrasonic processor.

(4) The measured EG was charged in a flask. The flask was set in a rotary evaporator and rotated at 303K under a pressure lower than atmosphere. Ethanol was removed from the flask.

(5) The mixed material in paste state in the flask was dried in an oven at 120°C for over 10 h. The final product was a dried mixed material.

Fig. 1(a) shows a SEM image of row expanded graphite. Fig. 1(b) shows the SEM image of EMC (n = 0.80, α = 0.10), which was mixed according to the above method [2].

The dispersion process of (3) using the ultrasonic processor before mixing with EG was useful for achieving homogeneous mixing, in comparison to the conventional stirring process.

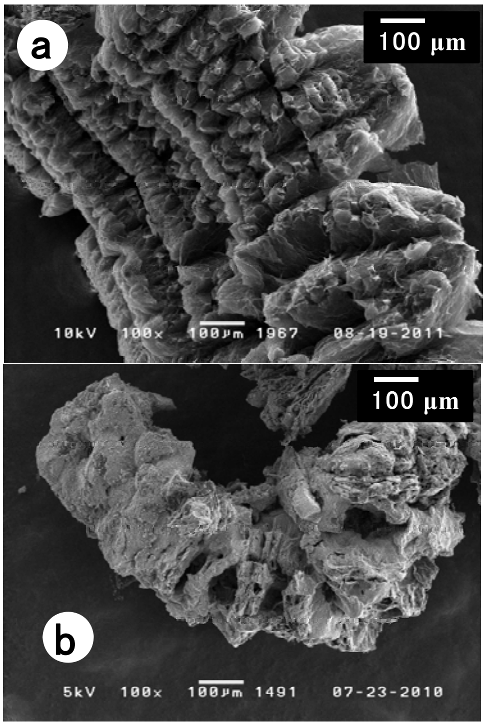

Fig. 1. SEM image of (a) expanded graphite and (b) EMC (n = 0.80, α = 0.10).

3. Results

The high thermal conductivity of EG positively affects $Mg(OH)_2$ dehydration by enhancing the thermal conductivity of the mixture and the high porosity of the worm form of EG increases the reaction surface area of the material. It is expected that these aspects will induce an increase in the dehydration rate. Therefore, dehydration experiments were conducted according to mixing weight ratio change to determine the effect of the amount of EG in EMC.

Fig. 2 shows the effect of the mixing weight ratio, n, on the reacted mole fraction in of $Mg(OH)_2$ dehydration at 300°C. From Fig. 2, it was confirmed that the dehydration rate increased as the amount of EG in EMC increased. It was thought that the addition of EG to the EMC mixture enhanced thermal conductivity, vapor diffusivity, and dehydration reactivity.

The kinetics of dehydration were evaluated by an integration method on the assumption that dehydration occurs homogeneously and the reaction order of dehydration is unity. The dehydration rate equation can be written as follows:

$$-\frac{dy}{dt_{\mathrm{d}}} = k_{\mathrm{d}} y \qquad (4)$$

where t_d [s] is the reaction time and k_d [s^{-1}] is the dehydration rate constant.
Eq. 4 can be integrated; then Eq. 5 is obtained.

$$y = y_0 \exp\left(-k_{\mathrm{d}} \cdot t_{\mathrm{d}}\right) \qquad (5)$$

where y_0 is determined to be 0.95 for the y intercept in this study. **Eq. 5** can be converted to natural logarithm form:

$$\ln y = -k_{\mathrm{d}} t_{\mathrm{d}} + \ln y_0 \qquad (6)$$

From **Eq. 6**, k_d can be obtained as the slope of a plot of t_d vs. ln y.

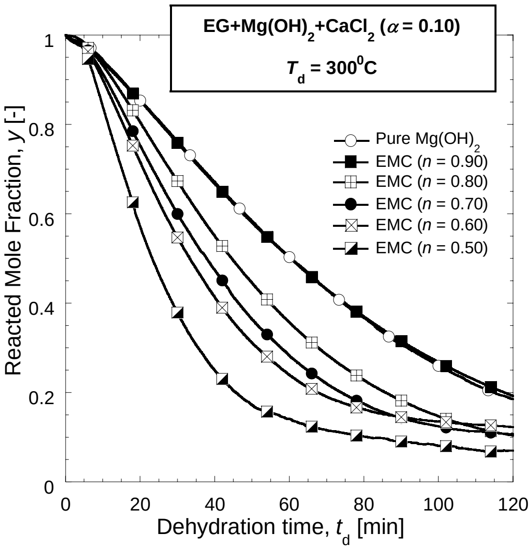

Fig. 2. Dependency of n on dehydration of EMC at 300°C.

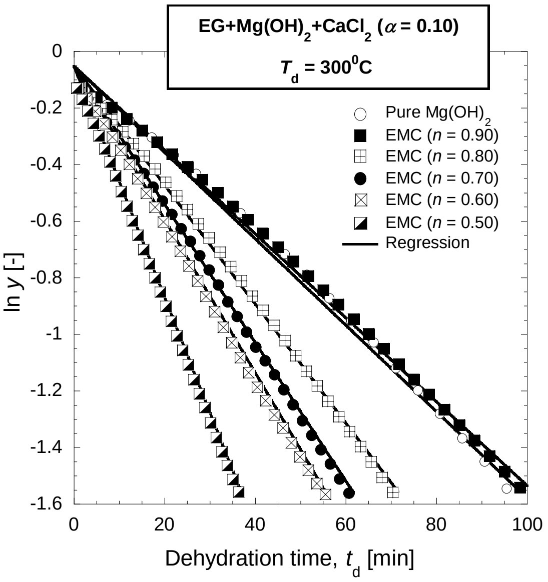

Fig. 3 Dependency of *n* on and ln *y* for EMC.

Reaction rate analysis plots of $Mg(OH)_2$ in EMC according to changing mixing weight ratios between EG and $Mg(OH)_2$ based on Eq. 6 are shown in Fig. 3. The range of y employed for kinetic analysis was $0.20 \leq y \leq 0.90$, ($-1.6 \leq \ln y \leq -0.11$). From the derived k_d values of EMC, it was found that k_d decreased as the amount of $Mg(OH)_2$ in EMC increased.

Dehydration experiments for the optimized EMC, which had an optimized n value of 0.80 at α of 0.10, were conducted under five temperatures (260, 270, 280, 290, and 300°C). Dehydration of pure $Mg(OH)_2$ was also conducted under three temperatures (280, 290, and 300°C). Two samples of each material were examined and the results are shown in Fig. 4. The line shows averaged results derived from two sample results at each reaction condition. It was confirmed that the EMC had a higher dehydration rate than pure $Mg(OH)_2$ under all experimental dehydration temperatures.

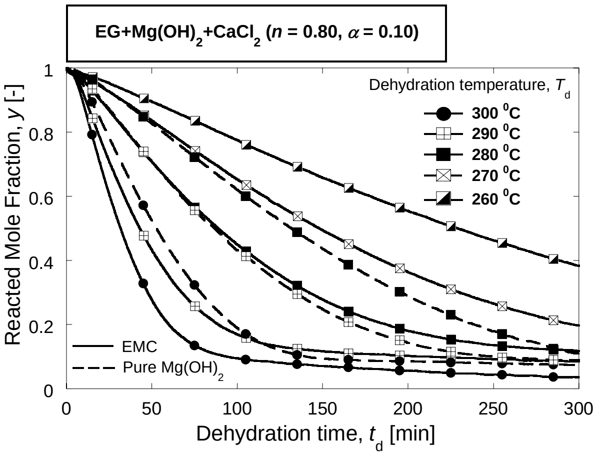

Fig. 4 Reacted fraction change profiles of optimized EMC (n = 0.80 and α = 0.10) and pure $Mg(OH)_2$ for dehydration at some temperatures.

Conclusions

EMC, a $Mg(OH)_2$ composite material mixed with expanded graphite and $CaCl_2$, was developed as a packed bed reactor material for MgO/H_2O chemical heat pumps. Dehydration rates increased with decreasing mixing weight ratio, n.

Dehydration rate constants were obtained from the experimental results. It was suggested on the basis of a discussion on the multiplied value of Φ that the optimized value of n at a value of 0.10 for the mixing molar ration, α, was approximately 0.80.

The dehydration performance of optimized EMC and pure $Mg(OH)_2$ were examined, and their reaction rate constant equations proposed. The reaction rate constant values of optimized EMC were higher than that of pure $Mg(OH)_2$ under all dehydration temperatures. It was thought that the thermal conductivity enhancement resulting from the introduction of EG and the water transfer capability resulting from the introduction of $CaCl_2$ positively contributed to the frequency factor and k_d of optimized EMC.

It was concluded that EMC had better thermal storage performance than pure $Mg(OH)_2$. Optimization of the mixing molar ratio of EMC and an evaluation of the hydration performance of optimized EMC under various experimental conditions will be needed in the next study.

References

[1] Y. Kato, N. Yamashita, K. Kobayashi, and Y. Yoshizawa, Kinetic study of the hydration of magnesium oxide for a chemical heat pump, *Applied Thermal Engineering,* **16** (1996) 853-862.

[2] Seon Tae KIM, Junichi RYU, Yukitaka KATO, "The optimized mixing ratio of expanded graphite mixture for packed bed reactor of chemical heat pump", *Applied Thermal Engineering*, **50**, pp. 485-490 (2013).

[3] Andrew Mills, Mohammed Farid, J.R. Selman, and Said Al-Hallaj, Thermal conductivity enhancement of phase change materials using a graphite matrix, *Applied Thermal Engineering,* **26** (14-15) (2006) 1652-1661.

[4] K. Fujioka, K. Hatanaka, and Y. Hirata, Composite reactants of calcium chloride combined with functional carbon materials for chemical heat pump, *Applied Thermal Engineering,* **28** (2008) 304-310.

[5] S. Mauran, P. Prades and F. L'Haridon, Heat and mass transfer in consolidated reacting beds for thermochemical systems, *Heat recovery systems & CHP,* **13**(4) (1993) 315-319.

[6] L.W. Wang, Z. Tamainot-Telto, S.J. Metcalf, R.E. Critoph, and R.Z. Wang, Anisotropic thermal conductivity and permeability of compacted expanded natural graphite, *Applied Thermal Engineering,* **30** (13) (2010) 1805-1811.

[7] Jianguo Zhao, Quangui Guo, Jingli Shi, Lang Liu, Jinsheng Jia, Yuecheng Liu, and Haiqing Wnag, Carbon nanotube growth in the pores of expanded graphite by chemical vapor deposition, *Carbon,* **47** (7) (2009) 1747-1751.

[8] Keiko Fujioka, Kensuke Hatanaka, Yushi Hirata, Composite reactants of calcium chloride combined with functional carbon materials for chemical heat pump, *Applied Thermal Engineering,* **28** (4) (2008) 304-310.

[9] R. G. Oliveira, R. Z. Wang, A consolidated calcium chloride-expanded graphite compound for use in sorption refrigeration systems, *Carbon,* **45** (2007) 390-390.

[10] Seon Tae KIM, Junichi RYU, and Yukitaka KATO, Reactivity enhancement of chemical materials used in packed bed reactor of chemical heat pump, *Progress of Nuclear,* **53** (2011) 1027-1033.

A.6 Dehydration Behavior of $Mg(OH)_2$-$Ni(OH)_2$ Composite Prepared by Mechano-chemical Method

Junichi RYU and Yukitaka KATO

Introduction

In recent years, the technologies of chemical heat pump and chemical heat storage are widely studied for the reduction of energy consumption and CO_2 emission. Chemical heat pump system with the reaction between magnesium oxide (MgO) and water vapor has been reported by our group. [1]

$$MgO + H_2O \rightleftarrows Mg(OH)_2 \quad \Delta H = -81.2 \text{ kJ mol}^{-1}$$

In this system, thermal energy above 350°C is required for practical heat storage operation. Recently, chemically modified magnesium hydroxides were proposed as new type material for chemical heat storage by our group. These materials can store thermal energy around 280 °C. [2,3] The heat storage density of these materials are higher than authentic magnesium hydroxide under 280°C of heat storage condition. In this work, dehydration behaviour of $Mg(OH)_2$-$Ni(OH)_2$ composites prepared by mechano-chemical method as a new material for chemical heat storage were studied by TG method.

Experimental

$Mg(OH)_2$-$Ni(OH)_2$ composite was prepared by mechano-chemical method. Authentic $Mg(OH)_2$ and $Ni(OH)_2$ were used as precursor. Mixture of $Mg(OH)_2$ and $Ni(OH)_2$ with several molar ratio were milled in planetary ball mill under 400rpm of rotation speed. Solid state reaction with milling treatment was confirmed by FT-IR. Dehydration reaction of the prepared samples were tested by thermogravimetric method with 5K/min of temperature increasing rate under Ar flow. The molar fraction of hydroxide in the sample and reaction conversion were calculated from the weight change of sample.

Results

FT-IR spectra of $Mg(OH)_2$-$Ni(OH)_2$ (5:5) are shown in Figure 1. Before the treatment, the OH group peak of $Mg(OH)_2$ and $Ni(OH)_2$ are exist at 3697 cm^{-1} and 3638 cm^{-1}, respectively. The peak at 3697 cm^{-1} was shifted lower wave number with milling time. On the other hand, the peak at 3638 cm^{-1} was disappeared after 20h of milling time. Dehydration behavior of prepared samples are shown in Figure 2. The dehydration temperature of $Mg(OH)_2$-$Ni(OH)_2$ composites were shifted lower with increase of $Ni(OH)_2$ content. These results indicate Mg-Ni mixed hydroxide was synthesized by mechano-chemical method with ball milling treatment.

The hydration behavior and the stability for cyclic operations under practical conditions should be studied further.

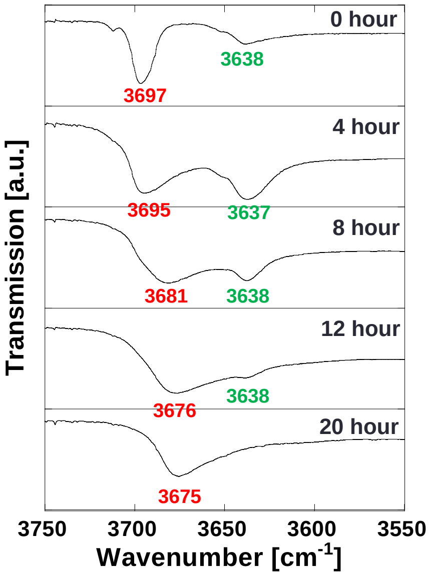

Figure 1 FT-IR spectra of $Mg(OH)_2$-$Ni(OH)_2$ composites with changing of treatment time.

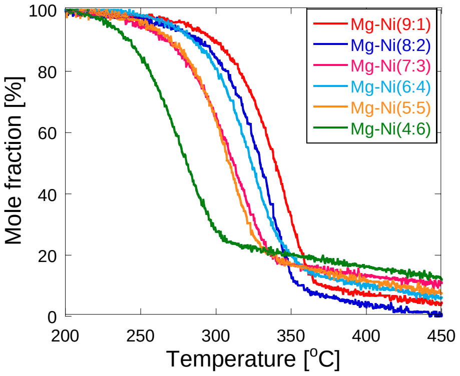

Figure 2 Dehydration behavior of $Mg(OH)_2$-$Ni(OH)_2$ composites.

References

1 Y. Kato et al., *Appl. Therm. Eng.*, **16**, 852 (1996).
2 J. Ryu et al., *J. Chem. Eng. Jpn.*, **40**, 1281 (2007).
3 H. Ishitobi et al., *Ind. Eng. Chem. Res.*, **52**, 5321 (2013).

A.7 Velocity measurement of electro-magnetically driven shock wave by laser refraction for dissociated gas-beam interaction experiments

Kotaro KONDO, Yoshiyuki OGURI

1. Introduction

Stopping power is defined as the average energy loss of a particle per unit path length in the target. The evaluation of ion stopping power which depends on the target temperature and density is important for heavy ion fusion target design and heavy-ion-driven high energy density physics experiments. Particularly, the stopping power for low energy beam depends strongly on the electronic state of the target. For example, the stopping power in a high temperature and low density plasma is larger than that in room temperature gas because free electrons in the plasma are efficient carriers of energy between the incident ion beam and the target. The effects of dissociation of the target molecules in stopping cross section have not been experimentally investigated, whereas the experiments on the ionization effects in stopping power were performed.

Electro-magnetically driven shock wave was proposed as a tool for production of well-defined dissociated targets, which are desirable for the stopping power measurement. The shock wave method has an advantage that Rankine-Hugoniot relations with shock wave velocity can give the information of the physical state behind the shock wave. Using this method, we generated quasi-steady and one-dimensional strong shock wave [1]. A previous study showed that the duration of the shocked region between the shock front and the discharge plasma is required to be in the order of microseconds for the stopping power measurement. Generally, it is expected that a long shock tube can generate the dissociated hydrogen target with long duration time because the shock-compressed region between the shock and the piston surface increases with the propagation length of the shock wave. From the consideration above, we developed a shock tube with long propagation section. A shock velocity of 25 km/s was required to produce completely dissociated hydrogen gas without ionization. We need precise shock velocity measurement because the property of the shocked region is sensitive to the velocity. In this paper, the laser refraction, which needs only simple and compact devices, is proposed as the method of velocity measurement. We present the experimental results on the electro-magnetically driven shock velocity.

2. Experimental method

2.1. Electro-magnetically driven shock tube

Fig. 1 shows the experimental setup. Hydrogen gas with pressure from 300 to 1000 Pa was filled in the electro-magnetically driven shock tube. The electrodes were connected with a gap switch and capacitors with a total capacitance of 3.5 μF. The charging voltage was from 16 to 18 kV. The central electrode, which works as the anode with a 12-mm outer diameter, is 180 mm longer than the previous tube. The inner diameter of the cathode is 30 mm. The discharge plasma is generated between the electrodes after the trigger signal is sent to the gap switch. The discharge current sheet, which is accelerated by the magnetic pressure, produces a shock wave. The dissociated hydrogen target can be formed between the shock front and the discharge plasma when we have a proper shock velocity.

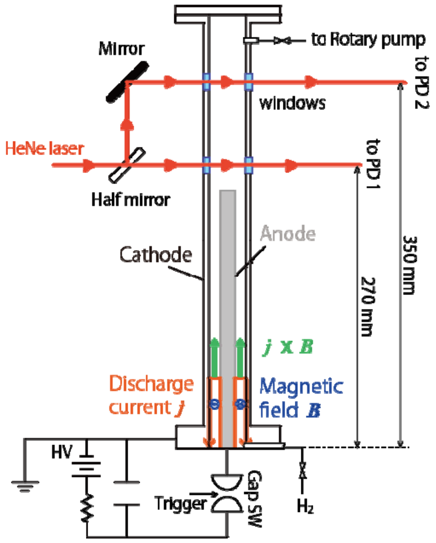

Fig. 1 This experimental setup consists of electro-magnetically driven shock tube, equivalent circuit, and He-Ne laser with optical devices for shock measurement.

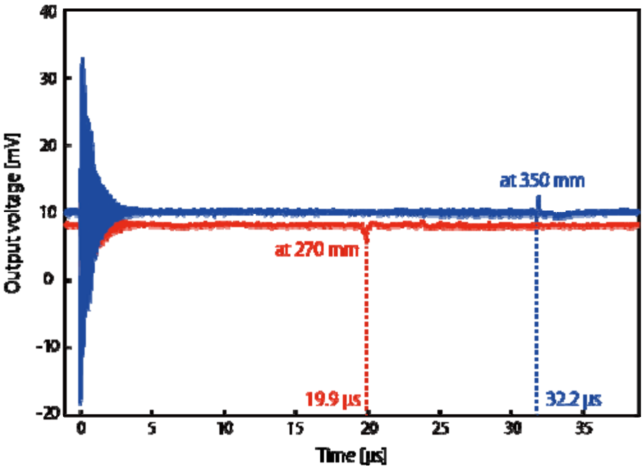

Fig. 2 Output signals from the two photodiodes (PD1 and PD2).

2.2. Velocity measurement using laser refraction

The degree of dissociation is sensitive to the shock velocity. In order to measure the velocity, we propose a laser refraction method as shown in Fig. 1. Probe lasers were led to the two photodiodes (PD1 and PD2) via the optical windows on the outer hollow cylinder. When shock wave reaches to the window position, the density gradient at the shock front causes a laser refraction. At this moment, the photodiode (S5972, Hamamatsu, Inc.) behind the shock tube detects the change of the laser signal. PD1 and PD2 were placed at 270 mm and at 350 mm from the bottom of the central electrode, respectively. From the two photodiode signals, the averaged shock velocities were estimated.

2.3. Experimental procedure

A delay pulse generator (DG535, Stanford Research System, Inc.) with amplifiers, which supplies the trigger signal to the gap switch, controlled the main discharge. In this experiment, dependence on the initial hydrogen gas pressure and the charging voltage was investigated. In order to investigate the reproducibility, three measurements were repeated for each experiment.

3. Experimental results

3.1. Photodiode signal

Output signals from the photodiodes are shown in Fig. 2. The vertical axis stands for the time after the discharge. The discharge voltage was 16 kV and the initial hydrogen gas pressure was 1000 Pa. The signal baselines of PD1 and PD2 were 8 mV and 10 mV, respectively because the CW lasers were used. Noise signals from the both photodiodes were observed until 5 μs due to the discharge. We observed change of the diode signals at 19.9 μs and at 32.2 μs for PD1 and PD2, respectively.

3.2. Initial gas pressure dependence

The measured average shock wave velocities for different initial hydrogen gas pressures are shown in Fig. 3.

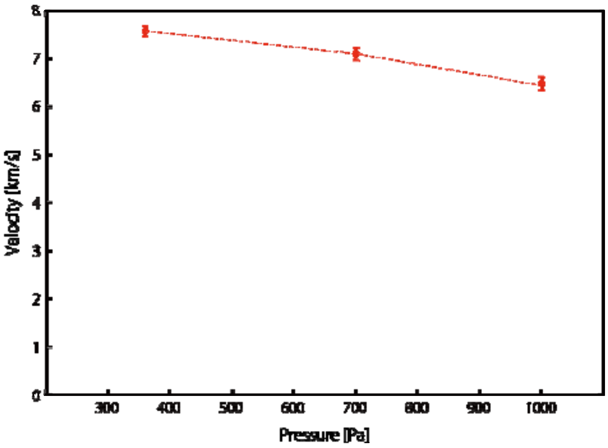

Fig. 3 Average shock wave velocity VS initial pressure (360 Pa, 700 Pa, and 1000 Pa). The discharge voltage was fixed at 16 kV. The dots show the average values for three measurements and error bars show the standard deviation.

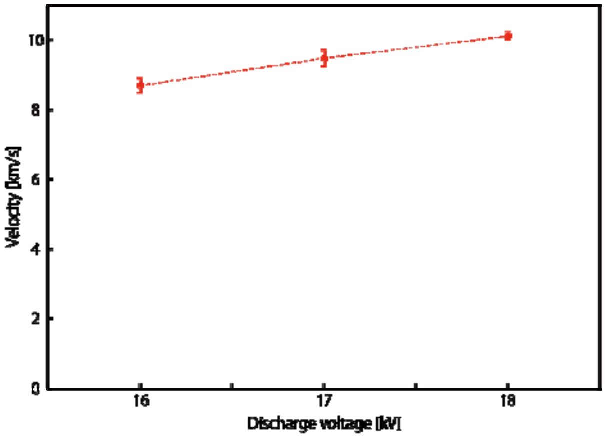

Fig. 4 Average shock wave velocity VS charging voltage (16 kV, 17 kV, and 18 kV). The initial pressure was fixed at 1000 Pa. The dots show the average values for three measurements and error bars show the standard deviation.

These results show that higher velocities were observed for lower initial pressures.

3.3. Discharge voltage dependence

Fig. 4 shows the dependence of the average shock wave velocity on the charging voltage. These results show that higher shock wave velocities were observed for the high charging voltages.

4. Summary

We successfully measured the average shock wave velocity by the laser refraction proposed in this work. The velocity measurement by this method can be reliable because the qualitatively measured dependences on the initial gas pressure and discharge voltage were consistent with a simple consideration based on energy conservation. On the other hand, we found that the shock wave velocity is not enough to dissociate hydrogen gas. The more input energy is required to produce a completely dissociated hydrogen gas target with a large volume using the long shock tube studied in this work.

Acknowledgement

We would like to thank S. Matsui for preparation of the experimental devices.

References

[1] K. Kondo, M. Nakajima, T. Kawamura and K. Horioka: “Compact pulse power device for generation of one-dimensional strong shock waves”, *Rev. Sci. Instrum.* **77**, No.3, pp. 036104-1-3, 2006.

B.1 Study of Neutron Capture Cross Sections of Long-Lived Fission Products

Masayuki IGASHIRA, Tatsuya KATABUCHI and Kazushi TERADA

1. Introduction

Nuclear waste contains long-lived radioactive materials, which are long-lived fission products (LLFP) and minor actinides. Currently, the deep geological disposal of nuclear waste is the national policy in Japan. However, it needs the long-term management that prevents the public from suffering radiological hazard. To decrease the hazard of nuclear waste for future generation, nuclear transmutation systems, in which LLFPs and MAs are transmuted into stable or shor-lived nuclides, become an attractive option.

In order to design a nuclear transmutation system, reliable nuclear data of LLFPs and MAs are necessary. We are measuring the neutron capture cross sections of LLFPs and their stable isotopes as a part of the project “Systematic Study on Neutron Capture Reaction Cross Sections for the Technological Development of Nuclear Transmutation of Long-Lived Nuclear Wastes” [1]. The project is financially supported by the Grants-in-Aid for Scientific Research (KAKENHI) of the Japan Society for the Promotion of Science. The purpose of this project is systematic study of neutron capture cross sections of LLFPs and MAs for nuclear transmutation of nuclear waste. Neutron beam lines of the three facilities, J-PARC (Japan Proton Accelerator Research Complex), Tokyo Tech and KURRI (Kyoto University Research Reactor Institute), are used for measurements.

In 2012 fiscal year, our Tokyo Tech group carried out experiments in Tokyo Tech and J-PARC. The experiments are summarized in the following sections.

2. Tokyo Tech

We measured the keV-neutron capture cross sections of Pd stable isotopes by the time-of-flight (TOF) method in Tokyo Tech. Nuclear data of Pd stable isotopes are important for study on nuclear transmutation of ^{107}Pd. Stable Pd isotopes are inherently contained in ^{107}Pd batch in reprocessing unless isotope separation is performed. In addition, it is not so easy to prepare an enough amount of ^{107}Pd sample for neutron capture cross section measurement. Only a few measurements have been done and consequently the existing cross section data of ^{107}Pd are not reliable. Thus, reliable systematic experimental data of stable Pd isotopes are useful to find a systematics of the model parameters of theoretical calculations of Pd isotopes. Then, the capture cross section of ^{107}Pd can be calculated from the model calculation.

A Pelletron accelerator in the Research Laboratory for Nuclear Reactors of Tokyo Tech was used to produce neutrons via the ^{7}Li(p,n)^{7}Be reaction. We have prepared isotopically enriched samples of five Pd isotopes, $^{104, 105, 106, 108, 110}$Pd. In 2012 fiscal year, capture cross sections of $^{104, 105, 106, 108}$Pd were measured at an incident neutron energy of approximately 550 keV. Gamma-rays from the neutron capture reaction were detected with an NaI(Tl) detector with anti-Compton shield. A pulse height weighting technique is employed to derive neutron capture yields. The ^{197}Au(n,γ)^{198}Au evaluated cross section of JENDL-4.0 was used as standard cross section.

In 2010-2011, measurements in the neutron energy region from 15 keV to 100 keV were already completed for all Pd samples [2]. After planned measurement of ^{110}Pd at 550 keV in 2013, systematic measurements of the Pd isotopes in the two energy regions will be accomplished. The cross section data set of the Pd isotopes will be used to find the optimal model parameters for theoretical calculations.

3. J-PARC

We utilized a high intensity neutron beam from a spallation neutron source of the Materials and Life Science Facility (MLF) of J-PARC for neutron capture cross section measurement. In a collaborative project involving our research group, the Accurate Neutron-Nucleus Reaction Measurement Instrument (ANNRI) was built for nuclear data measurement at the No. 4 beam port in 2007 [3]. We have installed NaI(Tl) detectors at a flight length of 27.9 m in ANNRI. We intend to use the NaI(Tl) detectors for capture cross section measurement, employing the pulse-height weighting technique which has been already established in our group in Tokyo Tech in the past decades.

In early part of 2012 fiscal year, we invested time to develop a new signal processing technique to facilitate capture cross section measurement in J-PARC. The high intensity pulsed neutron beam of J-PARC enables capture cross section measurements for micro amount samples such as radioactive materials. However the counting rate is inherently high due to the high neutron flux. Moreover, previous experiments have revealed that strong γ-ray bursts called γ flush emitted from the neutron source at the beginning of the TOF cycle saturated processing capacity of the conventional pulse height analysis system which consists of an analogy shaping amplifier and a peak hold analog-to-digital converter. The saturation of the electronics capacity lasted more than 10 μsec and precluded measurement in the fast TOF region. To overcome these issues, we developed a new signal processing method based on pulse width measurement using a fast time digitizer (FAST ComTec MCS6). The anode output signal from photomultiplier tubes of the NaI(Tl) detector was connected to the time digitizer directly without any analog devices. The pulse width of the anode signal was measured as duration of time the signal stays over the preset threshold level. In the test experiments using known-energy discrete γ-rays from standard γ-ray sources and neutron-induced reactions, we determined a suitable function to convert the pulse width to the pulse height. The pulse height spectra were successfully reconstructed by the conversion function. The signal processing speed of the time digitizer is much faster than the conventional pulse height analysis systems. Saturation of signal processing capacity by the γ flush was not observed.

After the previous data acquisition system was replaced with the new pulse width analysis system, we measured the capture cross sections of ^{99}Tc and ^{107}Pd. Data analysis of the experimental data to derive the capture cross sections is ongoing.

Acknowledgment

This work is supported by JSPS KAKENHI Grant Number 22226016.

References

[1] M. Igashira, “Systematic Study on Neutron Capture Reaction Cross Sections for the Technological Development of Nuclear Transmutation of Long-Lived Nuclear Wastes”, http://www.jsps.go.jp/j-grantsinaid/12_kiban/ichiran_22/e-data/e66_igashira.pdf

[2] K. Terada *et al.*, *Proceedings of the 14th International Symposium on Capture Gamma-Ray Spectroscopy and Related Topics*, World Scientific, pp. 456-461, May. 2013.

[3] Y. Kiyanagi *et al.*, *Journal of Korean Physical Society*, **59** (2011) 1781-1784.

B.2 Recovery Behavior of Point Defects after Low-Dose and Low Tempereature Neutron Irradiation of Sintered 6H-SiC

Toyohiko YANO, Yusuke FUTAMURA and Katsumi YOSHIDA

To evaluate neutron-irradiation-induced crystalline defects and its thermal stability, α-SiC sintered bodies consisting of mainly 6H polytype were neutron irradiated using the JMTR up to 1.9×10^{23} n/m^2 (E>0.1MeV) at a low temperature of ~150^{o}C. Changes in the lattice parameters and macroscopic lengths resulting from post-irradiation isothermal annealing up to 6 h between room temperature and 1400^{o}C were measured. Macroscopic volume swelling coincided well to those of unit cell volume changes, indicating the presence of only simple defects. The recovery behavior of the macroscopic length and lattice parameters showed almost the same tendencies, although residual changes in the c-axis length slightly exceeded that of the a-axis length at temperatures lower than 1273K. Difference in these axes lengths diminished at temperatures above 1273K. Calculation of activation energies revealed that length recovery behavior between 200 and 1300^{o}C could almost be completely explained by a first-order reaction, and three stages with activation energies of 0.14, 0.26, and 1.13eV. The results indicated the presence of several kinds of point defects, some of which induced anisotropic lattice expansion [1].

1. Introduction

Research on SiC or SiC/SiC composites, which are promising candidates as structure and blanket materials for future fusion reactors, has continued for more than a few decades because of the advantages of low-Z, high temperature mechanical stability, relatively low neutron activation, and quick decay of radioactivity. However, neutron-irradiation-induced crystalline defects degrade the material properties. It is generally accepted that, in the intermediate temperature range (from ~150 to ~1050^{o}C), swelling induced by point defects and their small complexes saturates at less than 1 dpa. The saturated swelling is inversely related to the irradiation temperature. Recombination of point defects is mainly caused by the migration of interstitial atoms in this temperature range, but the kinds and stabilities of induced defects have not yet been explained satisfactorily.

Our previous study examined two kinds of α-SiC (mainly a 6H polytype and a mixture of 6H and 4H polytypes) irradiated under different conditions but with the same level of swelling. We reported a slight change in recovery behavior of point defects during long-time thermal annealing using a precise dilatometer. The SiC specimen containing Al_2O_3 (a mixture of 6H and 4H polytypes) showed a large change in the activation energy of length recovery at ~950^{o}C and 1200^{o}C, and the activation energy of the SiC specimen containing B_4C (mainly the 6H polytype) showed large changes at ~800^{o}C, 950^{o}C, and 1200^{o}C. Activation energies of macroscopic length recoveries for both specimens from the irradiation temperature to the lower temperature boundary were 0.1~0.2 eV, and those of the second temperature range were 0.8~0.9 eV, respectively [2].

In this study, our goal was to confirm that the effects of neutron irradiation on physical property changes of SiC ceramics consisted mainly from the 6H polytype (α-SiC). Changes of lattice parameters and macroscopic lengths resulting from post-irradiation isothermal annealing up to 6 h between room temperature and 1400^{o}C are measured.

2. Experimental Procedures

SiC used in this study was pressureless-sintered α-SiC ceramics containing B_4C as a sintering additive, the same material used in our previous study [2]. These specimens, which were 2 x 4 x 25 mm in size, were neutron-irradiated in the Japan Materials Testing Reactor (JMTR) up to a fluence of 1.9×10^{23} n/m^2 (E_n>0.1MeV, ~0.02 dpa) at a relatively lower temperature of ~150^{o}C. Two different methods were used to measure the macroscopic lengths of the specimens. The first method used a point-type micrometer at room temperature after each isochronal annealing. The second method involved length changes by dilatometry. The length change of the rectangular specimens was continuously measured in situ at high temperature using a precision dilatometer from the irradiation temperature up to 1400^{o}C with a step-heating temperature interval of 50^{o}C in He atmosphere, as described previously [2, 3].

Lattice parameter changes were measured by powder X-ray diffractometry (XRD). The bulk specimen of the same lot used for length measurements was pulverized, and then mixed with an internal Si standard. The mixed powder was placed on a sample holder made of silica glass. The whole specimen holder filled with the mixed powder was annealed in a vacuum furnace (~10^{-1} Pa) up to 1000^{o}C, i. e., annealing and lattice parameter measurement were conducted alternately for the same sample. Above 1050^{o}C, other small bulk specimens of the same bar mentioned above were heated separately at each temperature using another vacuum furnace and then pulverized for XRD measurement. The isochronal annealing time was 6 h. XRD profiles were obtained by the step scan method from 80 to 140^o at 24±1^{o}C. To check the effect of different annealing atmospheres, another set of the measurements on a specimen from the same lot used for length measurements

Table 1 Lattice parameter change and macroscopic length change of the selected α-SiC specimens after irradiation of 1.9×10^{23} n/m^2 at ~150°C.

Specimen ID number	Lattice parameter				Macroscopic length change (%)
	axis	Before irradiation (nm)	After Irradiation (nm)	Change (%)	
21	a-axis	0.3078	0.3091	0.42	0.448
	c-axis	1.5102	1.5173	0.47	
23	a-axis	0.3078	0.3092	0.45	0.468
	c-axis	1.5102	1.5176	0.49	
28	a-axis	0.3077	0.3090	0.42	0.436
	c-axis	1.5107	1.5172	0.43	
17	-	-	-	-	0.450

was conducted using the helium atmosphere furnace of the dilatometer (10^5 Pa) in all temperature ranges for 3 h at each step.

3. Results and Discussion

The results of lattice parameter change and macroscopic length change of α-SiC due to our neutron irradiation is shown in **Table 1**. These specimens were the same lot from the same manufacturer, and irradiated in the same capsule. Whereas small variations due to independent measurements were observed, lattice parameter changes mostly matched well with that of the macroscopic length change. It was noted that there are small differences in the a- and c-axis parameter changes. Expansion of the c-axis is slightly larger than that of the a-axis.

Recovery behavior of the a- and c-axis lengths of the specimen ID=21 and 23 by isochronal annealing under vacuum for 6 h from 150 to 1400°C is shown in **Fig. 1**. The lattice parameter gradually decreased with increasing annealing temperature and mostly saturated around 1300°C. It is clear that, from room temperature to 1000°C, the residual lattice parameter change of the c-axis after each annealing exceeded that of the a-axis, but beyond 1000°C, the difference mostly disappeared.

Variations of the ratio of (c-axis length change)/(a-axis length change) by isochronal annealing for the specimens shown in Fig. 1 are presented in **Fig. 2**. The ratio is roughly constant at 1.05~1.1 up to 600°C but peaks slightly at ~300°C. Beyond ~600°C, It was observed a large peak with maximum at ~900°C. This means that the c-axis length expansion significantly exceeds that of the a-axis around that temperature region. On the contrary, at over ~1200°C, the ratio is less that unity, indicating that the expansion ratio of the a-axis is larger than that of the c-axis. Larger variations at higher temperatures can be attributed to very small absolute values of less than 0.05%, i.e., close to the detection limit.

Fig. 3 compares recoveries of both the macroscopic volume changes and unit cell volume changes for the specimen (macroscopic length measurement for the specimen ID=17 and unit cell volume change measurements for specimen ID=21 and 23, annealed in vacuum). It is clear that these values agree very well for the full range of annealing temperatures.

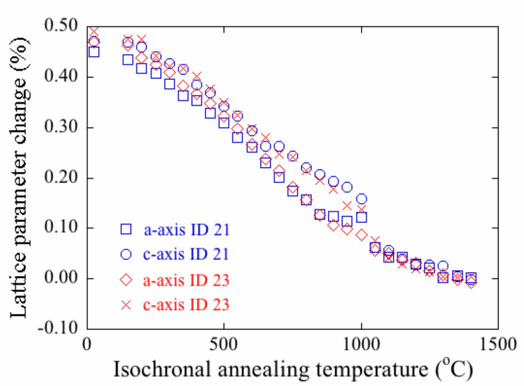

Fig. 1 Lattice parameter changes measured at ambient after 6 h isochronal vacuum anneals in 50°C steps from RT to 1400°C for specimens 21 and 23 (see Table 1) .

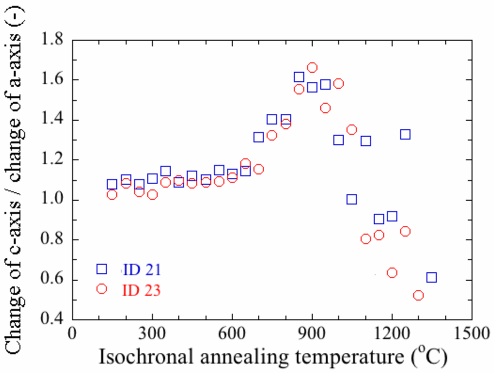

Fig. 2 Ratio of c-axis/a-axis lattice parameter changes for specimens 21 and 23 shown in Fig. 1.

To analyze the recovery rate of macroscopic length at each isothermal annealing temperature, rate constants were calculated using annealing curves observed by in situ dilatometry measurements for the specimen ID=28, as mentioned previously [2]. When the recovery process is governed by the recombination of interstitial atoms and vacancies (i.e., Frenkel pairs), it can be explained as a first-order reaction. The length change plotted in logarithmic scale yields a nearly straight line up to 3 h and the slope of the straight lines in the isothermal recovery process corresponds to the rate coefficients k of the first-order reaction.

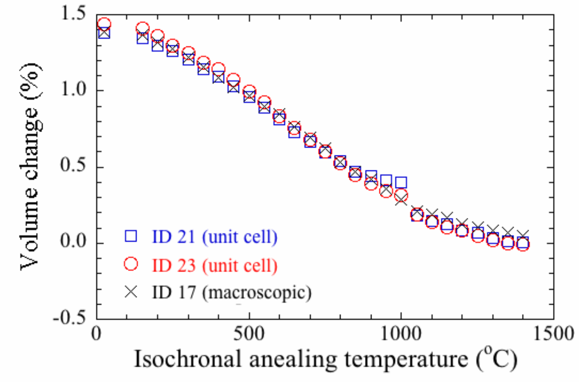

Fig. 3 Comparison of unit cell volume change of specimens 21 and 23 and macroscopic volume change of specimen 17 by isochronal vacuum anneals for 6 h.

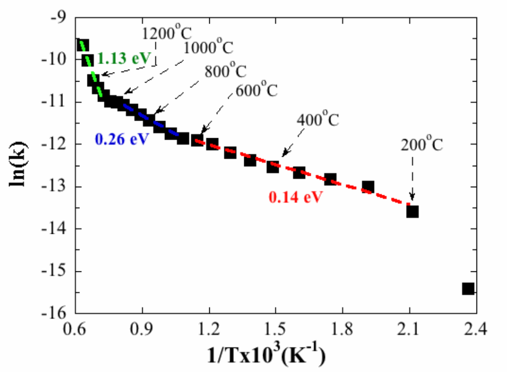

Fig. 4 Arrehenius plot of reaction rate constants derived from precise dilatometer macroscopic length change measurements for bar specimen 28 (see Table 1) during 3 h isothermal anneals in helium.

Fig. 4 shows an Arrhenius plot of the rate coefficients for macroscopic length recovery resulting from annealing of the SiC specimen (specimen ID=28). The value of *k* of each annealing temperature was obtained by applying a least-squares method to length change data. Each R^2 for fitting was generally more than 0.95. The rate coefficients increased gradually from 200°C (near the irradiation temperature) to 600°C, and could be fit to a straight line. Rate coefficients from 650 to 950°C could be fit to another slightly steeper straight line, and at temperatures higher than 1050°C a steeper slope was observed. From these Arrhenius plots, activation energies of the macroscopic length recovery were obtained by applying a least-squares method. The activation energies obtained were 0.14 eV for 200~600°C, 0.26 eV for 650~950°C, and 1.13 eV for 1100 ~1300°C. Slight changes in the rate constant around 600~ 650°C and 950~1050°C were observed. We concluded that the length recovery stage occurs in at least three stages between 200 and 1300°C. However, at higher temperatures (>1100°C) more complex recombination reactions may occur so that there is a possibility that second-order reactions should be expected for higher dose cases.

In a previous report on the same SiC specimens irradiated under the same conditions [2], the activation energies for length recovery for 6 h were reported to be 0.11~0.12eV for 200~800°C and 0.78~0.79eV for 800~ 950°C. The former value is similar to that of lowest temperature range value obtained here. The activation energy is possibly affected by the selected temperature range or data time range for each annealing step.

4. Conclusions

Results for the precise measurements of lattice parameter and macroscopic length change due to isothermal and isochronal annealing for α-SiC (6H polytype) ceramic, neutron-irradiated up to 1.9x10^{23} n/m^2 (E>0.1MeV) at ~150°C, were obtained. The results are summarized below:

(1) The residual c-axis lattice parameter change exceeded that of the a-axis parameter change up to 1000°C, but the difference in both axes diminished after annealing at temperatures higher than 1050°C.

(2) The c/a ratio was mostly constant with a value ~1.1 until ~600°C and then it peaked up to about 1.6 at 900°C, finally the anisotropy mostly diminished at temperatures higher than ~1050°C.

(3) The activation energies for macroscopic length recovery were 0.14 eV for 200~600°C, 0.26 eV for 650~ 950°C, and 1.13 eV for 1100~1300°C.

(4) During annealing up to ~1000°C, the ratio of point defects that induce anisotropic lattice expansion changes gradually. Beyond 1000°C, only the point defects that induce isotropic lattice expansion remains and these point defects finally are annihilated at approximately 1300°C.

References

[1] T. Yano, Y. Futamura, S. Yamazaki, T. Sawabe and K. Yoshida, "Recovery behavior of point defects after low-dose neutron irradiation at ~423K of sintered 6H-SiC by lattice parameter and macroscopic length measurements", *J. Nucl. Mater.*, **442** (2013) S399-S403.

[2] S. Yamazaki, K. Yoshida and T. Yano, "Comparative Experimental Study on Recovery Behavior of Point Defects in Neutron-Irradiated SiC", *J. Nucl. Mater.*, **417** (2011) 425-429.

[3] S. Yamazaki, M. Imai and T. Yano, "Recovery of Neutron-Induced Damage of SiC by Thermal Annealing up to 1400°C", *Progress in Nuclear Energy*, **50** (2008) 601-605.

B.3 Extraction Chromatographic Separation of MA (Am(III)) and Ln (Eu(III)) By TPEN-Immobilized Gel

Kenji TAKESHITA , Hiroshi OAKI and Yusuke INABA

The radioactivity of HLLW (High-level Liquid Wastes) is caused by some fission products and these daughter nuclides for the first 300 years and after that by MAs (Minor Actinides). If the partitioning of MAs from HLLW and the transmutation of MAs by fast reactors are realized, the long-term radiotoxicity of HLLW can be reduced, significantly.

In this study, a TPEN derivative with 4 vinyl groups,*N*,*N*,*N*',*N*'-tetrakis-(4-propenyloxy-2-pyridylmethyl) ethylenediamine (TPPEN) was synthesized for the separation of trivalent MA (Am(III)) and Ln (Eu(III)). A copolymer gel with TPPEN and *N*-isopropylacrylamide (NIPA) showed a high separation factor of Am(III) over Eu(III) (SFAm/Eu), which was evaluated to be 26 at pH 5. And, thin film of NIPA-TPPEN gel (average thickness: 2-40 nm) was immobilized on the pore surface of the porous silica particles (particle diameter: 50μm, average pore diameter : 50 and 300 nm) and a chromatographic column (diameter: 6mm, bed height: 11mm) packed with the gel-coated particles was prepared. A small amount of weakly acidic solution (pH4) containing Am(III) and Eu(III) was supplied to the column and the elution tests of Am(III) and Eu(III) were carried out. Eu(III) and Am(III) were recovered separately by a weakly acidic eluent (pH4) at 313K and a highly acidic eluent (pH2) at 298K, respectively (Fig.1)[1-7].

These results suggest that the contentious separation of MAs and Lns is attainable by a new extraction chromatographic process consisted of the two columns adjusted to 298K and 313K (Fig.2).

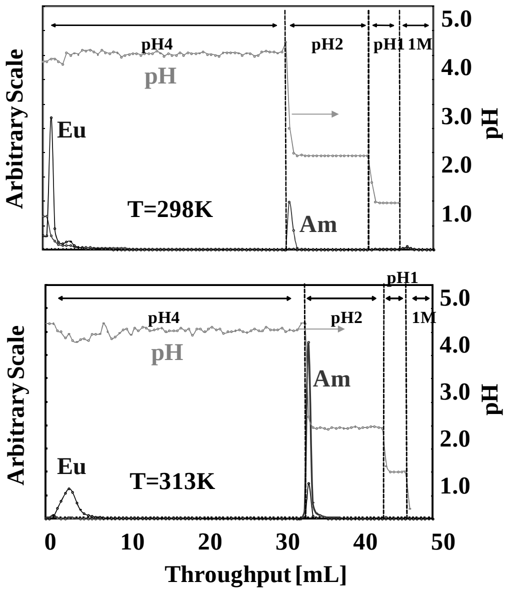

Fig.1 Elution cureves of Am(III) and Eu(III) at 298K and 313K

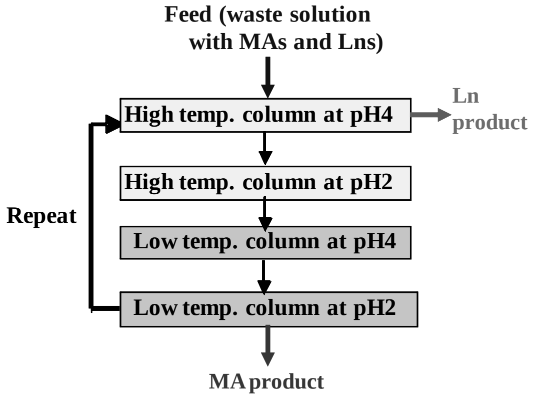

Fig.2 Operations of proposed two-column process.

References

[1] M. Ozawa, S. Suzuki and K. Takeshita, “Advanced Hydrometallurgical Separation of Actinides and Rare Metals in Nuclear Fuel Cycle”, *Solvent Extr. Res. Dev., Jpn.*, **17**, 19-34 (2010).

[2] T. Matsumura, K. Takeshita, “Extraction separation of trivalent minor actinides from lanthanides with hydrophobic derivatives of TPEN,” *Progress in Nuclear Energy*, **50**(2-6), 470-475 (2008).

[3] K. Takeshita, T. Matsumura, Y. Nakano, “Separation of americium (III) and europium (III) by thermal-swing extraction using thermosensitive polymer gel,” *Prog. Nucl. Energy*, **50**(2-6), 466-469 (2008).

[4] K. Takeshita, T. Matsumura, Y. Nakano, “Thermal-swing extraction separation of Am (III) and Eu (III) with poly-NIPA gel cross linked with TPEN derivative,” *J. Nucl. Sci. Technol.*, **44**(12), 1481-1483 (2007).

[5] T. Matsumura, Y. Inaba, A. Mori, K. Takeshita, “Am/Eu Separation with a New Ligand, *N,N,N’,N’*-tetrakis((4-butoxypyridin-2-yl)methyl)ethylenediamine (TBPEN), a Hydrophobic Derivative of TPEN”, *J. Nucl. Sci. Technol.*, **47**(2), 123-126 (2010).

[6] S. Koyama, M. Suto, H. Ohbayashi, K. Takeshita, T. Ogata, H. Oaki, Y. Inaba, “Recovery of Minor Actinides from Spent Fuel via an Extraction Chromatographic Technique Using TPPEN- Immobilized Gels”, *Sep. Sci. Technol.*, **47**(14-15)**,** 2024-2028 (2012).

[7] S. Fukuoka, T. Kida, Y. Nakajima, T. Tsumagari, W. Watanabe,Y. Inaba, A. Mori, T. Matsumura, Y. Nakano, K. Takeshita, “Thermo-responsive Extraction of Cadmium(II) Ion with TPEN-NIPA Gel. Effect of the Number of Polymerizable Double Bond toward Gel Formation and the Extracting Behavior”, *Tetrahedron*, **66**(9), 1721-1727 (2010).

B.4 Restoration of Environment Contaminated by Radioactive Cesium Released From Fukushima Dai-ichi NPP

Kenji TAKESHITA, Hideharu TAKAHASHI and Yusuke INABA

In the Fukushima Dai-ichi NPP Accident, large amounts of volatile radioactive nuclides, such as ^{131}I, ^{134}Cs and ^{137}Cs, were released to the atmosphere and huge areas surrounding the nuclear site were contaminated by the radioactive fallout.

In this study, a combined process with a hydrothermal-blasting process and a coagulation settling process was proposed for the separation of radioactive Cs from contaminated substances [1-2]. This process has excellent features such as a small quantity of secondary wastes and highly effective Cs recovery. Fig.1 shows the process configuration. In the hydrothermal decomposition process, water is added to Cs-contaminants (solid) and the obtained water-solid mixture is stirred under the subcritical water conditions (temperature range: 200 to 260ºC and pressure range: 2 to 4 MPa). The ionic product of water increases with increasing temperature and pressure. At 260ºC it reaches about 1000 times that of water at 25ºC. The decomposition of contaminated substances is promoted by the increase in the ionic product of water. After the hydrothermal operation, the high pressure is decreased sharply by opening a valve. This pressure release operation is called “blasting”, in which inorganic crystal substances can be destroyed partially. The treated water with hydrophilic decomposition products is transferred to the coagulation settling process. The remained solid is washed by water and the washing water is also transferred to the same process. Small amounts of coagulant and adsorbent powders are added to the collected water. Cs in the water is recovered as a precipitate.

The removal of Cs from real sewage sludge (100,000 Bq/kg) sampled in Fukushima-city was tested to demonstrate the validity of the combined process of hydrothermal decomposition and coagulation settling (Fig.2). 30g of the sewage sludge (about 3000 Bq) and 90g of water were added into a 500mL test tube in a hydrothermal decomposition device. The only hydrothermal operation was carried out under the conditions of 260ºC and 4.4 MPa for 30 min. The solid remained in the test tube was washed by 437g of water, which corresponds to about 14 times the weight of sewage sludge. Cs in the mixture of the treated water and the washed one was precipitated by the coagulation settling process using ferric ferrocyanide powder (1wt%) as an adsorbent and ion-reaction N (0.1 wt%, NPO Saiseisya, Saitama, Japan) as a coagulant. About 96% of Cs in the sewage sludge was removed successfully by combining simple hydrothermal decomposition and coagulation settling. As a result, we confirmed that the combined process with hydrothermal blasting and coagulation settling is applicable to the removal of Cs from highly contaminated substances.

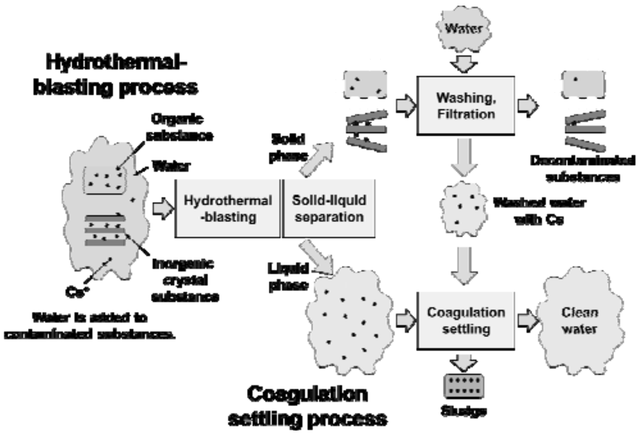

Fig.1 Cs recovery by combined process with hydrothermal -blasting and coagulation settling

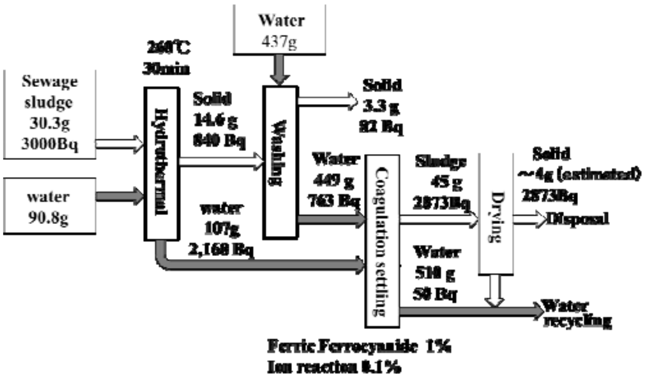

Fig.2 Decontamination of sewage sludge by the hydrothermal decomposition and coagulation-settling combined process

References

[1] K.Takeshita and T.Ogata, “Application of Ion exchange Technique to Decontamination of Polluted Water generated by Fukushima Nuclear Disaster”, *J. Ion Exchange*, **23**(1), 1-5 (2012).

[2] K.Takeshita, “Restoration Technology of Environment Contaminated with Radioactive Fallout by Fukushima Daiichi Nuclear Power Plant Accident”, *Hyomen Kagaku*, **34**(3), 108-118 (2013).

B.5 Structural Studies on Uranyl Species in Acetonitrile and 1-Ethyl-3-methylimidazolium Nitrate Dissolved $[EMI]_2[UO_2(NO_3)_4]$

Kotoe SASAKI, Tomoya SUZUKI, Yasuhisa IKEDA

Uranyl trinitrato complex in non-aqueous solvents and in solid state has been known to exist as $[UO_2(NO_3)_3]^-$ with D_{3h} symmetry [1-3]. Uranyl nitrato complexes in ionic liquids (ILs) have also been examined using spectroscopic methods such as UV-visible, EXAFS, and so on [4-7]. Such studies have clarified that the uranyl nitrato complexes in ILs exist as $[UO_2(NO_3)_3]^-$ with D_{3h} symmetry. However, recently it was reported that $[DMI]_2[UO_2(NO_3)_4]$ (DMI =1,3-dimethylimidazolium) is obtained as a single crystal and that uranyl species exist as $[UO_2(NO_3)_4]^{2-}$ in $[BMI][NO_3]$ (BMI = 1-butyl-3-methylimidazolium). In this complex, the equatorial plane of uranyl moiety is coordinated by two bidentate and two unidentate nitrates [8].

In the present study, to get more detail information on the structure of uranyl nitrato complexes, the structures of uranyl species in CH_3CN and $[EMI][NO_3]$ dissolved $[EMI]_2[UO_2(NO_3)_4]$(EMI = 1-ethyl-3-methylimidazolium) have been examined.

The $[EMI]_2[UO_2(NO_3)_4]$ complex was synthesized by adding four equivalent of $AgNO_3$ to $[EMI]_2[UO_2Cl_4]$ in CH_3CN, followed by filtration for removing AgCl and evaporation of CH_3CN. Sample solutions were prepared by dissolving $[EMI]_2[UO_2(NO_3)_4]$ complex into CH_3CN or $[EMI][NO_3]$. The UV-visible absorption spectra of solutions were measured by Shimadzu UV-3150 spectrophotometer.

UV-visible absorption spectrum of sample solution prepared by dissolving $[EMI]_2[UO_2(NO_3)_4]$ complex (0.024 M, M = mol dm^{-3}) into CH_3CN was measured. As a result, the absorption spectrum was found to be consistent with that of the $UO_2(NO_3)_3]^-$ species with D_{3h} symmetry. We also measured the absorption spectral changes with the addition of $[EMI][NO_3]$ (0.074, 0.12, 0.52, 1.5 M) to the above CH_3CN solution dissolved $[EMI]_2[UO_2(NO_3)_4]$ (0.024 M). The results are shown in Figure 1. The absorbance in the range of 420 to 440 nm is found to increase with appearance of isosbestic points at 465 and 469 nm. This phenomenon is similar to that reported by Ryan [2], i.e., the absorption spectra of CH_3NO_2 solutions dissolved $(C_2H_5)_4UO_2(NO_3)_3$ and $(C_2H_5)_4NNO_3$ showed the isosbestic points at 465.5 and 470.0 nm. These results indicate that the following equilibrium exists in the present system.

$$[UO_2(NO_3)_3]^- + NO_3^- = [UO_2(NO_3)_4]^{2-},$$

Based on the absorption spectral changes, the equilibrium constant (K) was evaluated as 3.85 M^{-1}, which is in agreement with that reported by Ryan, 4.74 M^{-1} [2].

Furthermore, we measured UV-visible absorption spectrum of $[EMI][NO_3]$ solution dissolved $[EMI]_2[UO_2(NO_3)_4]$ at 50 ºC (see Figure 1, neat). The spectrum was found to be consistent with that of $[EMI][NO_3]$ dissolved $UO_2(NO_3)_2{\cdot}6H_2O$.

From these results, it is proposed that in the $[EMI][NO_3]$, the $[UO_2(NO_3)_4]^{2-}$ species is formed.

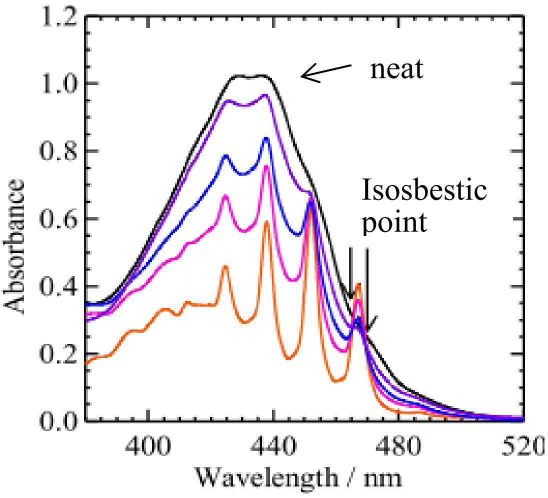

Fig. 1. UV-vis absorption spectral changes with the addition of $[EMI][NO_3]$ (0.0, 0.074, 0.12, 0.52, 0.15 M) to CH_3CN dissolved $[EMI]_2[UO_2(NO_3)_4]$ (24 mM). Temp. 323 K.

Reference

1. T L.K. Kaplan, R.A. Hildebrandt, and M. Ader, *J. Inorg. Nucl., Chem.*, **2**, 153 (1956).
2. J.L. Ryan, *J. Phys. Chem.*, **65**, 1099 (1961).
3. R.D. Denning, D.N.P. Foster, T.R. Snellgrove, and D.R. Woodwark, *Mol. Phys.*, **37**, 1089 (1979).
4. K. Servaes, C. Hennig, I. Billard, C. Gaillard, K. Binnemans, C.G-.Walrand, and R.V. Deun, *Eur. J. Inorg. Chem.*, 5120 (2007).
5. P. Nockemann, K. Servaes, R.V. Deun, K.V. Hecje, L.V. Meervelt, K. Binnemans, and C.G-Walrand, *Inorg. Chem.*, **46**, 11335 (2007).
6. D.L. Quach, C.M. Wai, and S.P. Pasilis, *Inorg. Chem.*, **49**, 8568 (2010).
7. S. Georg, I. Billard, A. Ouadi, C. Gillard, L. Petitjean, M. Picquet, and V. Solo'ev, *J. Phys. Chem. B*, **114**, 4276 (2010).
8. C. Gaillard, O. Klimchuk, A. Ouadi, I. Bikkard, and C. Hennig., *Dalton Trans.*, **41**, 5476 (2012).

B.6 *Après ORIENT*, A P&T-based New Resource Strategy in Nuclear Fuel Cycle

Masaki OZAWA, Chi Young Han, Toshitaka KANESHIKI, and Mikael NILSSON*
*University of California, Irvine

The **Après ORIENT** research program, recently initiated in 2011, will deal with transmutation of radioactive FPs to create rare metals / rare earth (RE) elements (defined as secondary Nuclear Rare Metal, ^{2nd}NRM) by (n,γ) reaction succeeded by β^- decays:

$$^{A}_{Z}FP(n,\gamma)^{A+1}_{Z}FP \xrightarrow{\beta^-} {}^{A+1}_{Z+1}NRM$$

Target $^{A}_{Z}FP$ are radioactive FPs and any created $^{A+1}_{Z+1}NRM$ should be more valuable and non-, or significantly less, radioactive than the $^{A}_{Z}FP$. In the case of transmutation of radioactive Ba (i.e., non RE element) to La (i.e., light RE), the yield of ^{139}La was low < 3.5 % with 5 years irradiation at thermal neutron energy conditions. However, by neutron irradiation in the fast reactor blanket region corresponding to a resonance energy range of 10 ~ 100 keV with an expected cross section, $\sigma_\gamma = 0.27\ b$, of ^{139}Ba a higher transmutation rate of more than 12 % / 5 y was obtained when the neutron flux is 1.0×10^{15} n / cm^2-sec. Created La will be perfectively non-radioactive (< 0.001 Bq / g) despite that natural La is slightly radioactive ca. 1 Bq/g. To facilitate Ba / La separation various kinds of crown ether (CE) resins were tested. The highest separation of Ba^{2+} / La^{3+} was obtained by a newly synthesized Benzo-18-Crown-6 (BC18) -substituted resin indicating $SF_{Ba/La}$ > 1,000 at 5 mol/l HCl medium. To confirm scientific feasibility on such new P&T, actual irradiation tests by various target materials in a test reactor and separation & analysis of the products are required. While the test reactor available at UC Irvine has a steady state flux on the order of 1.0×10^{12} n / cm^2-sec which is at least 2 orders of magnitude lower than a conventional power reactor, proof-of-concept investigations will be carried out since the production of nuclides should scale up linearly with the neutron flux.

1. Introduction

After the catastrophe of Fukushima Daiichi NPP on March 11, 2011, the sentiment of the Japanese people on nuclear energy has been drastically shifted to a negative mindset. However, the role of the nuclear fuel cycle to maintain a sustainable, carbon-emission free energy resource (*i.e.*, ^{238}U–^{239}Pu) and energy security is still, or is becoming, even more important. In this context, radioactive waste management will require further technological innovation. In the ***Adv.-ORIENT*** (Advanced Optimization by Recycling Instructive Elements) ***Cycle*** concept[1] initiated in 2006, spent nuclear fuel and high level liquid waste (HLLW) are recognized as an artificial vein of ore. Separation and utilization research have been carried out for so-called nuclear rare metals such as light platinum group metals (PGM), Tc as well as all of the actinides (An) and lanthanides (Ln) (defined as the first Nuclear Rare Metal, ^{1st}NRM). Through this program the eventual reduction of radioactive toxicity and amount of HLLW will be foreseen. The ***Après ORIENT*** research program was recently initiated in 2011. This program will deal with transmutation of radioactive FPs to create rare metals / rare earth (RE) elements (defined as the secondary Nuclear Rare Metal, ^{2nd}NRM) by (n,γ) reaction succeeded by β decays. The overall process can be written as the following reaction:

$$^{A}_{Z}FP(n,\gamma)^{A+1}_{Z}FP \xrightarrow{\beta^-} {}^{A+1}_{Z+1}NRM \qquad (1)$$

The creation of such nuclear rare metals by neutron irradiation depends on the capture cross-section of the target FP, neutron flux, and decay constant of the parent nuclide. The produced rare metal may be transmuted into a corresponding radioactive isotope by neutron capture during the neutron irradiation. This would cause the formed isotope to decay to a different nuclide. Therefore, the net creation of a nuclear rare metal results from the competition of production and destruction caused by neutron capture.

The annual transmutation rate (R_{tr}) by neutron capture can be expressed as:

$$R_{tr} = 1 - e^{-\sigma_\gamma \phi t} \qquad (2)$$

where σ_γ is the capture cross-section, □ is the neutron flux, and t = 1 year. It can be written in the transmutation half-life (T_{tr}) defined as:

$$T_{tr} = \frac{\ln 2}{\sigma_\gamma \phi} \qquad (3)$$

In considering the neutron flux (~10^{14} to ~10^{15} n / cm^2-sec) of typical thermal or fast reactors, the capture cross-section larger than about 1 barn is required for the transmutation rate of 10 % / y, which corresponds to the transmutation half-life of about 6.6 years.

2. Transmutation of Fission Products For Creation of Rare Metals (^{2nd}NRM)

2.1. Creation of Rare Earth Metals (REE)

The transmutation feasibility is discussed to produce rare earth metals such as La, Nd, and Dy from FPs (Ba, Pr, and Tb) in the spent fuel by neutron irradiation of nuclear reactors.

La can be created from Ba, of which most in the spent fuel is non-radioactive since all radioactive Ba isotopes are short-lived except for ^{133}Ba. La isotopes are all radioactive except for ^{139}La which can be created by β^- decay of ^{139}Ba, of which the isotope fraction in a PWR spent fuel reaches about 80 %. Thus, the La creation from Ba in the spent fuel has a high feasibility in the view point of the large isotope fraction of ^{138}Ba and the simple path of ^{139}La creation from ^{138}Ba. ^{139}La has a larger capture cross-section by one order of magnitude, which leads to ^{140}La ($T_{1/2}$ = 1.7 d) production. Therefore, La creation from Ba is not feasible under the neutron irradiation of typical nuclear reactors[2]. However, ^{138}Ba has a larger resonance for the higher neutron energy compared to ^{139}La. Considering the neutron spectrum of fast reactors, a proper moderation of neutrons in blanket of a fast reactor may provide a higher creation rate of La. By the neutron irradiation at the fast reactor blanket region corresponding to a resonance energy range of 10 ~ 100 keV with the expected $\sigma_\gamma = 0.27\,\mathrm{b}$ of ^{139}Ba, a higher transmutation rate of more than 12 % / 5 y was obtained when the neutron flux is 1.0×10^{15} n / cm^2-sec[3].

Nd can be created from Pr, of which most in the spent fuel is ^{141}Pr (stable) since all radioactive Pr isotopes are short-lived. ^{142}Nd, ^{143}Nd, ^{145}Nd, and ^{146}Nd are non-radioactive and only ^{144}Nd is very long-lived. The capture cross-section of ^{142}Nd is comparable with that of ^{141}Pr in thermal energy region and is lower in resonance region. Therefore, the long-lived ^{144}Nd, which is produced by two consecutive neutron captures from ^{142}Nd, is hard to be created from ^{141}Pr. Thus, non-radioactive Nd can be created from Pr in the spent fuel by the simple transmutation path of ^{142}Nd creation from ^{141}Pr. The creation rate of Nd from Pr is expected to be 1.2 % / y in a typical PWR, and 1.2 % / y and 0.6 % / y in core and blanket, respectively, in the MONJU fast reactor[2,4]. Such low creation rates are due to small capture cross-sections of ^{141}Pr (< 1.0 barn in PWR). The creation rate can be improved by a softer neutron spectrum than the thermal spectrum of typical PWRs. An investigation with changing pitch-to-diameter (P / D) ratio of a typical PWR fuel pin for softer neutron spectrum shows that the creation rate can be increased to more than 3 % / y with a larger P / D ratio[2]. The resonance integral of ^{141}Pr is evaluated as 18.3 barns by JENDL-4.0 library. Similarly to the discussion about the La creation, as an alternative, a proper moderation of neutrons in blanket of a fast reactor, concentrating on the energy range of 0.1 ~ 10 keV, may give a higher creation rate of Nd.

Dy can be created from Tb, of which most in the spent fuel is ^{159}Tb (stable). Therefore, ^{160}Dy is first produced by neutron capture of ^{159}Tb followed by β^- decay of ^{160}Tb, which can alternatively be transmuted into ^{161}Tb ($T_{1/2}$ = 6.9 d), ^{162}Tb ($T_{1/2}$ = 7.6 m), ^{163}Tb ($T_{1/2}$ = 19.5 m), and ^{164}Tb ($T_{1/2}$ = 3.0 m) by successive neutron capture. All daughter nuclides produced by the decay of the respective terbium isotopes are stable: ^{161}Dy, ^{162}Dy, ^{163}Dy, and ^{164}Dy. Thus, non-radioactive Dy can be created from Tb in the spent fuel by the two main transmutation path of ^{160}Dy and ^{161}Dy creation from ^{159}Tb. The creation rate of Dy from Tb is expected to be 11.3 % / y in a typical PWR, and 18.9 % / y and 8.1 % / y in core and blanket, respectively, in the MONJU fast reactor[2,4]. Such high creation rates is led to by relatively large capture cross-sections of ^{159}Tb (13.2 barns in PWR) and ^{160}Tb (115.4 barns in PWR).

2.2. Creation of Platinum Group Metals (PGM)

PGMs such as Ru, Rh, and Pd are currently considered as target elements created from FPs in the spent fuel by neutron irradiation of nuclear reactors.

Ru can be created from Tc, of which most in the spent fuel is ^{99}Tc, which is known as a representative long-lived fission product being able to be transmuted in fission reactors because it has a relatively large capture cross-section compared to other long-lived fission products. ^{100}Ru is created by neutron capture of ^{99}Tc followed by β^- decay of ^{100}Tc ($T_{1/2}$ = 15.8 s). The created ^{100}Ru may be transmuted into a higher-mass isotope by successive neutron captures. All expected isotopes are stable or short-lived. Therefore, non-radioactive Ru can be created from the long-lived fission product, Tc, in the spent fuel by neutron irradiation. The creation rate of Ru from Tc is expected to be ~2 % / y in PWRs, and ~5 % / y in blanket of fast reactors[5,6]. Mo in the spent fuel is another candidate element for Ru creation. It is non-radioactive since all radioactive Mo isotopes are short-lived except for ^{93}Mo, which is not found in the spent fuel. First, Tc is produced by neutron capture of Mo succeeded by β^- decay and, in the case of ^{101}Tc, a second decay to Ru with a short-half life. The isotope fraction of ^{98}Mo and ^{100}Mo in a PWR spent fuel is each about 25~30 %. Ru created from Mo in the spent fuel is also non-radioactive. The creation rate is expected to be low due to low capture cross-sections of ^{98}Mo and ^{100}Mo.

Rh can be created from Ru, of which most in the spent fuel is non-radioactive or short-lived except for ^{106}Ru, of which the isotope fraction is about 0.2 % in PWR spent fuel. Since only ^{103}Rh is stable, the available transmutation path is ^{103}Rh creation from ^{102}Ru. However, the produced ^{103}Rh may be transmuted again into its short-lived isotopes ^{104}Rh by neutron capture during the neutron irradiation because ^{103}Rh has a much larger capture cross-section than ^{102}Ru. A low creation rate of Rh can therefore be expected, especially in thermal reactors.

Pd can be created from Rh, of which most in the spent fuel is ^{103}Rh (stable) since all radioactive Rh isotopes are short-lived except for ^{101}Rh and ^{102}Rh. ^{104}Pd is created by neutron capture of ^{103}Rh followed by β^- decay of ^{104}Rh. The created ^{104}Pd may be transmuted into a higher-mass isotope by successive neutron capture. All expected isotopes are stable or short-lived except for ^{107}Pd, which is produced by three consecutive neutron captures from ^{104}Pd. The capture cross-section of ^{104}Pd is even lower than that of ^{103}Rh. Therefore, almost non-radioactive Pd can be created from Rh in the spent fuel. In addition, since the capture cross-section of ^{103}Rh is large, especially at the thermal energy as mentioned before, a high creation rate of Pd from Rh can be expected in thermal reactors. However, a low creation rate of about 1 % / y[5] is expected in the blanket of a fast reactor due to low capture cross-sections in the fast energy region. Ru in the spent fuel is another candidate element for Pd creation. However, the creation rate is expected to be low due to low capture cross-sections of ^{102}Ru and ^{104}Ru.

3. Chromatographic Separation of Ba^{2+} (FP) and La^{3+} (NRM)

The distribution coefficient (Kd) of Ba^{2+} (FP) and La^{3+} (NRM) were measured using three kinds of macrocyclic resins, as shown in Fig. 1, from HCl and HNO_3 media at room temperature.

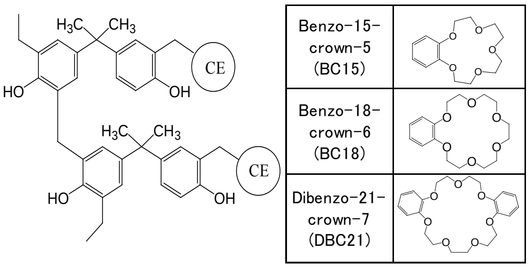

Fig. 1. Structure of the newly synthesized macrocyclic resin with functional crown ether groups.

The results for HCl medium, Fig. 2, show that La^{3+} was less absorbed to all CE-resins (*e.g.,* Kd < 0.1 at 5 mol HCl), while Ba^{2+} was well absorbed in the higher HCl concentration for all CE-resins (*e.g.,* Kd > 10 at 5 mol HCl).

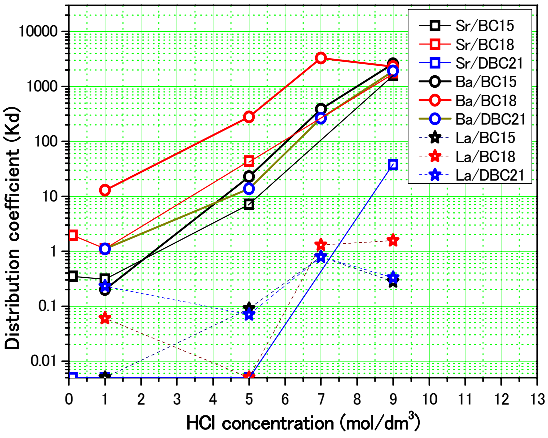

Fig. 2. Distribution coefficient (Kd) of La, Ba and Sr for three CE-resins in HCl medium.

Among these, the highest separation of Ba^{2+} / La^{3+} was obtained by BC18-resin indicating $SF_{Ba/La}$ > 1,000 at 5 mol / l HCl medium, where only Ba^{2+} would be absorbed. However as shown in Fig. 2, Sr^{2+} will behave in the same absorption manner as Ba^{2+} by BC18- and BC15-resins, and may thus disturb both Ba^{2+} separation from the high level liquid waste (HLLW) and the Ba target fabrication processes. However, the differences of their Kds at lower than 2 mol / l HCl will allow for preferential elution of Sr^{2+} to Ba^{2+}. As shown in Figs. 3 and 4, separation of Ba^{2+} / Sr^{2+} and Ba^{2+} / La^{3+} was possible using a chromatographic column with BC18-resin, by changing elute HCl concentration.

In light of these results, BC18 resin was confirmed to be a vital decontamination tool for recovery of radioactive Sr^{2+} at > 5 mol / l HCl medium.

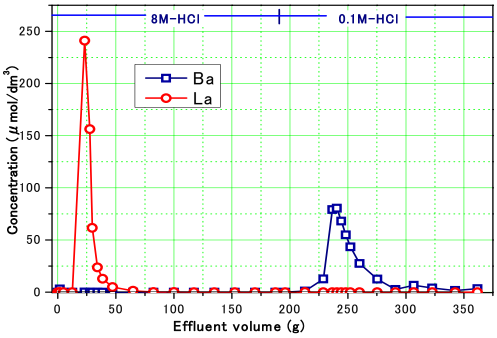

Fig. 3. Chromatogram of Ba^{2+} / La^{3+} separation by BC18 resin.

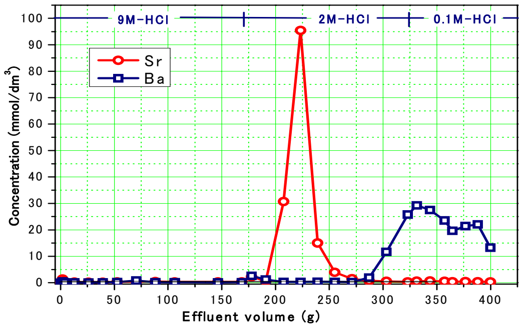

Fig. 4. Chromatogram of Sr^{2+} / Ba^{2+} separation by BC18 resin.

4. Partitioning and Transmutation experiments at the TRIGA reactor at UC Irvine

To confirm scientific feasibility on such new P&T, actual irradiation tests by various target materials in a test reactor followed by separation and analysis of the products are required. While the test reactor available at UC Irvine has a steady state flux of thermal neutrons on the order of 1.0×10^{12} n / cm^2-sec which is at least 2 orders of magnitude lower than a conventional power reactor, proof-of-concept investigations will be carried out since the production of nuclides should scale up linearly with the neutron flux.

Below is shown a calculation of successive neutron capture in 1g of natural barium during an irradiation in the UC Irvine TRIGA® reactor, Fig. 5. This simplified calculation only takes into account the thermal neutron cross sections. This calculation assumes that as the ^{139}Ba is produced in the reactor it is continuously removed from the reactor core. For a stationary target the results in the figure would differ only very slightly due to the relatively low flux of the UC Irvine reactor and short irradiation times. However, for longer irradiation times and higher flux the barium target would eventually contain higher barium isotopes ^{140}Ba, ^{141}Ba as well as ^{140}La, ^{141}La, and ^{140}Ce etc. The continuous removal of the neutron capture product will be made available in the UC Irvine TRIGA® reactor through a sample loop recently installed in the reactor, see Fig. 6. Studies underway at UC Irvine have shown the possibility to prepare a porous target material that may be irradiated by thermal neutrons whereby the activated atoms are recoiled out into a capture solvent using the principle of the Szilard-Chalmers method. A suitable barium target will be prepared and irradiated inside the PEEK cup shown in Fig. 6 placed at the bottom of the test loop. A liquid, capture matrix, will be pumped from outside the reactor core into the PEEK cup where the ^{139}Ba produced by neutron capture and recoiled out of the target will be captured and transported out of the core. Thus we will avoid any successive neutron capture of ^{139}Ba to reach the heavier barium isotopes. Once the fluid is recovered outside the reactor core the solution may be left to let the ^{139}Ba decay to ^{139}La and finally a suitable CE resin may be used to separate the produced ^{139}La from any remaining Ba that may have been dissolved into the capture matrix. The capture matrix, stripped of La, may be re-circulated into the reactor core for additional production of ^{139}La.

This preliminary test will allow us to show proof-of-principle for the continuous transmutation of elements representative of spent nuclear fuel.

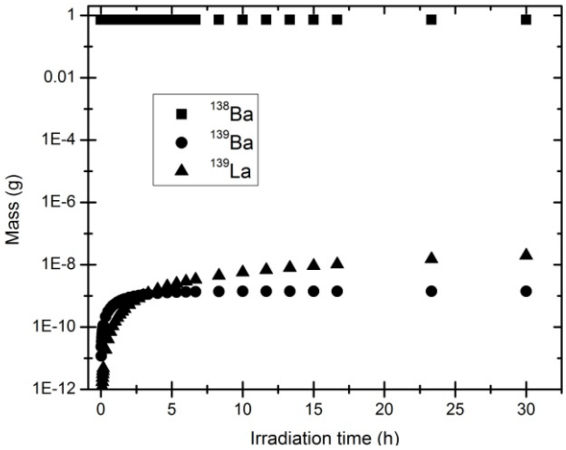

Fig. 5. Theoretical calculation of the formation of ^{139}Ba and ^{139}La from irradiation of 1 g of natural barium in the UC Irvine TRIGA® reactor at 250 kW steady state thermal power.

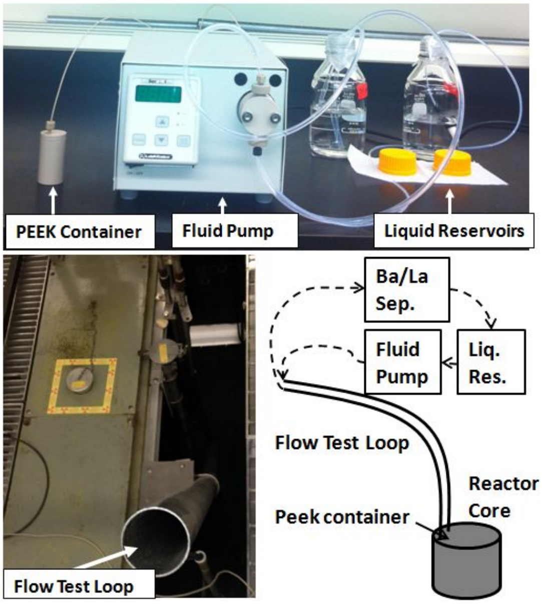

Fig. 6. Schematic of experimental setup for continuous irradiation and separation of material in the UC Irvine TRIGA® reactor.

5. Conclusions

The paper describes the new concept of ***Après ORIENT***, to create rare metals, rare earth from the nuclear radioactive wastes, by the approaches with neutron capture transmutation,

$$ {}^{A}_{Z}\mathrm{FP}(n,\gamma)^{A+1}_{Z}\mathrm{FP} \xrightarrow{\beta^-} {}^{A+1}_{Z+1}\mathrm{NRM}, $$

in the reactors, and chemical separation of ${}^{A}_{Z}\mathrm{FP}/{}^{A+1}_{Z+1}\mathrm{NRM}$ at the reprocessing plant.

Their high feasibilities are expected when using high neutron flux FBR and chromatographic separation by macrocyclic, crown ether resins. In parallel with the calculation science, actual irradiation and separation experiments are planned in the collaboration of Japan / US Universities. This new P&T approach will contribute not only to national resource strategy on rare metal / rare earth, but also bring the synergistic effect to nuclear fuel cycle by decreasing the radioactive fission products and wastes.

Acknowledgement

The authors wish to acknowledge Drs. M. Nomura and S. Koyama, through the technological discussions and the past financial support from Japan Atomic Energy Agency (JAEA).

Reference

1. M. OZAWA, T. SUZUKI, S. KOYAMA, H. AKATSUKA, H. MIMURA and Y. FUJI, “A New Back-end Cycle Strategy for Enhancing Separation, Transmutation and Utilization of Materials (*Adv.-ORIENT Cycle*),” *Progress in Nuclear Energy*, **50**, 476-482 (2008).
2. Y. SAKATA, C. Y. HAN, M. OZAWA and M. SAITO, “Nd and Dy Creation by Transmutation in Nuclear Reactors,” *The 29th Symposium of the Rare Earth Society of Japan*, Hokkaido, Japan, 2012. (in Japanese).
3. M. OZAWA, C. Y. HAN, T. KANESHIKI and M. NOMURA, “Element Strategy on Nuclear Fuel Cycle (II) Separation and Transmutation of Radioactive Barium to Rare Earth Elements,” *2013 Annual Meeting of the Atomic Energy Society of Japan*, ISBN978-4-89047-155-3, 2013 (in Japanese).
4. Y. SAKATA, “A Study on Transmutation of Radioactive Rare Earth Metals in Nuclear Reactor,” Dissertation for the Undergraduate Degree, Tokyo Institute of Technology, 2012. (in Japanese).
5. T. YOSHIOKA, “A Study on Creation of Platinum Group Metals in Nuclear Reactor,” Dissertation for the Master Degree, Tokyo Institute of Technology, 2012. (in Japanese).

B.7 Overview of Recent Studies Related to Lead-Alloy-Cooled Fast Reactor

Minoru TAKAHASHI, Rongyuan SA, Asril PRAMUTADI, and Eriko YAMAKI-IRISAWA

1. Introduction

Lead alloys are attractive candidate coolants and target materials for lead alloy-cooled fast reactors (LFR) and the accelerator-driven system (ADS), respectively, where the lead alloy includes both of pure lead and lead-bismuth eutectic (LBE or 45%Pb-55%Bi). Feasibility studies of LFRs have been performed so far for the LBE-Cooled Long-Life Safe Simple Small Portable Proliferation -Resistant Reactor (LSPR) (53 MWe/150MWt), the Pb-Bi-cooled Direct Contact Boiling Water Small Fast Reactor (PBWFR) (150MWe/450MWt), etc. Various studies have been performed for the development of LFRs. The present paper overviews our recent studies for the following items:

(1) Compatibility of structural and cladding materials with lead alloys
  i. Corrosion under steady condition
  ii. Corrosion under transient condition
  iii. Employment of ceramics for cladding materials
  iv. Properties of lead alloys related to corrosion
(2) Safety issues
  i. Water injection into reactor for decay heat removal
  ii. Accident in direct contact of water/steam-lead alloy

2. Compatibility of Structural and Cladding Materials with Lead Alloys

2.1. Corrosion under steady condition

2.1.1 Background

Lead alloys are corrosive to steels in general, and the corrosion rate of steels increases in about one order of magnitude with an increase in temperature by 100°C. Therefore, structural and cladding materials and operating temperature must be chosen based on compatibility data of the materials with lead alloy at high temperature. The compatibility of the materials should be investigated taking account of the factors below:

(1) The primary coolant temperature ranges in 350-400°C for core inlet, and on 450-550°C for core outlet in most of the LFRs. Therefore, the structural materials in the cold leg will be exposed to lead alloy at the temperature less than 400°C where corrosion rate is low. Stress due to pumping and coolant static pressures acts on reactor vessel. The pressure in reactor vessel is as high as 7MPa in PBWFR.
(2) On the other hand, the structural materials in the hot leg will be exposed to lead alloy at the temperature higher than 450°C where corrosion rate is high. Steam generator (SG) tubes in the hot leg are exposed to the high temperature lead alloy and inner steam pressure.
(3) In these cases, cladding tubes at hot spot may reach 650°C and have inner pressure of fission product (FP) gases. In addition, at UTOP, ULOF and ULOHS events, the temperature of cladding materials at hot spot reaches as high as 700-800°C even for a short time.
(4) The materials such as cladding and SG tubes will be fabricated by welding. The effects of the welding on corrosion are also important.
(5) Mass transport of dissolved metals in lead alloy has a large influence on liquid metal corrosion, or dissolution type of corrosion. The transport is dominated by diffusion of metals in a flow circuit. The diffusion coefficients of metals in lead alloy are important factors for the estimate of each rate.

Therefore, the compatibility studies were performed taking account of the factors mentioned above.

2.1.2 Commercialized steels

Corrosion experiment in flowing LBE was conducted for structural materials such as commercialized steels under the hot leg condition of 550°C. Oxygen potential was adequately chosen so that oxide protection layers were formed on steel surfaces. LBE velocity was 1 and 2 m/s. It was found that single or multiple oxide layers formed on the steel surfaces protected the material from corrosion. Ferritic-martensitic steels with higher Cr content were more corrosion-resistant. Austenitic stainless steel, SS316, was corroded by selective dissolution of Ni into LBE. The result of weight loss of 25 g/m^2 in HCM12 and HCM12A corresponds to corrosion depth of 0.9 mm for thirty year-operation, and that of 60 g/m^2 in SS316 corresponds to that of 2 mm for the same operation period. Even if SG tubes are made of HCM12 or HCM12A, they must be replaced in shorter operation period than reactor life time.

In the same type of LBE corrosion experiment, serious erosion occurred when the oxygen concentration was lower than the Fe oxide formation conditions, i.e., the oxygen concentration of 2x10^{-9} wt%. This suggests the necessity of adequate control of oxygen potential in lead alloy.

2.1.3 Al- and Si-added steels

The addition of Si and Al improves the corrosion resistance drastically. That is because very thin and stable Si- or Al-oxide layers in the thickness of approximately 1 m is formed and self-healed. Since their oxide formation potentials are very low, the corrosion is inhibited even under very low oxygen concentration in LBE. Si- and Al-rich steels, SUH3 (10Cr-1Mo-2Si), NTK04L (18Cr-3Al) and Recloy10 (18Cr-1Al-1Si), were immersed in a flowing LBE for 500 to 2,000 h under the oxygen concentration of 1.7x10^{-8} - 1x10^{-6}wt%. It was found that the addition of Si and Al is good for improvement of corrosion resistance for cladding steels.

2.1.4 Surface-coated steels with and without bending load

It is possible to improve the corrosion resistance only by changing the surface of material with Al-Fe alloy coating. Thus, the test steels, T91, E911 and ODS, were surface-treated and Al-alloyed by pulsed electron beam (GESA—GepulsteElektronenStrahlAnlage). Then, a corrosion test was performed for the specimens in a flowing LBE at 550ºC under the oxygen content of 10^{-6} wt% for 2000 h.

As the other surface Al-alloying technique, the unbalanced magnetron sputtering (UBMS) method with Al and SS304 targets was adopted. Surface-coated steels were tested by means of stirred-type LBE corrosion test at 700 ºC for 1000 h. Oxygen concentration was $4.5\text{x}10^{-7}$ - $5\text{x}10^{-6}$wt%. The results showed that a very thin oxide layer was formed on the coating layer and protected the material from corrosion attack.

External stress acts on structural materials, and influences the corrosion process in certain cases. A SS316 tube filled with LBE ruptured due to cyclic thermal stress. Liquid metal embrittlement took place in the tube wall.

The stress has the influence of damage on the Fe-Al alloy coating layer. It was investigated under bending stress condition. LBE pool was at the low oxygen concentration (up to 5.2×10^{-8} wt%) and 550 and 650°C. Under a tensile stress condition, Fe-Al alloy-coated HCM12A exhibited the penetration of LBE into the base metal and dissolution of base metal to LBE around cracks of the coating layer. Under a compression stress condition, the coating layers detached from the base metal. LBE corrosion was not observed appreciably at 550°C. At 650°C, Fe-Al coating layer was not corroded by LBE, and the penetration of LBE to base metal and dissolution of base metal into LBE occurred.

Heat treatment to the FeAl coating layer for strengthening had no appreciable effect on corrosion of material under the bending stress. Again, the coating layer was effective to reduce the surface of the matrix to be corroded by LBE.

2.1.5 Welded steels

Compatibility of welded structure with LBE at high temperature should be taken into account for the design of LFRs. Thus, the effect of welding on steel corrosion was investigated at 600ºC for 500 h. Several welding methods, TIG, YAG laser and electron beam welding, were applied to the steel: HCM12A. Oxygen concentration was $4.7\text{x}10^{-6}$wt%. Grain structure around fusion zone was coarse, and grain structure in base metal was typical ferritic-martensitic. Cr-rich spinel oxide layer was much thicker in the fusion zone: 18-30μm, than in the base metal: 10-15μm. The same type of experiment was conducted in LBE at 650ºC under oxygen concentration of $7\text{x}10^{-7}$ wt% for 500 h. Oxide layer was larger in the weld zones than base metal.

2.2. Corrosion under transient condition

2.2.1 Background

Fuel and cladding temperatures at hot spot will reach 700-800ºC at the UTOP and ULOF events in LSPR. The cladding temperature at hot spot reaches 792ºC in ULOHS (Unprotected Loss of Heat Sink)/ULOF (Unprotected Loss of Flow) event in PBWFR. It is concerned that lead alloy may become much corrosive at the transient temperature higher than 700ºC.

2.2.2 Corrosion of Steels in Lead-Bismuth Eutectic under Transient Temperature Conditions

The corrosion characteristics of candidate materials was investigated under transient temperature conditions. The concentration of oxygen was 10^{-6} (550ºC) - $2\text{x}10^{-5}$ (800ºC) for the transient case 1 and 10^{-6} wt% (550ºC-800ºC) for the transient case 2.

An Al-Fe-coating layer remains intacted on the base metal. The coating layer with ~20 μm in thickness was the same as before the immersion test. There is no penetration of LBE into the matrix of material and dissolution of constituent metals from the matrix into LBE. A coating layer remains intacted on the base surface with ~10 μm in thickness, which was the same as that before the test. There was no penetration of Pb-Bi into the matrix of material and dissolution of constituent metals to Pb-Bi.

2.3. Employment of ceramics for cladding materials

2.3.1 Background

Ceramics materials, silicon carbide (SiC) and its composites, may be promising cladding and structural materials for high temperature LFR, since they are expected to be compatible with high temperature lead-alloys. They have the superior high-temperature properties, thermo-chemical stability, irradiation tolerance, inherent low activation and low-after heat properties. The neutronic performance of the core and corrosion resistance of ceramics with lead alloys were investigated.

2.3.2 Neutronic performance of core with ceramics cladding

Neutronics of a reactor core with SiC cladding and structure was compared with that with steel cladding and structure analytically for small lead-cooled fast reactors. The analytical result indicated that neutron energy spectrum was slightly softer in the core with the SiC cladding and structure than that with steel cladding and structure. The SiC type core can be designed smaller than the steel type core.

2.3.3 Compatibility of ceramics with lead alloys

Corrosion characteristics of ceramic materials SiC and Si_3N_4 in a flowing lead-bismuth (Pb-Bi) for 2,000 h were investigated compared with those of high chromium steels. The surfaces of the specimens were smooth without corrosion after the exposure of the specimens to the flowing Pb-Bi. No appreciable oxide layer was formed, and no chemical segregation layer was observed near the surfaces. The weight losses were negligibly small, and were much lower than those of 9Cr steels. Corrosion test of SiC and Ti_3SiC_2 in a pot was carried out in stagnant lead alloys at 700ºC. The ceramics exhibited high corrosion resistance.

2.4. Properties of Lead Alloys Related to Corrosion

2.4.1 Background

One of main factors which cause steel corrosion in LBE is the dissolution of metallic elements in steels, such as Fe, Cr and Ni, into the liquid LBE. The diffusion characteristics of these dissolved elements in the liquid LBE are important factors for prediction of dissolution type of corrosion and the transport of the elements in a LBE circuit. Especially, Ni has high solubility into LBE and the preferential dissolution of Ni causes the dissolution corrosion of austenitic stainless steels.

2.4.2 Diffusion of metal elements in lead-bismuth eutectic

The diffusion coefficient of Ni in LBE was determined in the temperature range from 550 to 650˚C by means of Capillary method. The inner diameter of the capillary was 2 mm, and the length was 50 mm. The Ni concentration distribution in LBE was determined by means of the inductively coupled plasma mass spectroscopy (ICP-MS) method. The diffusion coefficients of Ni were determined from the measure profiles.

3. Safety Issues

3.1. Water injection into reactor for decay heat removal

3.1.1 Background

The conceptual designs of LFRs are equipped with decay heat removal systems: PRACS and RVACS which work with natural circulation of primary coolant. However, if the coolant level-down terminates the natural circulation, the function of decay heat removal is lost. In order to avoid the core disruptive accident (CDA) in this event, a water can be injected into the core like the emergency core cooling systems (ECCS) of LWRs. However, there is the possibility of re-criticality in the water injection.

3.1.2 Criticality of core in case of water injection

A scenario for prevention of the CDA with the ECCS was examined for PBWFR. The possibility of the re-criticality was evaluated analytically. It is found that the reactor becomes super-critical when the core is filled with water. It is necessary to prepare the ECC system with boric acid and additional backup rods for sub-critical core in water injection.

3.2. Accident in direct contact of water/steam-lead alloy

3.2.1 Background

One of the advantage of LFR is the elimination of the secondary lead alloy loop and installation of SG inside the reactor vessel. However, there is additional concern of SG pipe break. Rapid vaporization of the discharged water into LBE will bring sloshing motion of the heavy primary coolant and impact pressure to the reactor structures. It is necessary to avoid the mechanical damage to the structures. Although there is no SG pipe break in PBWFR, the feed water injected into LBE coolant may induce violent boiling. It is necessary to make the interaction of LBE with water mild in the chimney.

3.2.2 Visualization of bubbles in lead-bismuth eutectic

For the experimental study of LBE-water interaction, a new bubble visualization method was developed by means of gamma-ray radiography. ^{60}Co with 11 TBq was used as gamma–ray source, and a multi-crystal Gd_2O_2S (Tb) scintillator was employed as a gamma–ray detector. The bubble behavior was visualized successfully. Void fraction distributions were obtained by processing the visualized images.

3.2.3 Thermal interaction of lead alloy droplet with subcooled water

The lead alloy droplet and water micro interaction was experimentally clarified. Characteristics of thermal-hydraulic interaction of LBE and lead droplets with subcooled water in water pool were investigated. Two kinds of interaction zones (deformation and fragmentation) and three kinds of interaction zones (solidification, deformation and fragmentation) were observed. The fragmentation zone (FZ) could be bounded by two border lines: spontaneous nucleation temperature and minimum film boiling temperature.

Fragmentation behavior of molten lead alloy droplet in water was investigated experimentally by releasing liquid LBE and lead droplets into a pool of subcooled water. The fragmentation occurred when the temperature of the interface was higher than the spontaneous nucleation temperature of water and lower than the minimum film boiling temperature.

Preliminary experiments at low temperature jet boiling were performed by using ethanol as jet, and transparent fluorinert (FC-3283) as hot liquid, to understand the fundamental physical phenomena of the jet boiling of a water jet into LBE. Jet boiling occurred at bottom part of jet first and developed to the upper part of jet within very narrow area around jet.

4. Conclusions

Fundamental studies have been performed for development of LFRs. The recent progress of the studies are summarized below.

The compatibility of candidate structural and cladding materials has been clarified under steady and transient temperature conditions. Higher Cr steels, Si- and Al-added steels and Al-Fe alloy-coated steels exhibited good performance of corrosion resistance as structural materials, cladding materials and special high temperature materials, respectively. The Al-Fe alloy-coated steel was not corroded even high temperature transient conditions. The ceramics of SiC and and Si_3N_4 are expected to be used as cladding material for the core of high temperature LFR, since they were highly corrosion resistant both in a flowing condition and in high temperature condition. For the consideration of mass transport in corrosion process, the diffusion coefficient of metallic impurity, Ni, could be measured using the capillary and ICP-MS methods. A new bubble visualization method in LBE using the gamma-ray radiography was developed. The thermal interaction of LBE and lead droplets with sub-cooled water, and the fragmentation of droplets in the same system were investigated, and the visualization of injection of volatile liquid into high temperature transparent liquid were achieved.

Reference

M. Takahashi, R. Sa, A. Pramutadi, E. Yamaki-Irisawa, “Overview of Recent Studies Related to Lead-Alloy-Cooled Fast Reactors,” American Institute of Physics (AIP) Conference Proc. Series, 1448, pp.39-49 (2012).

B.8 Anomaly in the Infrared Phonon Intensity of One-dimensional Uneven Peanut-shaped C_{60} Polymer

Jun ONOE, Akito TAKASHIMA, Shota ONO, Hiroyuki SHIMA, and Toshiyuki NISHII

1. Introduction

Since nanocarbon family such as fullerenes, nanotubes, and graphene exhibit novel properties different from those of conventional carbon allotropes, they are expected to replace silicon-based devices in near future [1].

A one-dimensional (1D) uneven peanut-shaped C_{60} polymer was formed when pristine C_{60} films were irradiated using electron beam (EB) with an incident energy of 3 keV [2, 3]. Comparison between *in situ* infrared (IR) spectra and first-principle calculations indicated that the 1D polymer has a cross-linked structure close to that of P08 C_{120} stable isomer obtained from the general Stone-Wales rearrangement, as shown in Fig. 1 [3].

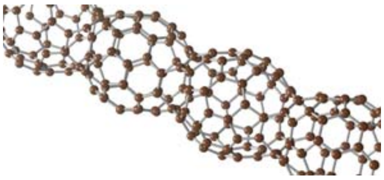

Fig. 1. Schematic illustration of 1D uneven peanut-shaped C_{60} polymer.

Since this polymer has positive and negative Gaussian curvatures (k) [4], it differs from the other nanocarbon allotropes [graphene ($k = 0$), fullerenes ($k > 0$), nanotubes ($k = 0$)]. Femtosecond carrier dynamics [5] and infrared (IR) phonon spectra [6] of the 1D peanut-shaped C_{60} polymer respectively showed a carrier lifetime of ca. 500 fs and a Peierls transition associated with charge-density-wave below 50 K corresponding to an energy gap of 15 meV. In addition, we have recently obtained from *in situ* high-resolution (12 meV) photoemission spectra that the polymer exhibits a Tomonaga-Luttinger liquid (TLL) state [7]. These anomalous behaviors can be attributed to the uneven structure of the 1D C_{60} polymer [8, 9], and furthermore suggest their superiority as quantum wires which conductance can be artificially tunable [10].

One of important consequences for the 1D uneven peanut-shaped C_{60} polymer is an occurrence of the van Hove singularities (VHSs) [11] in the density of states (DOS) of both electronic and phonon spectra. Recently, VHSs for the 1D nanotubes and 2D graphenes have been focused from a viewpoint of not only basic science but also electronic device applications [12-14]. In particular, since VHSs are related to superconductivity via electron-phonon couplings [15, 16], it is of interest to examine VHSs of not only electron but also phonon properties for the low dimensional nanocarbons [13, 14]. In a similar reason for nanotubes and graphenes, it is of much interest to examine VHSs for the electron and phonon properties of the 1D uneven peanut-shaped C_{60} polymer, which is strongly related to superconductor. More recently, we have observed an anomalous enhancement (by more than 10 times) in the IR mode intensities at 565 and 1340 cm^{-1}, which are respectively due to radial and in-plane (tangential) motions of the 1D uneven peanut-shaped C_{60} polymer [3], and speculated that the enhancement might be caused by VHSs [11].

In the present study, we confirmed whether or not the anomalous increase in the IR intensity can be explained by VHSs, using an extended thin-shell elastic model fully considering the effects of periodic radius modulation inherent to the 1D uneven peanut-shaped C_{60} polymer [17].

2. Experiments and Theory

2.1. Experiments

Details of the present apparatus used for measuring *in situ* high-resolution (0.25 cm^{-1}) IR spectra of the 1D peanut-shaped C_{60} polymer in an UHV chamber (a base pressure of 2×10^{-7} Pa) have been described elsewhere [18]. C_{60} films (ca. 300 nm thick) were formed on cesium iodide (CsI) substrates (20 mm in diameter and 2 mm thick) by thermal evaporation of C_{60} powder (Matsubo, 99.98% pure) in the Knudsen-cell at 673 K for 30 min after residual organic solvents in the powder were completely removed at 473 k for 2 h in the same UHV chamber. After the films were irradiated with EB (3 kV, 0.5 mA) until EB-polymerization was saturated, we measured *in situ* IR spectra of the 1D peanut-shaped C_{60} polymer. All the IR spectra were recorded with a resolution of 0.25 cm^{-1} and with 1000 scans ($S/N > 300$) at room temperature.

2.2. Theory

To explain the anomalous enhancement in the IR intensity of the tangential vibration arising from the whole cross-linkage of the 1D peanut-shaped C_{60} polymer, we used a 1D uneven peanut-shaped structure model with a unit cell consisting of two particles at the first stage, as shown in Fig. 2. The displacements along the 1D chain direction are denoted by u_s and v_s with an integer of s. The equations of motion for those oscillating particles can be written as,

$$M\frac{d^2u_s}{dt^2}=C_d\left(v_s-u_s\right)-C_{d-d}\left(u_s-v_{s-1}\right) \qquad (1),$$

$$M\frac{d^2v_s}{dt^2}=C_{d-d}\left(u_{s+1}-v_s\right)-C_d\left(v_s-u_s\right) \qquad (2),$$

where, M is the mass of the particles, while C_d and C_{d-d} are force constants.

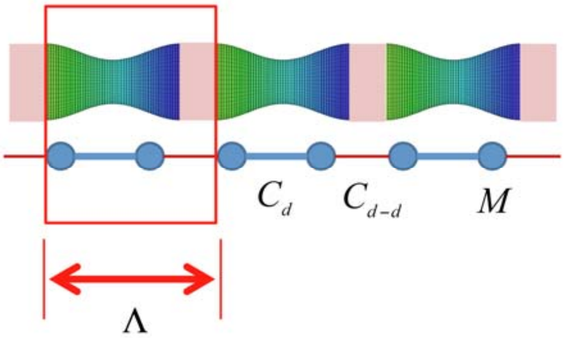

Fig. 2. Schematic illustration of an extended thin-shell elastic model considering the effects of periodic radius modulation inherent to the 1D uneven peanut-shaped C_{60} polymer.

The plane waves, $u_s = u\exp[i(sk\Lambda - \omega t)]$ and $v_s = v\exp[i(sk\Lambda - \omega t)]$, with the amplitude of u and v satisfy Eqs. (1) and (2), where, ω, k, and Λ denote the vibrational frequency, wave vector, and the length of the unit cell, respectively. When the plane waves are introduced into the equations, we obtain the eigenvalue equation, $\boldsymbol{A}\boldsymbol{x} = \omega^2\boldsymbol{x}$, in which $\boldsymbol{x} = [u,v]^T$ and

$$\boldsymbol{A} = \frac{1}{M}\begin{bmatrix} C_d + C_{d-d} & -C_d - e^{-ik\Lambda}C_{d-d} \\ -C_d - e^{ik\Lambda}C_{d-d} & C_d + C_{d-d} \end{bmatrix} \quad (3).$$

Solving the secular equation,

$$\det\left(\boldsymbol{A} - \omega^2\boldsymbol{I}\right) = 0 \quad \boldsymbol{I} = \begin{pmatrix} 1 & 0 \\ 0 & 1 \end{pmatrix},$$

we obtain the following dispersion relation,

$$\omega_{\pm}(k) = \sqrt{\alpha \pm \sqrt{\alpha^2 - 4\beta^2 \sin^2\left(\frac{k\Lambda}{2}\right)}} \quad (4),$$

where, $\alpha = \frac{C_d + C_{d-d}}{M}$ and $\beta = \frac{\sqrt{C_d C_{d-d}}}{M}$. The dispersion consists of two branches denoted using ω_+ (upper branch) and ω_- (lower branch), respectively. For each branch, the density-of-states (DOS) is calculated using the following equation,

$$D(\omega) = \frac{N\Lambda}{2\pi\left(\frac{d\omega}{dk}\right)} \quad (5).$$

Here, N is the number of the point mass.

To obtain the frequency and force constant of individual IR modes attributed to the waist cross-linked structure of the 1D uneven peanut-shaped C_{60} polymer, we have carried out first-principles density-functional calculations of IR spectra of the peanut-shape cross-linked region (see Fig. 3), using the GAUSSIAN03 package [19]. We employed a 6-31g (d) basis set and the Perdew-Burke-Ernzerhof (PBE) exchange-correlation potential [20], because these conditions have been shown to provide a good agreement in the energy gap and IR spectra between computational and experimental results for C_{60} [21, 22]. For example, the energy gap of C_{60} was estimated to be 1.67 eV, which is in an excellent agreement with the values of 1.6–1.85 eV obtained experimentally [23]. We analyzed individual IR peaks (frequency, intensity, force constant, and vibrational vector) obtained theoretically and assigned which of them to the cross-linked regional motions except edges.

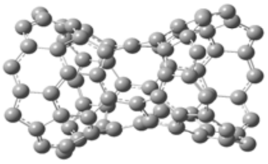

Fig. 3. Schematic representation of the waist cross-linked structure (consisting of 5-, 6-, and 7-membered rings) close to that of the 1D uneven peanut-shaped C_{60} polymer.

3. Results and Discussion

In our previous work, Fig. 3 of Ref. 3 has demonstrated that when the pristine C_{60} films were completely transformed into the 1D peanut-shaped C_{60} polymer, two anomalous intense IR peaks appeared at 1340 and 565 cm^{-1}, which are respectively attributed to the in-plane motion of the whole cross-linkage and to its radial motion for the 1D polymer. To understand the anomalous enhancement in the intensity of the two IR peaks, we examined the dependence of the two IR peak intensities on EB-irradiation time.

Fig. 4 shows the time evolution of IR spectra for C_{60} films with respect to EB-irradiation time in the range of 0–14 h. Where, the ω_1–ω_4 show IR modes of pristine C_{60} films, whereas the ω_5 and ω_6 show those of the 1D metallic peanut-shaped C_{60} polymer. As shown in Fig. 4, the ω_5 and ω_6 began to appear after 6 h EB-irradiation. Their intensities drastically and suddenly increased after 6.5 h EB-irradiation, immediately decreased after 7 h irradiation, and finally seemed to be constant after 14 h irradiation (this implies that the 1D polymer shown in Fig. 1 is very stable). To understand the behavior of the two intense peaks with respect to EB-irradiation time more clearly, we next examined the variation of the ω_5 and ω_6 peak intensities with respect to EB-irradiation time.

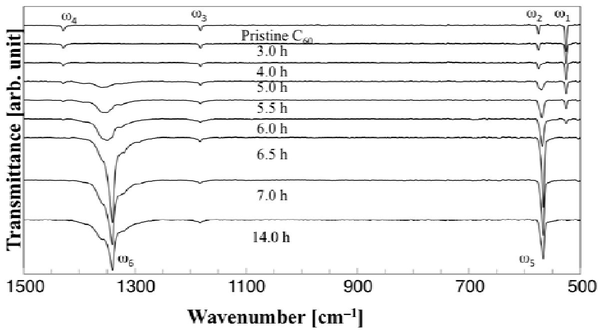

Fig. 4. Time evolution of infrared spectra of EB-irradiated C_{60} films, along with pristine C_{60} film.

Fig. 5 shows the plot of the ω_5 and ω_6 peak intensities (the 1D peanut-shaped C_{60} polymer) as a function of EB-irradiation time, together with the ω_2 and ω_4 peaks (pristine C_{60} film). It is interesting to note that the intensity of both ω_5 and ω_6 peaks suddenly increases after 6 h EB-irradiation and becomes the maximum at 6.5 h irradiation when the ω_2 and ω_4 peaks disappear.

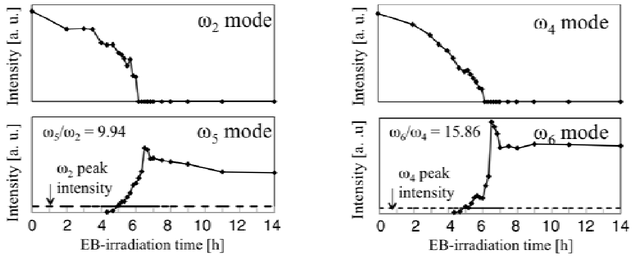

Fig. 5. EB-irradiation time dependence of the IR intensity for pristine C_{60} (ω_2, ω_4) and 1D exotic-nanocarbon (ω_5, ω_6).

To estimate the enhancement in the intensity of both peaks, we evaluated the maximum of both ω_5/ω_2 and ω_6/ω_4 ratios, and obtained to be ca. 10 and 16, respectively. Table 1 summarizes the results of the ω_6/ω_4 ratio obtained under several different conditions, and shows the reproducibility of the anomalous enhancement by more than 10 times.

Table 1. Summary of the enhancement in the ω_6 infrared peak obtained under several kinds of experimental conditions.

C_{60} film Thickness [nm]	IR resolution $[\mathrm{cm}^{-1}]$	ω_6/ω_4 ratio [–]
60	4.0	35.6*
60	4.0	12.4
60	0.25	21.6
300	0.25	12.3
300	0.25	15.8**

*Ref. 3, **the present work

Since the ω_2 and/or ω_4 peak intensity for pristine C_{60} film is obtained to be the sum of the corresponding IR intensity of individual C_{60} molecules observed within the IR measurement area, the intensity of the ω_5 and/or ω_6 peak is, in a similar manner, the sum of the corresponding intensity of individual cross-linked regions. Accordingly, the intensity of the ω_5 and/or ω_6 peak should be comparable to that of the ω_2 and/or ω_4 peak. However, the present results demonstrate that the intensity of the ω_5 and ω_6 peaks is greater by one-order than that of the ω_2 and ω_4 peaks.

As described above, since the peanut-shaped C_{60} polymer has been found to exhibit 1D physical properties, it is reasonably considered that the anomalous enhancement is due to one-dimensionality of the peanut-shaped C_{60} polymer, namely, due to 1D VHS [11], though there is the other possible explanation to cause the enhancement based on the charged phonon mechanism [24]. We will discuss the anomalous enhancement by examining the vibrational DOS of the 1D uneven peanut-shaped tube (see Fig. 2) with a cross-linked structure shown in Fig. 3. As shown in Fig. 5, the intensity of both ω_5 and ω_6 peaks suddenly decreases to some extent at 7 h irradiation and thereafter changes gradually and finally is saturated even after 12 h irradiation. These behaviors may be due to the interactions between adjacent 1D uneven peanut-shaped C_{60} polymer chains.

Fig. 6 shows the irradiation-time dependence of the wave number and intensity of the ω_3 peak due to a mixture of tangential (a major contribution) and radial motions arising from C_{60} molecule itself [25] which part remains as the positive Gaussian curved region of the 1D polymer (thus ω_3 mode can be still observed even after C_{60} molecules were completely polymerized).

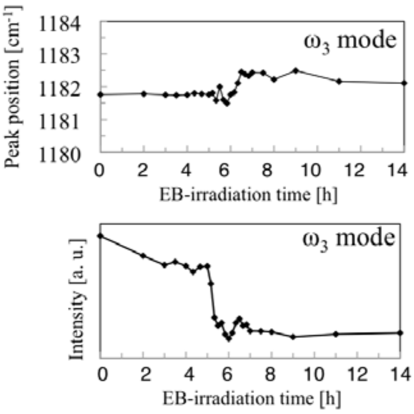

Fig. 6. EB-irradiation time dependence of the wave number and intensity for the ω_3 mode.

Both the wave number and the intensity are found to change drastically with the rapid increase in the intensity of the ω_5 and ω_6 peaks (in other words, with the beginning of formation of 1D peanut-shaped C_{60} polymers). The interaction between adjacent 1D polymer chains inhibits the tangential motion of the ω_3 peak to some extent, thus making both the peak position shifted to a higher wave number and the peak intensity weakened [18].

To confirm whether or not the intensity of the two IR modes is enhanced by VHS, we first examined the IR-active in-plane vibrational modes of the cross-linked structure (see Fig. 3) as a unit cell of the 1D uneven peanut-shaped polymer, using the first-principles density-functional calculations. Among all IR modes, by excluding the IR modes due to the edge region of Fig. 3, Table 2 shows that in-plane IR modes originating from the flat region of Fig. 3 are found to appear in the range of 1230–1300 cm^{-1}, whereas those from the waist (concave) region in the range of 800–880 cm^{-1}.

Table 2. The wave number and force constant of IR peaks originating from the waist cross-linked structure shown in Fig. 3. The IR modes due to the edge region were excluded.

Wave number [cm^{-1}]	Intensity [arb. unit]	Force constant [mDyne/Å]
807.5	2.7	4.6
825.0	23.5	4.8
834.3	5.4	4.9
842.1	6.9	5.0
844.5	33.2	5.0
852.9	17.9	5.1
861.7	20.8	5.3
874.6	91.3	5.4
1237.0	2.9	10.8
1247.6	5.9	11.0
1249.4	8.2	11.0
1268.3	8.6	11.4
1274.1	2.2	11.5
1295.8	47.0	11.9

Based on the results of Table 2, we obtained the dispersion curve and DOS of both ω_+ and ω_- branches, as shown in Fig. 7, when the unit cell is connected with each other to form the 1D uneven peanut-shaped polymer (see Fig. 2). Figure 7 (b) shows the divergence (namely, VHS) of the DOS at an eigen frequency of $\omega_-\left(\frac{\pi}{\Lambda}\right)$, $\omega_+\left(\frac{\pi}{\Lambda}\right)$, and $\omega_+(0)$. Since the first two eigen modes belonging to $k \neq 0$ are IR inactive, only the uppermost VHS (indicated by a red arrow) should be relevant to the intense IR peak appearing at 1340 cm^{-1}.

The estimation of $\omega_+(0)$ requires the values of C_d and C_{d-d}. As the IR anomaly is related to the vibration in the vicinity of the waist region, it is reasonable to assume C_d = 5.4 mDyne/Å that corresponds to that of the most intense IR mode at 874.6 cm^{-1}, as shown in Table 2. In addition, C_{d-d} should be larger than C_d, because the number of C-C bonds at the bulgy region is larger than that at the waist region. Assuming that C_{d-d} is 7.3 mDyne/Å, we obtained $\omega_+(0)$ to be 1340 cm^{-1}, which well reproduces the present results.

The large enhancement in the intensity of the ω_5 mode, unfortunately, cannot be explained using the present model, thus the origin to cause that is still unclear. This is because a model considering a larger part (consisting of at least 180 carbon atoms) of the 1D polymer than that shown in Fig. 3 will be necessary for estimating the force constants of radial IR motions, because a part of the tangential motions is possible to be contained in the ω_5 mode, in a similar manner to that for C_{60} [25].

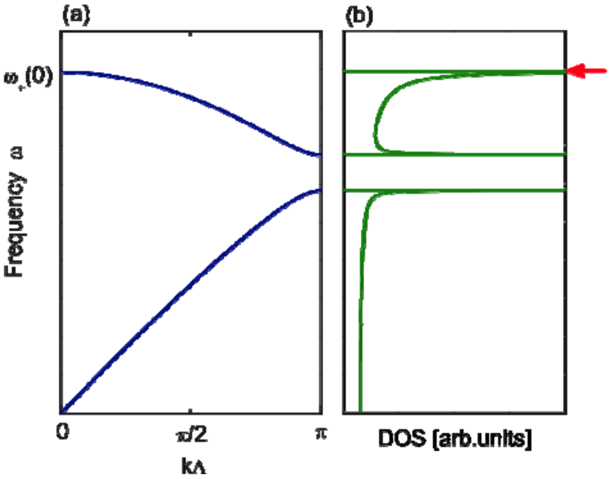

Fig. 7. The dispersion curve (a) and DOS (b) of both ω_+ and ω_- branches obtained using Eq. (4).

4. Summary

We examined the evolution of *in situ* IR spectra of a C_{60} film with respect to electron-beam irradiation time, and confirmed whether or not the anomalous enhancement in the IR intensity of the two intense IR peaks attributed to the radial (ω_5) and tangential (ω_6) motions of the 1D uneven peanut-shaped C_{60} polymer is caused by van Hove singularities (VHS), using an extended thin-shell elastic model fully considering the effects of periodic radius modulation inherent to the 1D polymer. We succeeded in explaining the enhancement in the ω_6 peak intensity using VHS, whereas the origin to cause that in the ω_5 peak intensity is still unclear. It is necessary to employ the 1D model considering the real carbon atom network of the 1D polymer, instead of using the simple 1D model shown in Fig. 2.

Acknowledgment

The present work was supported by a Grant-in-Aid for Scientific Research on Innovative Areas (No.21200032) of MEXT (The Ministry of Education, Culture, Sports, and Technology).

Reference

[1] N.P. Guisinger and M.S. Arnold, *MRS Bull.* **35**, 273 (2010) and references therein.

[2] J. Onoe, T. Ito, S. Kimura, H. Shima, Y. Toda, and H. Yoshioka, *Fullerenes, Nanotubes and Carbon Nanostructures* **20**, 1 (2012), and references therein.

[3] A. Takashima, J. Onoe, and T. Nishii, *J. Appl. Phys.* **108**, 033514 (2010), and references therein.

[4] The Gaussian curvature (K) at a given point on a general curved surface is defined to be the product of the maximum (κ_{max}) and minimum (κ_{min}) curvatures obtained among a myriad of curved lines generated when a myriad of normal surfaces cross the given point on the curved surface.

[5] Y. Toda, S. Ryuzaki, and J. Onoe, *Appl. Phys. Lett.* **92**, 094102 (2008).

[6] J. Onoe, A. Takashima, and Y. Toda, *Appl. Phys. Lett.* **97**, 241911 (2010).

[7] J. Onoe, T. Ito, H. Shima, H. Yoshioka, and S. Kimura, *Europhys. Lett.* **98**, 27001 (2012).

[8] H. Shima, H. Yoshioka, and J. Onoe, *Phys. Rev. B* **79**, 201401(R) (2009).

[9] S. Ono and H. Shima, *J. Phys. Soc. Jpn.* **80**, 064704 (2011).

[10] S. Ono and H. Shima, *Europhys. Lett.* **96**, 27011 (2011).

[11] L. Van Hove, *Phys. Rev.* **89**, 1189 (1953).

[12] Ge.G. Samsonidze *et al.*, *Appl. Phys. Lett.* **85**, 5703 (2004).

[13] J.L. McChesney *et al*., *Phys. Rev. Lett.* **104**, 136803 (2010).

[14] Li. Guohong *et al*., *Nature Phys.* **6**, 109 (2010).

[15] W. Kohn and J.M. Luttinger, *Phys. Rev. Lett.* **15**, 524 (1965).

[16] E. Cappelluti and L. Pietronero, *Phys. Rev. B* **53**, 932 (1996).

[17] J. Onoe, A. Takashima, S. Ono, H. Shima, and T. Nishii, *J. Phys.*: *Condens. Matter* **24**, 175405 (2012).

[18] J. Onoe and K. Takeuchi, *J. Phys. Chem.* **99**, 16786 (1995).

[19] M. J. Frisch, G. W. Trucks, H. B. Schlegel, G. E. Scuseria, M. A. Robb, J. R. Cheeseman, J. A. Montgomery, Jr., T. Vreven, K. N. Kudin, J. C. Burant, J. M. Millam, S. S. Iyengar, J. Tomasi, V. Barone, B. Mennucci, M. Cossi, G. Scalmani, N. Rega, G. A. Petersson, H. Nakatsuji, M. Hada, M. Ehara, K. Toyota, R. Fukuda, J. Hasegawa, M. Ishida, T. Nakajima, Y. Honda, O. Kitao, H. Nakai, M. Klene, X. Li, J. E. Knox, H. P. Hratchian, J. B. Cross, C. Adamo, J. Jaramillo, R. Gomperts, R. E. Stratmann, O. Yazyev, A. J. Austin, R. Cammi, C. Pomelli, J. W. Ochterski, P. Y. Ayala, K. Morokuma, G. A. Voth, P. Salvador, J. J. Dannenberg, V. G. Zakrzewski, S. Dapprich, A. D. Daniels, M. C. Strain, O. Farkas, D. K. Malick, A. D. Rabuck, K. Raghavachari, J. B. Foresman, J. V. Ortiz, Q. Cui, A. G. Baboul, S. Clifford, J. Cioslowski, B. B. Stefanov, G. Liu, A. Liashenko, P. Piskorz, I. Komaromi, R. L. Martin, D. J. Fox, T. Keith, M. A. Al-Laham, C. Y. Peng, A. Nanayakkara, M. Challacombe, P. M.W. Gill, B. Johnson, W. Chen, M. W. Wong, C. Gonzalez and J. A. Pople, GAUSSIAN 03, REVISION B.05 (Gaussian, Inc., Pittsburgh PA, 2003).

[20] J. P. Predew, K. Burke and M. Ernzerhof, *Phys. Rev. Lett.* **77**, 3865 (1996).

[21] T. A. Beu and J. Onoe, *Phys. Rev. B* **74**, 195426 (2006).

[22] T.A. Beu, J. Onoe and A. Hida, *Phys. Rev. B* **72**, 155416 (2005).

[23] R. K. Kermer, *Appl. Phys. A* **56**, 211 (1993).

[24] M.J. Rice and H.-Y. Choi, *Phys. Rev. B* **45**, 10173 (1992).

[25] R.E. Stanton and M.D. Newton, *J. Phys. Chem.* **92**, 2141 (1988).

B.9 Mechanisms of the Recruitment of XRCC4/DNA Ligase IV Complex To DNA Damage Sites for Final Joining

Sicheng LIU and Yoshihisa MATSUMOTO

1. Background and purpose of this study

DNA, the carrier of genetic information, continuously suffers from damage caused endogenously and exogenously, among which DNA double-strand break (DSB) is considered the most critical. Eukaryotic cells have evolved two major pathways to repair DSBs, *i.e.*, homologous recombination (HR) and non-homologous end-joining (NHEJ).

NHEJ requires six core proteins (1). Ku heterodimer consisting of Ku70 and Ku86 (also known as Ku80) first recognizes DSB (Fig.1, (i)) and, in turn, recruits DNA-PK catalytic subunit (DNA-PKcs) (ii). When the DSBs are not readily ligatable, processing takes place prior to ligation (iii). DSBs are finally joined by DNA ligase IV (LIG4), which is in tight association with XRCC4 (iv). XRCC4-like factor (XLF, also known as Cernunnos), is essential at this step, especially when two ends are not compatible. However, there are several important problems unsettled. First, despite the lines of evidence indicating the requirement for the protein-phosphorylating activity of DNA-PKcs in NHEJ, it is unknown which protein should be phosphorylated for proper NHEJ reaction. Second, large remains unknown how these proteins are recruited to and assembled at DSB to constitute the repair machinery.

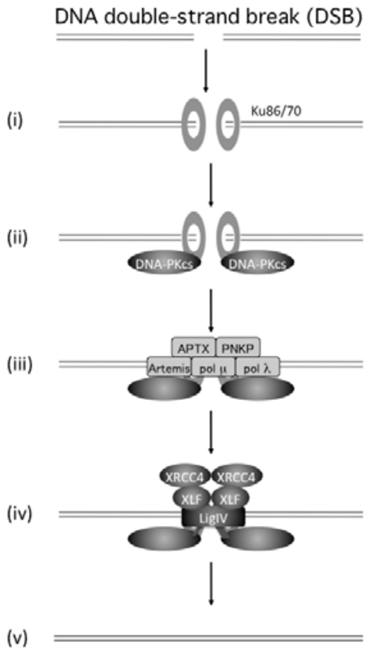

Fig. 1 General model for NHEJ reaction
From ref.1, modified.

We recently established a procedure to examine the chromatin binding of XRCC4 using a biochemical fractionation analysis using a detergent Nonidet P-40 (2). A subpopulation of XRCC4 changed into a form that is resistant to the extraction with 0.5 % Nonidet P-40-containing buffer after irradiation. This form of XRCC4 was liberated by micrococcal nuclease treatment, indicating that it had been tethered to chromatin DNA. This work explored the role of LIG4 and its subdomains in the recruitment of XRCC4/LIG4 complex to chromatin using this procedure (3).

2. Findings in this study

2.1. The chromatin binding of XRCC4 is dependent on the presence of LIG4.

We analyzed the chromatin binding of LIG4 and XRCC4 in human pre-B leukemia cell line Nalm-6 cell and its LIG4$^{-/-}$ derivative (generous gift by Dr. Adachi, Yokohama City University). We found that the chromatin binding of XRCC4, as well as that of LIG4, was diminished in LIG4$^{-/-}$ (Fig.1). When we introduced the *LIG4* cDNA into LIG4$^{-/-}$ (+LIG4), chromatin binding of XRCC4 , as well as that of LIG4, was restored. These results indicated that LIG4 is required for the chromatin binding of XRCC4.

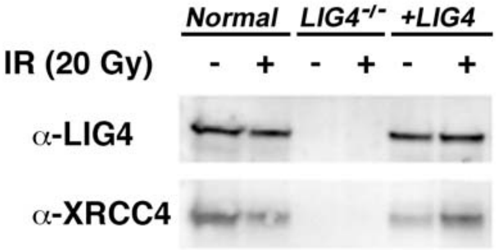

Fig. 1 Chromatin binding of LIG4 and XRCC4 in LIG4-deficient and reconstituted cells.
From ref. 3, modified.

2.2. BRCT domains in LIG4 are essential for the chromatin binding of XRCC4/LIG4 complex.

We next examined which part of the LIG4 was responsible for the chromatin binding. LIG4 consists of several domains: N-terminal region contain DNA binding, adenylation and oligo-binding domains, essential for catalytic function. C-terminal region (amino acids 638-911, denoted LIG4-CT hereafter) contains two BRCT domains, BRCT-I and BRCT-II, and XIR (XRCC4-interacting) domain in between (Fig.2). We introduced R278H (means arginine residue at 278th position from N-terminus changed to histidine), W725R and W893R mutations, respectively, in adenylation, BRCT-I and BRCT-II domains.

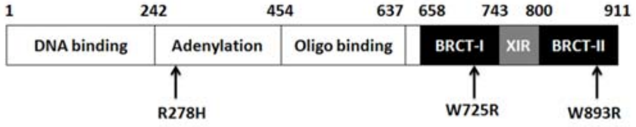

Fig. 2 Domain structure of LIG4.
From ref. 3, modified.

In W725R and W893R mutant, the chromatin binding of LIG4 was considerably reduced as compared to non-mutated LIG4 and the chromatin binding of XRCC4 was almost undetectable (Fig.3). These results indicated that BRCT-I and/or BRCT-II domains are essential for the chromatin binding of LIG4 and XRCC4. It is noted, however, that BRCT-II might be essential for the maintenance of LIG4 stability itself, as the abundance of LIG4 in free (not bound to chromatin) fraction was also greatly diminished.

In agreement with this, it was also found that W725R and W893R mutants were more radiosensitive than normal LIG4-expressing cells, substantiating the importance of BRCT domains in DSB repair.

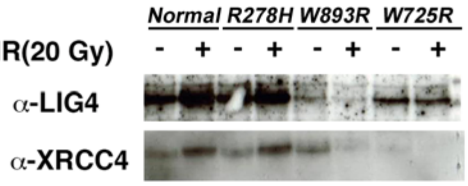

Fig.3 Chromatin binding of LIG4 and XRCC4 in LIG4 mutants.
From ref. 3, modified.

2.3. C-terminal fragment of LIG4 is capable of binding to chromatin with XRCC4.

We finally found that the expression of LIG4-CT in LIG4$^{-/-}$ restored XRCC4 as well as itself in F-IV (Fig.4), indicating that C-terminal fragment of LIG4 DNA ligase IV could drive XRCC4/LIG4 DNA ligase IV to the chromatin.

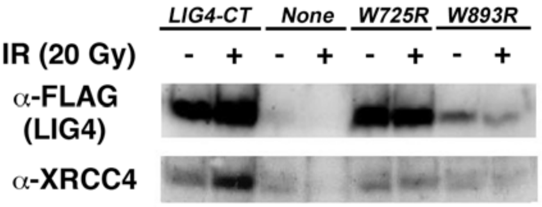

Fig.4 Chromatin binding of LIG4-CT and XRCC4.
From ref. 3, modified. Note that LIG4-CT was fused with FLAG epitope sequence to enable detection by anti-FLAG antibody.

3. Significance and perspectives of this study

This study demonstrated that the chromatin binding of XRCC4 is dependent on LIG4 and that C-terminal region, containing two BRCT domains, is essential. The ability of C-terminal region, in addition to DNA binding domain in N-terminus, to interact with chromatin might have an implication in the mechanisms of DSB repair through NHEJ. For example, the presence of two DNA binding domain would enable “hooking” another DNA end.

The present results would also provide a new strategy for radiosensitization for further improvement of cancer radiotherapy. As LIG4-CT alone can interact with XRCC4 and bind to chromatin, it would compete with normal LIG4 and interfere with its function, leading to the inhibition of DSB repair. Studies are ongoing to examine possible radiosensitizing effects of LIG4-CT upon introduction to cells with normal LIG4.

Acknowledgment

We thank Dr. Noritaka Adachi for the gift of DNA Ligase IV-deficient cells, without which this study was never possible, Mr. Isao Yoda (Cobalt Irradiation Facility) for cell irradiation and the laboratory members, especially Ms. Masami Kitamura, for assistance in cell culture and experiments. This work was supported in part by Grant-in-Aid for Young Scientists (A) (21689033). Initial part of this study is the result of “Study on Initiating Events in the Recognition and Repair of DNA Double-Strand Breaks” carried out under the Strategic Promotion Program for Basic Nuclear Research by the Ministry of Education, Culture, Sports, Science and Technology of Japan.

References

1. Y. Matsumoto, S. Imamichi, M. Fukuchi, S. Liu, R. Wanotayan, S. Kuniyoshi, K. Yoshida, Y. Mae, M.K. Sharma. Radiosensitization strategy through modification of DNA double-strand break repair. In “DNA Repair-New Research Directions”, Edit. Chen, C. ISBN 980-953-307-746-3, InTech (2013)
2. R.P. Kamdar, Y. Matsumoto. Radiation-induced XRCC4 Association with Chromatin DNA Analyzed by Biochemical Fractionation. *Journal of Radiation Research*, **51**, 303-313 (2010).
3. S. Liu, X. Liu, R.P. Kamdar, R. Wanotayan, M.K. Sharma, N. Adachi, Y. Matsumoto. C-terminal region of DNA ligase IV drives XRCC4/DNA ligase IV complex to chromatin. *Biochemical and Biophysical Research Communications*, **439**, 173-178 (2013).

B.10 Synthesis of Stimulus-Responsive Polymer-Silica Hybrid Particles using Surface-Initiated Atom Transfer Radical Polymerization (SI-ATRP) and its application for the mutual separation of lanthanides

Takehiko TSUKAHARA and Ki Chul PARK

This study aims at investigating the adsorption mechanism of Ln(III) by using non-crosslinked NIPAAm-based polymers in order to screen out the effect of inter-penetrating network (IPN) textures, where brush-like polymers immobilized on silica (SiO_2) surface were employed for easy handling of the water-soluble polymers.

The applicability of atom transfer radical polymerization (ATRP) to the copolymerization of *N*-isopropylacrylamide (NIPAAm) with *N*-vinyl-2-pyrrolidone (NVP) was examined in CuCl/CuCl2-catalyst system using tris[2-(dimethylamino)ethyl]amine (Me6TREN) and 1,4,8,11-tetramethyl-1,4,8,11-tetraazacyclo-tetradecane (Me4Cyclam) as ligands (Fig 1). In the Me6TREN system, less reactive NVP was not only hard to quantitatively copolymerize but also interfered with the homo-polymerization of NIPAAm units. In contrast, the Me4Cyclam system under heating was more active, although the controllability for polymer homogeneity is lower than in Me6TREN system. The application of active Me4Cyclam system to surface-initiated ATRP has successfully prepared silica beads surface-modified with the copolymers of NIPAAm with NVP and 4-vinylpyridine (VPy). The thermo-responsive behavior of the surface-grafted NIPAAm-based polymers was investigated for lanthanide trivalentions (Ln(III)). In less acidic aqueous solutions, all the surface-grafted polymers including poly(NIPAAm) exhibited only adsorption behavior with regular selectivity (Eu^{3+}>Sm^{3+}>Nd^{3+}>Ce^{3+}>La^{3+}) at below the phase-transition temperatures (Fig. 2). In more acidic solutions, the surface-grafted poly(NIPAAm) exhibited adsorption and desorption at below and above the phase-transition temperature, respectively. However, the copolymerization with NVP and VPy have deteriorated the desorption functions of poly(NIPAAm). In this study, a possible adsorption/desorption mechanism of Ln(III) on surface-grafted NIPAAm-based polymers is discussed.

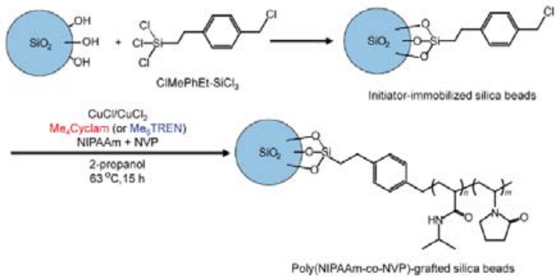

Fig. 1 Synthetic pathway of poly (NIPAAm–co-NVP)-grafted silica surface via surface-initiated ATRP.

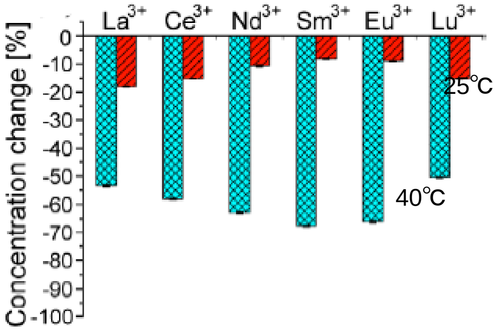

Fig. 2 Thermal-responsive adsorption/desorption behavior of poly(NIPAAm-co-VPy)-SiO_2 beads for $Ln(NO_3)_3$ aqueous solutions of pH = ca. 5.4–5.6.

B.11 Highly Effective Solvent Extraction of Radioactive Elements using Microfluidic Device

Takehiko TSUKAHARA

Microfluidic devices have been recognized as innovative research tools in the fields of general chemical analyses, because of their specific features such as laminar flow, short molecular diffusion distances, and large surface to volume ratio. Previously, we have demonstrate that actinide and lanthanide species could be extracted with higher speed (~sec) and smaller solution volume (~nL) in aqueous-organic two-phase microflows [1-3]. However, two-phase microflows are often unstable and difficult to control. Therefore, in this study, we develop a novel microfluidic device which makes it possible to control the complicated microflows, and realize highly effective solvent extraction of uranyl ions. A microchannel composed by a pinched-structure and a stairs-structure (shallow and deep channels) was fabricated on a glass chip, and their channel surfaces were hydrophobically modified by means of micro fabrication and surface patterning techniques (Fig. 1).

When aqueous and organic solutions were introduced into the microchannel, we found that the immiscible solutions formed aqueous-organic emulsion flow, and that were converted to plug flow at the pinched structure point. Furthermore, converted plug flow could be completely separated at the stairs-structure point, because only organic plugs passed through to the hydrophobic shallow channel according to Laplace pressure, which was induced at the interface between deep channel and shallow channel. Using the microfluidic device, the chelate extraction experiments of uranyl ions were carried out.

The results showed that almost 100 % extraction of uranyl ions from aqueous phase to organic phase could be achieved at about 10 second after starting of reaction. This new extraction concept will provide significant advantages in the field of nuclear fuel cycle.

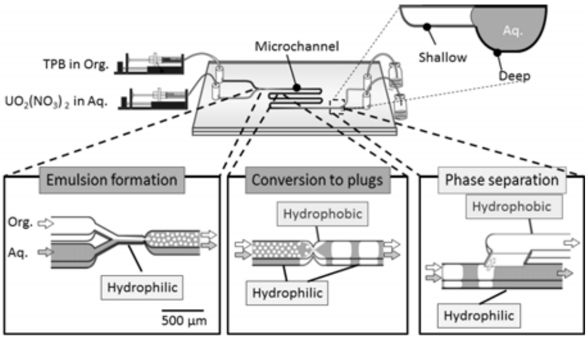

Fig. 1 A novel microfluidic device for the extraction of uranium.

Reference

[1] T. Tsukahara, K. Mawatari, T. Kitamori, *Chem. Soc. Rev*. **39**, 1000 (2010).

[2] K. Mawatari, Y. Kazoe, A. Aota, T. Tsukahara, K. Sato, T. Kitamori, *J. Flow Chem*. **1**, 3, (2011).

B.12 Local Structural Analysis of Thorium Compounds in Molten Fluoride Mixtures for Molten Salt Reactor Concept

Haruaki MATSUURA, Atsushi NEZU and Hiroshi AKATSUKA

Molten salt reactor (MSR) is one of the concepts of promising reactor type in the 4th generation. Actually, at the Oak Ridge National Laboratory (ORNL) in 1960s, the molten salt reactor experiment (MSRE) had been successfully performed for a few years. However, the project at the ORNL had been quitted until the proposal of the idea of a molten salt breeder reactor, which has been introduced two innovative ideas after the MSRE, that is, introduction of a second coolant loop and an online fuel cleaning process in the first coolant/fuel loop. For the development of the on-line recycling process, the electrochemical method is one of the options to separate actinides (An) from lanthanides (Ln). To find better electrolysis conditions to improve the efficiency of the pyrochemical reprocessing, systematic clarification of the correlation between structures of molten An (Ln)F_n and their physico-chemical properties is useful. In this study, ThF_4-LiF mixtures are focused on the structural investigation by EXAFS.

ThF_4 was synthesized from ThO_2 under fluorine gas (40 ml/min) at 650 ^{o}C for 4 h. Mixtures of ThF_4 and LiF were melted once in a glassy carbon crucible at 1073 K in a quartz chamber filled with an argon atmosphere in high purity. Then, they were mixed with boron nitride powder, and pressed into pellets in 7 mm diameter and 1 mm thickness. The mixing weight ratio of ThF_4 to BN was ca. 1: 2.5. To prevent chemical reaction of sample and contamination of ThF_4 to outside during heating process in EXAFS experiments, these pellets were installed in a double barrier cell. The 1st barrier is made with pyrolytic boron nitride and the 2nd barrier is made with boron nitride (HP) [1-3]. The electric furnace was filled with He gas at ca. 30 kPa. The Th L_{III}-edge EXAFS spectra have been collected with fixed time scan method by the X-ray from a double Si (111) crystals monochromator in transmission mode at BL27B/PF/KEK, Japan. EXAFS data were analysed by using the WinXAS ver.3.1.

The temperature dependence of EXAFS structure functions of certain sample is shown in Fig. 1 [4]. Unfortunately, this sample contains few percent of thoria identified by powder X-ray diffraction analysis. With increasing temperature, the intensity of the 1st neighbour contribution which is mainly attributed to Th^{4+} – F^{-} correlation has been reduced. This fact is typical behaviour of temperature effect caused by an anharmonic oscillation. Over the melting point, the spectra at 600^{o}C and 800^{o}C are similar to each other. It means that the most of the part of sample had been already molten below 600^{o}C. The most striking fact is the spectra of before heating and after cooling down are nearly similar to each other. The small peak at ca. 4 Å is corresponding to multiple scattering caused by thoria, since the spectra of thoria indicates that even larger contribution exists in 2nd coordination than that in 1st coordination. The ratio of the intensity of the 1st and the 2nd coordination peak is constant before and after heating, therefore, molten fluoride can stably co-exist with thoria. The behaviour of oxide species should be clarified to make realization of the molten salt reactor concept, and this study would provide the valuable information for the future study.

This study was done by a collaboration research with Prof. N. Sato, Tohoku University and Dr. C. Bessada, CEMHTI, CNRS, France.

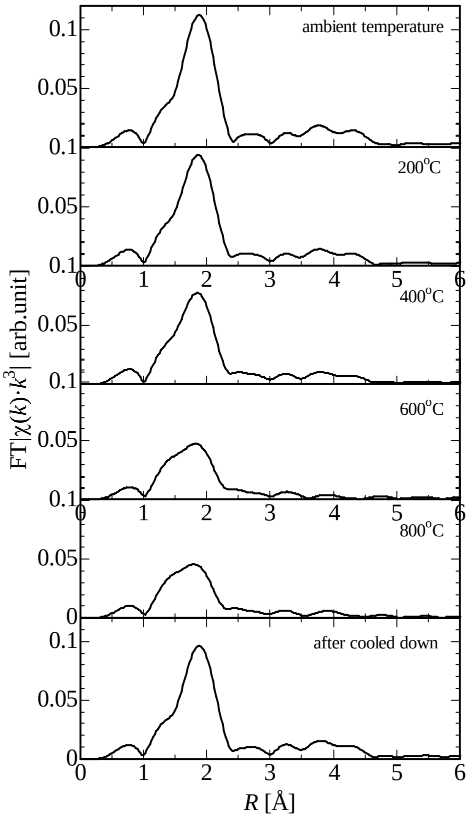

Fig. 1 Structure functions of LiF-ThF_4 (x_{ThF4} = 0.25) at various temperatures.

References

[1] M. Numakura, et al, *Prog. Nucl. Ener.* **53**, (2011) 994.

[2] C. Bessada, et al, *Nucl. Sci. NEA/NSC/DOC 15* (2009) 117.

[3] M. Numakura, *Doctor Thesis, Tokyo Institute of Technology* (2011).

[4] H. Matsuura et al *Proc. AMS4* (2012) 249.

B.13 Fluoride Addition Effect on the Electrochemistry and Local Structure of Neodymium Cation in Molten LiCl-KCl

Haruaki MATSUURA, Atsushi NEZU and Hiroshi AKATSUKA

Neodymium magnet has the strongest magnetism among the magnets currently industrialized, thus it has been used as motors in hybrid cars, electric vehicles, wind farms and medical instruments which are required with strong magnetism. However, over 90 % of the first resource of rare earths including neodymium is now produced in China. If the demand of the electric vehicles and wind farms rapidly increases in the world, it leads to special concern about the lacking of rare earth resource. Therefore, we have focused on nickel misch metal hydride batteries as a secondary resource of rare earths, and investigated applicability of molten salt electrolysis to extract neodymium from them [1]. To find out much efficient electrochemical condition for the separation of neodymium, the electrochemical behaviour of neodymium in molten LiCl – KCl eutectic coexisting various amount of LiF has been examined. To elucidate the relationship between the variation of electro-reduction potential and local structure around neodymium cation depending on fluoride concentration in molten chloride, EXAFS and UV-vis-NIR experiments of neodymium cation in molten LiCl – KCl – LiF have been performed.

Electrochemical study

Cyclic voltammograms and differencial pulsed volatammograms have been measured in an argon circulated glove box by using the electrodes as follows: working electrodes: tungsten or nickel electrode, counter electrode: glassy carbon, and reference electrode: Ag in LiCl-KCl eutectic + AgCl (1mol%), respectively. Molten LiCl-KCl eutectic and glassy carbon was chosen as an electrolyte and a container, respectively. To observe the fluoride addition effect, varous amount of LiF was added to be the ralative concentration upto 12 times to the concentration of rare earths. Differential pulsed voltammograms of LiCl-KCl-$NdCl_3$-LiF by scanning 5 mV s^{-1} are shown in Fig. 1. It has been found that the electro-reduction potential of neodymium metal depending on fluoride concentation is shifted positively once until the 3 times of concentration of LiF, and shifted negatively over the 3 times of concentration of LiF, which was also observed in La and Ce containing melts[2].

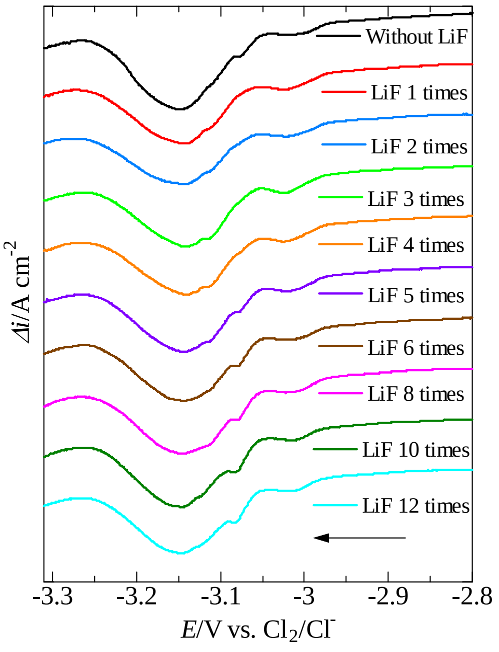

Fig. 1 differential pulsed voltammograms of cathodic sweep of neodymium in molten LiCl-KCl-LiF.

Extended X-ray absorption fine structure [3]

EXAFS spectra of Nd L_{III}-edge (6.209 keV) were collected with a fixed time scan method by using Si (111) double crystal monochromator in transmission mode at BL27B/PF/KEK, Japan. Mixtures of $NdCl_3$ (x = 5mol%) in eutectic LiCl – KCl with LiF in the amount of various times to the concentration of $NdCl_3$ (0 to 15), were melted once in a glassy carbon crucible at 873 K in a glove box filled with an argon atmosphere in high purity. Then, they were mixed with boron nitride powder, and pressed into pellets. To prevent from the chemical reaction during heating process in EXAFS measurements, these pellets were installed in a cell made with pyrolytic boron nitride and the electric furnace was filled with He gas under 30 kPa. EXAFS data were analysed by using the WinXAS ver.3.1.

The inter-ionic distance between neodymium cation and anion of structural functions of molten $NdCl_3$ – LiCl – KCl – LiF (0 and 15 times of concentration of Nd) at 298 K and 1073 K are shown in Fig. 2. In both temperatures, with increasing fluoride concentration, inter-ionic distance between Nd^{3+} and anion decreases, that is corresponding to the fact that chloride anions in the 1st coordinated sphere around Nd^{3+} are exchanged by fluoride anions. The most striking feature derived from the figure is that the inter-ionic distance in molten state (at 1073 K) approaches to the value at pure fluoride at 8 – 10 times of LiF concentration while the one at solid state (at 298 K) rapidly reaches to the value at fluoride at 3 times of LiF concentration. It is considered that even larger coodinated structure with 8 or 10 anions can be expected in fluoride melts, while the 6 coordinated octahedron is well known to be predominantly existing in various chloride melts.

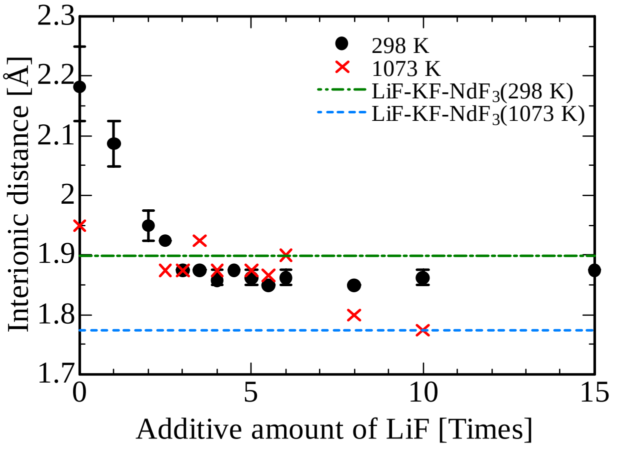

Fig. 2 inter-ionic distances between Nd^{3+} and anion of structural functions of molten $NdCl_3$ – LiCl – KCl – LiF (0 and 12 times of concentration of Nd) at 298 and 1073 K.

UV-vis-NIR spectroscopy

UV-vis-NIR spectroscopy of molten salts containing neodymium cation has been carried out by using the spectrophotometer (JASCO V-500) at the hot labo in KURRI, Japan. The solvent salts of LiCl-KCl or NaCl-2CsCl was initially molten in a quartz cell (light path: 1cm) installed in the argon circulated glove box and the background absorption spectrum was measured. Then, anhydrous neodymium chloride was added and electronic absorption spectrum of neodymium was obtained by the extraction of the background from the spectrum. In order to look at the effect of fluoride in absorption spectra, LiF (upto 35 times of the molar concentration of neodymium) or NaF (upto 10 times of the molar concentration of neodymium) was added stepwisely to molten LiCl-KCl or NaCl-2CsCl melts, respectively. Before the measurement, the molten salts containing fluoride were well confirmed that the mixtures were homogeneously mixed without any bubbles in the light path.

It is well known that the evolution of hypersensitive transition in the electronic absorption of neodymium is related to the indication of the symmetric characteristics of 6 anions octahedral coordinated species around neodymium cation. The electronic absorption spectra of neodymium in molten LiCl-KCl-LiF (Fig. 3a) shows that with increasing the concentration of LiF, the main absorption peak is slowly shifted to the lower wavelength and new absorption shoulder appears at ca 575 nm. Contrary to the case of LiCl-KCl-LiF, the electronic absorption spectra in molten NaCl-2CsCl-NaF (Fig. 3b) shows much drastic effect depending on fluoride concentration, i.e. molar absoptivity rapidly decreases until the concentration of 6 times to the neodymium and it seems saturated over this concentration. It can be clearly identified that the peak at ca. 575 nm is related to the fluoride coodinated species. The reason of the differency of the tendency would be the symmetric characteristics of neodymium species and/or the effect of the coulombic interaction between the cation existing in the 2nd coordination sphere (in this case Li^+ or Na^+) from neodymium.

Thus intermediately exchanged coordination by fluoride anion makes unstable local structure around neodymium cation in chloride melts, and this fact would result in positive shift of electroreduction potential in electrochemical behaviour. The similar strategy can be applicable to compounds containing actinide and the profound discussion on the relationship between electrochemical behaviour and local structure will be expected.

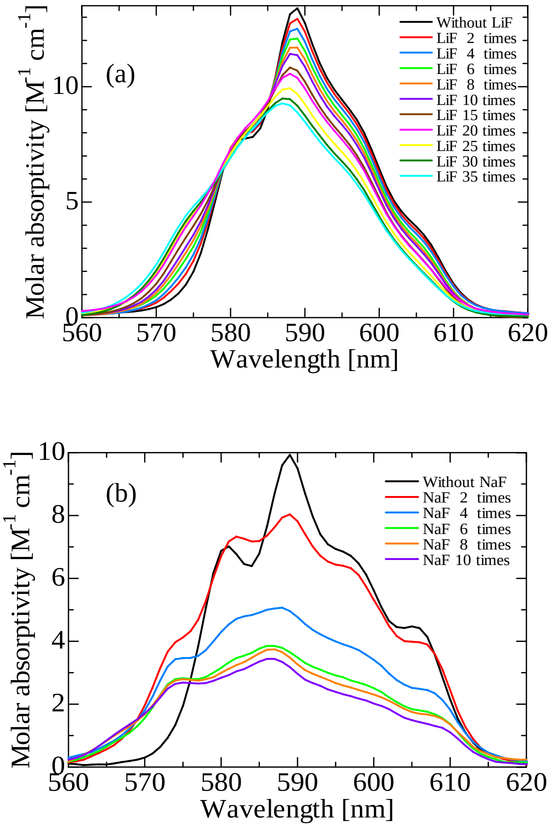

Fig. 3 electronic absorption spectra of neodymium in molten (a) LiCl-KCl-LiF and (b) NaCl-2CsCl-NaF.

This study is funded by the Fujikura Foundation. This study was done by a collaboration research with Profs. T. Fujii and H. Yamana, Kyoto University.

References

[1] H. Matsuura et al, *J. Phys. Chem. Solids*, **66** (2005) 439.
[2] Y. Shimohara et al *Proc. of 9th International Symposium on Molten Salts Chemistry & Technology* (2011).
[3] K. Fujita et al., *Proc. AMS4*, (2012) 264.

B.14 Mechanical Properties of Uni-directional SiC$_f$/SiC Composites with Carbon Interphase Formed by Electrophoretic Deposition Method

Katsumi YOSHIDA and Toyohiko YANO

1. Introduction

Continuous silicon carbide fiber-reinforced silicon carbide matrix composites (SiC$_f$/SiC) have been expected to be used as components for fission and fusion power reactors. It is important for achieving high-performance SiC$_f$/SiC composites to design optimum fiber/matrix interfaces and microstructures. The optimum fiber/matrix interfaces play an important role for the inhibition of reactions between fiber and matrix, and for the promotion of interfacial debonding and fiber pullout.

Electrophoretic deposition (EPD) is a colloidal process wherein ceramic bodies are shaped directly from a stable colloid suspension by a DC electric field, and EPD process can be applied for attaining complex shaped ceramics and a coating on the substrate. Present authors paid attention to EPD process, and we proposed the novel fabrication process including interfacial control of SiC$_f$/SiC composites based on EPD. In this study, interfacial control of uni-directional SiC$_f$/SiC composites were performed by EPD, and their mechanical properties at room temperature were evaluated. The effect of the thickness of carbon interphase on SiC fibers by EPD on mechanical properties of uni-directional SiC$_f$/SiC composites was also investigated.

2. Experimental

2.1.Carbon coating and SiC matrix formation for uni-directional SiC fiber preforms by EPD

Polycrystalline SiC fibers (Tyranno SA, fiber diameter; 10 μm, 800 filaments/yarn, Ube Industries, Ltd., Japan) were used as the reinforcement. The SiC fibers were uni-directionally aligned and then fixed on the jig. The SiC fiber preform was immersed in hot water in order to remove a sizing agent on the fibers. Silver paste was applied on the upside of the SiC fiber preform. Aqueous suspension of graphite particles for EPD was prepared using a commercial colloidal graphite aqueous solution. Concentration of colloidal graphite suspension was set at 0.1, 0.2 and 0.3 wt%. Small amount of *n*-butylamine was added to the suspension to adjust the pH of the suspension to 10. The uni-directional SiC fiber preform and graphite plates were used as the anode and the cathode, respectively. They were settled at a distance of 10 mm in the colloidal graphite suspension under an applied voltage of 3 V for 1 h. After EPD, they were dried at 120°C. Beta-SiC powder and sintering additives composed of α-Al_2O_3, Y_2O_3 and $CaCO_3$ were dispersed in distilled water using a commercial dispersant. The concentration of SiC with the sintering additives in the aqueous suspension was 10 wt%. Small amount of *n*-butylamine was added to the suspension, and the pH of the suspension was adjusted to 10. The carbon-coated SiC fiber performs and graphite plates were dipped into the SiC suspension as the anode and the cathode, respectively, and they were settled at a distance of 10 mm. SiC matrix with the sintering additives was infiltrated into the fiber preform by EPD under an applied voltage of 5 V for 1 h. Afterwards, the fiber preforms were dried at 120°C.

2.2.Fabrication of uni-directional SiC$_f$/SiC composites

SiC green sheet was prepared by tape casting using a laboratory-scale tape casting equipment. The slurry for tape casting was prepared using submicron-sized β-SiC powder, sintering additives (20 wt% α-Al_2O_3-Y_2O_3-CaO in total) and some organics. The thickness of the SiC green sheet was 90–100 μm. The SiC sheet and the uni-directional SiC fiber preform with carbon coating and SiC matrix were pasted with polyvinyl alcohol aqueous solution and stacked alternately, and then warm-pressed at 120°C for 10 min under a uniaxial pressure of 2 MPa. The stacked green body was heat-treated at 300°C for 24 h in air in order to remove organics. The compact was hot-pressed at 1700°C for 1 h in argon flow under a uniaxial pressure of 40 MPa.

2.3.Characterization and evaluation of uni-directional SiC$_f$ /SiC composites

The SiC$_f$/SiC composite was cut into rectangular bars (4.0 mm^w×2.6 mm^t×35 mm^l) along the fiber direction. Bulk density and open porosity of specimens were measured by Archimedes' method. Bending strength of specimens was measured by three-point bending test at room temperature with a span of 30 mm and a crosshead speed of 0.1 mm/min. Elastic modulus of the SiC$_f$/SiC composites was measured by ultrasonic pulse method at room temperature. Crack propagation in the specimen after three-point bending test was observed with an optical microscope. Microstructure and fracture surface of the specimens were observed with a field emission scanning electron microscope (FE-SEM).

3. Results and discussion

3.2.Characterization and microstructure of uni-directional SiC$_f$ /SiC composites

In the present report, uni-directional SiC$_f$/SiC composites with carbon-coated SiC fiber preforms by EPD using 0.1, 0.2 and 0.3 wt% colloidal graphite suspension are denoted as SC01, SC02 and SC03, respectively. Table 1 lists bulk density, open porosity and fiber volume fraction

Table 1 Bulk density (ρ_{bulk}), open porosity (P_o), fiber volume fraction (V_f), bending strength (σ_{3p}), fracture energy (Γ) and elastic modulus (E) of uni-directional SiC$_f$/SiC composites

Sample code	ρ_{bulk} (g/cm^3)	P_o (%)	V_f (%)	σ_{3p} (MPa)	Γ (J/m^2)	E (GPa)
SC01	2.89±0.04	4.7±0.5	48.2	236±64	0.56±0.17	344± 8
SC02	2.93±0.02	6.1±0.6	50.5	244±30	0.38±0.02	288±17
SC03	2.95±0.04	3.6±1.0	47.2	209±13	1.68±0.23	289±15

of the SiC$_f$/SiC composites. Fiber volume fraction of the SiC$_f$/SiC composites was 47.2–50.5%. Bulk density and open porosity of the SiC$_f$/SiC composites were 2.89–2.95 g/cm^3 and 3.6–6.1 %, respectively, and dense SiC$_f$/SiC composites were achieved.

Fig. 1 shows SEM micrographs of carbon coating on SiC fibers by EPD in the SiC$_f$/SiC composites. SEM micrographs suggested that the amount of carbon deposited on SiC fibers depended on the concentration of colloidal graphite suspension. The carbon coating on the SiC fibers in SC01 and SC02 was thin, and the average thickness of carbon coating was 42±18 nm and 68±31 nm, respectively. The carbon coating on SiC fibers in SC03 was much thicker than that in SC01 and SC02. The thickness of carbon coating in SC03 ranged from 50 to 400 nm, and the average thickness was 164±98 nm.

3.3. Bending strength and fracture behavior of uni-directional SiC$_f$ /SiC composites

Fig. 2 exhibits typical load–displacement curves of the SiC$_f$/SiC composites in three-point bending test at room temperature. Bending strength, fracture energy and elastic modulus of the SiC$_f$/SiC composites are listed in Table 1. SC01 and SC02 had a bending strength of 236 MPa and 244 MPa, respectively, and these values were higher than that of SC03 (209 MPa). This was because SC01 and SC02 did not have the optimal interfaces between fiber and matrix, and the interfaces did not act effectively. Microstructures of the interfaces in the SiC$_f$/SiC composites were discussed below. Elastic modulus of SC01 was slightly higher than SC02 and SC03, and the value was 344 GPa. SC02 and SC03 showed almost the same elastic moduli and the values were approximately 290 GPa. Elastic modulus of monolithic SiC has been reported to be 280–450 GPa, and the values of the SiC$_f$/SiC composites agreed with the literature values. In the load–displacement curves of SC01 and SC02, the proportional limit corresponded to the maximum load, i.e. a non-linear region did not appear below the maximum load. After the maximum load, the sudden reduction of load and the small tail were observed. SC01 and SC02 fractured in brittle manner, and their fracture energy was very low (0.4–0.6 kJ/m^2). In contrast, SC03 showed a pseudo-ductile fracture behavior, i.e. the non-linear region appeared clearly after the proportional limit, and the load gradually decreased after the maximum load. Fracture energy of SC03 was 3–4 times as high as those of SC01 and SC02, and the value

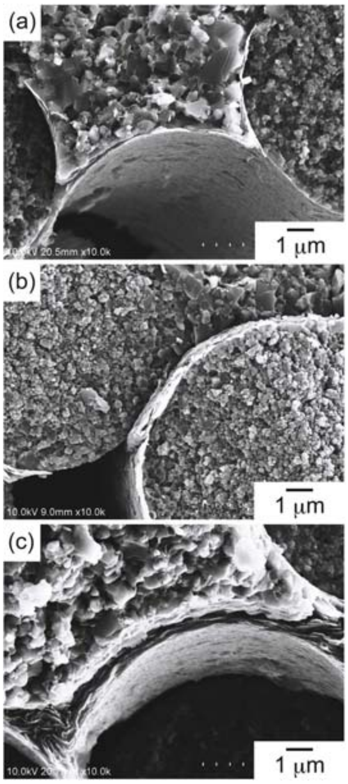

Fig. 1 SEM micrographs of carbon coating on SiC fibers by EPD using (a) 0.1 wt% (SC01), (b) 0.2 wt% (SC02) and (c) 0.3 wt% (SC03) colloidal graphite suspension in SiC$_f$/SiC composites

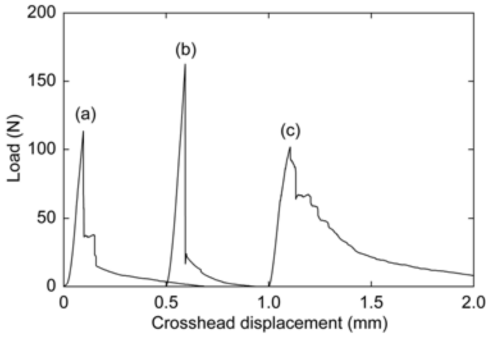

Fig. 2 Typical load-crosshead displacement curves of uni-directional SiC$_f$/SiC composites in three-point bending test at room temperature. Carbon-coated SiC fibers by EPD using (a) 0.1 wt% (SC01), (b) 0.2 wt% (SC02) and (c) 0.3 wt% (SC03) colloidal graphite suspension were used as the reinforcement

was about 1.7 kJ/m^2. Crack propagation in the SiC$_f$/SiC composites after three-point bending test at room temperature was observed with an optical microscope. Crack propagated across or along the fiber layers in SC01 and SC02, and fiber pullout was not observed, while long fiber pullout was observed in SC03 along the crack propagation.

Fracture surface of the SiC$_f$/SiC composites after bending test was observed by FE-SEM. The fracture surface of SC01 was stepwise without fiber pullout. In addition, fibers and matrix appeared to be attached firmly, and the fracture surface was almost flat. SC02 exhibited almost flat fracture surface with very short fiber pull out, and fiber and matrix in SC02 were also attached firmly similar with SC01, resulting in the flat fracture surface. On the other hand, SC03 exhibited a large number of fiber pullout, and the debonding along the fiber/matrix interfaces and fiber pullout were clearly observed. From the microstructure observation with optical microscope and SEM, the small tails observed in the load–displacement curves of SC01 and SC02 were considered to correspond to the stepwise fracture along the fiber layers and short fiber pullout. As the thickness of carbon coating on SiC fibers was thin, fiber pullout during fracture was inhibited because of high sliding frictional force between the fiber and the matrix. As a result, the SiC$_f$/SiC composite fractured in brittle manner without fiber pullout. In consideration of the present results, the thickness of carbon coating on SiC fibers should be at least 100 nm to obtain high-performance uni-directional SiC$_f$/SiC composites. In our previous works, two-dimensional SiC$_f$/SiC composites with the same sintering additives used in this study and BN-coated (CVD) SiC fiber cloths (Hi-Nicalon, Nippon Carbon Co., Ltd., Japan, BN coating thickness; 400 nm, fiber volume fraction; 52 %) were fabricated by sheet stacking and hot-pressing at 1700^{o}C. The SiC$_f$/SiC composites showed a bending strength and a fracture energy of 240 MPa and 1.2 kJ/m^2 at room temperature, respectively. In terms of mechanical properties, SC03 was comparable with or superior to the SiC$_f$/SiC composites described above. In addition, bending strength of the uni-directional SiC$_f$/SiC composites fabricated in this study was higher than that of the two-directional SiC$_f$/SiC composites using plain-woven SiC fiber cloths after carbon coating by EPD, and this result suggested that the interfacial control process based on EPD was optimized using uni-directional SiC fiber preforms.

From these results, it was concluded that the fabrication process based on EPD method is expected to be an effective way to control the interfaces of SiC$_f$/SiC composites and to obtain high-performance SiC$_f$/SiC composites.

4. Conclusion

Interfacial control of uni-directional SiC$_f$/SiC composites were performed by EPD, and their mechanical properties at room temperature were evaluated. The effect of the thickness of carbon interphase on SiC fibers by EPD on mechanical properties of uni-directional SiC$_f$/SiC composites was also investigated.

The surface of SiC fibers was wholly coated with flaky graphite particles by EPD, and relatively homogeneous carbon coating was formed on SiC fibers. The amount of carbon deposited on SiC fibers depended on the concentration of colloidal graphite suspension for EPD, and the average thickness of carbon coating on SiC fibers in SC01, SC02 and SC03 was 42±18 nm, 68±31 nm and 164 ±98 nm, respectively. The SiC$_f$/SiC composites were dense and their fiber volume fraction was 47–51 %. The SiC$_f$/SiC composites had a bending strength of 210–240 MPa. SC01 and SC02 fractured in almost brittle manner and their fracture energy was very low. In contrast, SC03 showed a pseudo-ductile fracture behavior, and its fracture energy was 3–4 times as high as those of SC01 and SC02, and the value was about 1.7 kJ/m^2. The fracture surface of SC01 was stepwise without fiber pullout, and SC02 exhibited almost flat fracture surface with very short fiber pull out. In SC01 and SC02, the fibers and matrix appeared to be attached firmly. On the other hand, SC03 exhibited a large number of fiber pullout, and the debonding along the fiber/ matrix interfaces were clearly observed. In consideration of the present results, the thickness of carbon coating on SiC fibers should be at least 100 nm to obtain high-performance uni-directional SiC$_f$/SiC composites.

The fabrication process based on EPD method is expected to be an effective way to control the interfaces of SiC$_f$/SiC composites and to obtain high-performance SiC$_f$/SiC composites.

Acknowledgment

This work was partially supported by The Kazuchika Okura Memorial Foundation, Ishikawa Carbon Science and Technology Foundation and JGC-S Scholarship Foundation.

Reference

[1] K. Yoshida, Y. Aoyagi, H. Akimoto, T. Yano, M. Kotani, T. Ogasawara, “Interfacial Control of Uni-Directional SiC$_f$/SiC Composites Based on Electrophoretic Deposition and Their Mechanical Properties,” *Compos. Sci. Technol.*, Vol.**72**, No.14, pp.1665-1670, September, 2012.

[2] K. Yoshida, H. Akimoto, Y. Aoyagi, M. Kotani, T. Ogasawara, T. Yano, “Interfacial Control of Uni-Directional SiC$_f$/SiC Composites Based on Electrophoretic Deposition Method,” *10th International Symposium on Ceramic Materials and Components for Energy and Environmental Applications*, Dresden, Germany, May 23, 2012.

[3] K. Yoshida, Y. Aoyagi, H. Akimoto, T. Yano, M. Kotani, T. Ogasawara, “Application of Electrophoretic Deposition For Interfacial Control of SiC$_f$/SiC Composites,” *Workshop on The Design of Ceramic-Fiber Based Composites for Service Above 1400 Centigrade*, Boulder, Colorado, USA, June 11, 2012.

B.15 Simplest Homoleptic Metal-Centered Tetrahedrons, $[M(OH_2)_4]^{2+}$, in 1-Ethyl-3-methylimidazolium Tetrafluoroborate Ionic Liquid (M = Co, Ni, Cu)

Koichiro TAKAO

1. Introduction.

Ionic liquids (ILs) consist of only molecular ions and possess unique characteristics, for instance a low melting point, very low volatility, high conductivity, and a wide electrochemical potential window. Because of these properties, ILs are regarded as alternative media in various fields, e.g., organic synthesis, electrochemical devices, and nuclear engineering.

Whole aspects on coordination and solution chemistry of metal ions (M^{n+}) in ILs are of great interest, not only in the fundamental science, but also for the multidisciplinary applications. Because such a medium comprises only completely dissociated molecular cation and anion, a strong ionic atmosphere is formed in this solvent. Furthermore, the anionic species of ILs are usually noncoordinating to M^{n+} (e.g., BF_4^-, PF_6^-) or very weakly Lewis basic (e.g., $R_fSO_3^-$, $(R_fSO_2)_2N^-$). On this basis, I wondered if a positively charged metal ion (M^{n+}) is able to be present in an IL as a naked ion without any solvation in the first-coordination sphere or appears at least as a less-solvated species.

To my best knowledge, the dehydration without successive insertion of any specific ligands has not been known for any aqua complexes, $[M(OH_2)_m]^{n+}$ so far. If this is the case for M^{n+} such as transition metals, the metal complex preparation would no longer suffer from competition between solvation and entering ligand(s). Therefore, a new strategy to synthesize functionalized metal-complexes superior to the HSAB principle could be provided. As a first step to develop this chemistry in ILs, I started from several 3d transition metal ions; Co^{2+}, Ni^{2+} and Cu^{2+}. 1-Ethyl-3-methylimidazolium tetrafluoroborate ([emim]BF_4) was selected as a IL solvent in this study because of non-coordinating character of BF_4^-.

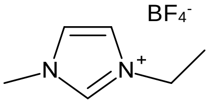

[emim]BF_4

2. Results and Discussion

Tetrafluoroborate or perchlorate salts of 3d-metal hexahydrated cations $[Co(OH_2)_6]^{2+}$, $[Ni(OH_2)_6]^{2+}$, and $[Cu(OH_2)_6]^{2+}$ were dissolved in H_2O and [emim]BF_4. The dissolution of the M^{2+} salts in the latter solvent was accelerated by heating under reduced pressure. During this process, vigorous evolution of water vapor was detected. Photographs of these solutions are displayed in Fig. 1. For each M^{2+}, the significant change and increasing intensity in color from the aqueous solution to [emim]BF_4 were observed; i.e., Co^{2+}: pink (aq) → sky blue ([emim]BF_4); Ni^{2+}: pale green (aq) → navy blue ([emim]BF_4); Cu^{2+}: pale blue (aq) → greenish yellow ([emim]BF_4). Such a remarkable solvatochromism clearly indicates that the structure of the first-coordination sphere around M^{2+} is completely different from that in aqueous solution, where M^{2+} occurs in octahedral coordination as $[M(OH_2)_6]^{2+}$. It is noteworthy that the only possible ligand in [emim]BF_4 is H_2O originating from the hydrated water in the starting salt, because the anionic component of the IL used here, BF_4^-, is regarded as a noncoordinating anion. Such color change could arise from the modification of the hydrated structure around M^{2+} in [emim]BF_4.

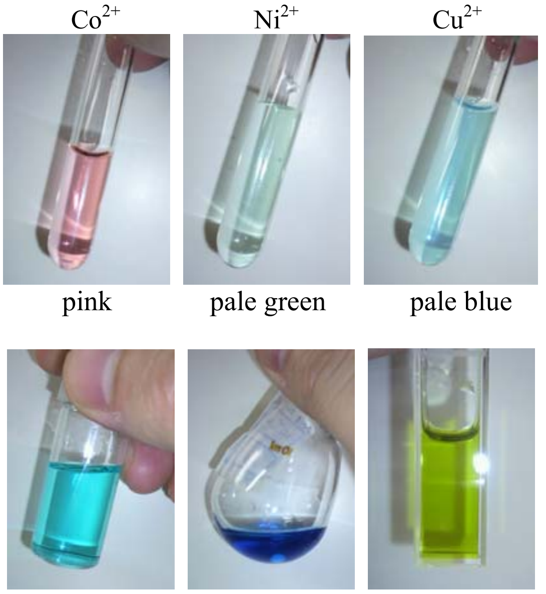

Fig. 1 Photographs of several 3d transition metal ions in H_2O (top) and [emim]BF_4 (bottom).

A UV-vis absorption spectrum of Co^{2+} in [emim]BF_4 shows strong bands at around 600-700 nm with ε = 550-570 $M^{-1}\cdot cm^{-1}$ at the peak maxima. These characteristic color and absorption spectrum of Co^{2+} indicate that the most plausible structure around Co^{2+} in [emim]BF_4 is tetrahedral (T_d) arrangement of water molecules, i.e., $[Co(OH_2)_4]^{2+}$. The well-resolved fine structure of the absorption band in [emim]BF_4 also suggests that the occurring Co^{2+} species forms the simple and homoleptic coordination. The similarly structured spectrum is known for the tetrachloro complex, $[CoCl_4]^{2-}$, which is also homoleptically four-coordinated in T_d geometry.

For the moment, trial to isolate a crystalline Co^{2+} salt from $[emim]BF_4$ is not successful. Instead, a Co K-edge extended X-ray absorption fine structure (EXAFS) spectrum was measured to extract the structural information of Co^{2+} in $[emim]BF_4$. As a result, it was clarified that Co^{2+} is surrounded by 4.2 O atoms with a Co–O distance of 2.17 Å, corroborating the T_d structure of $[Co(OH_2)_4]^{2+}$.

Solvation in the second-coordination sphere of the T_d $[Co(OH_2)_4]^{2+}$ in $[emim]BF_4$ is also of interest. This tetraaqua species has seven d-electrons, and results in $e^4t_2^3$ electronic configuration with $S = 3/2$ at the ground state, i.e., paramagnetic. Therefore, ^1H and ^{19}F NMR spectra of $[emim]^+$ and BF_4^- will be affected by this paramagnetism, providing the information of the second-coordination structure around $[Co(OH_2)_4]^{2+}$ in $[emim]BF_4$. As a result, a single pair of ^{19}F signals arising from $^{10}BF_4^-$ and $^{11}BF_4^-$ isotopomers has been observed at 3.88 and 3.93 ppm (vs. $^{11}BF_3{\cdot}Et_2O$) in the presence of $[Co(OH_2)_4]^{2+}$. This signal pair is significantly shifted to downfield by 625 Hz compared to the neat $[emim]BF_4$ (2.55 and 2.60 ppm vs. $^{11}BF_3{\cdot}Et_2O$). The former observation implies that the chemical exchange of BF_4^- in the second-coordination sphere with that in bulk is very rapid in the NMR time-scale. The paramagnetic shift ($\Delta\nu$) is regarded to arise only from the pseudocontact shift between BF_4^- and $[Co(OH_2)_4]^{2+}$ because of the poor coordinating character of BF_4^- to M^{n+}. The large paramagnetic shift of the ^{19}F signals of BF_4^- could be reasonable, because the positively charged $[Co(OH_2)_4]^{2+}$ attracts the negatively charged BF_4^- by the electrostatic interaction.

In the ^1H NMR spectra of the same solution, the paramagnetic downfield shifts similar to ^{19}F were also recognized for all the signals of $[emim]^+$. The magnitude of the shift of each signal is ranging 611-632 Hz, which is almost the same as that of BF_4^-. This is somewhat surprising because strong electrostatic repulsion was expected between $[Co(OH_2)_4]^{2+}$ and $[emim]^+$, and therefore the tetraaqua complex was predicted to be exclusively surrounded by BF_4^- rather than $[emim]^+$. The actual result implies that $[emim]^+$ also enters the second-coordination sphere of $[Co(OH_2)_4]^{2+}$ with the similar lifetime to stay there, because $\Delta\nu$ rapidly decreases as a function with the third power of the distance from the paramagnetic Co^{2+} center as long as the lifetimes of the cation and anion in the second-coordination sphere are the same. Therefore, one can imagine that both $[emim]^+$ and BF_4^- are randomly arranged around $[Co(OH_2)_4]^{2+}$.

Cu^{2+} in $[emim]BF_4$ was also examined by the same experiments. The intense greenish yellow color of Cu^{2+} in $[emim]BF_4$ results from a strong absorption at 400 nm with $\varepsilon = 1580\ M^{-1}{\cdot}cm^{-1}$, while a weaker and broader band centered at 900 nm ($\varepsilon = 190\ M^{-1}{\cdot}cm^{-1}$) is also lying. Furthermore, from the Cu K-edge EXAFS spectrum, it was suggested that 3.8 O atoms bind to Cu^{2+} with a distance 2.09 Å in $[emim]BF_4$. By comparing these findings with the much weaker blue color of $[Cu(OH_2)_6]^{2+}$ in aqueous solution ($\lambda_{max} = 800$ nm, $\varepsilon = 10\ M^{-1}{\cdot}cm^{-1}$), it can be concluded that the T_d $[Cu(OH_2)_4]^{2+}$ is also formed in $[emim]BF_4$. In line with the former reports on $[CuCl_4]^{2-}$, the $[Cu(OH_2)_4]^{2+}$ tetrahedron in $[emim]BF_4$ might be somewhat flattened. The four-coordinated Cu^{2+} usually prefers a square planar (*SP*) geometry because of the Jahn-Teller effect in d^9 electronic configuration. In contrast, $[Cu(OH_2)_4]^{2+}$ in $[emim]BF_4$ tends to be in the T_d coordination despite unlikelifood of the considerable steric crowding in the first coordination sphere. The preferred T_d form rather than *SP* is convincing from a viewpoint of uniform charge distribution around $[Cu(OH_2)_4]^{2+}$ immersed in the strong ionic atmosphere of $[emim]BF_4$. The paramagnetic shift for BF_4^- (108 Hz) is not very different from those for $[emim]^+$ (84-105 Hz), implying the random arrangement of $[emim]^+$ and BF_4^- in the second-coordination sphere of $[Cu(OH_2)_4]^{2+}$.

The study on Ni^{2+} in $[emim]BF_4$ was just started, and only the significant solvatochromism and color intensification displayed in Fig. 1 were confirmed at the moment. Combining this fact and the general trend found in Co^{2+} and Cu^{2+}, a similar T_d $[Ni(OH_2)_4]^{2+}$ can be reasonably expected to occur in $[emim]BF_4$. This hypothesis is also in line with the former isolation of blue-colored T_d Ni^{2+} complexes, $NiX_2(OAsPh_3)_2$ (X = Cl, Br).

3. Conclusion

In this study, solvation of Co^{2+}, Ni^{2+} and Cu^{2+} in $[emim]BF_4$ ionic liquid was investigated. In all the cases of M^{2+} studied, the starting hexahydrated M^{2+} exhausts 2 water molecules in $[emim]BF_4$, resulting in the tetrahedrally coordinated $[M(OH_2)_4]^{2+}$ as monitored by the significant solvatochromism and increasing intensity of the color. Although other homoleptic tetrahedral species have already been known (e.g., $[CoCl_4]^{2+}$), the tetraaqua 3d metal complexes in T_d symmetry are most fundamental in the coordination chemistry and observed for the first time in the present study.

Reference

K. Takao, Y. Tone, C. Hennig, S. Inoue, T. Tsubomura, *Inorg. Chem.*, Vol.**51**, pp. 4850-4854 (2012).

C.1 Progress in Innovative Nuclear Reactor Study

Toru OBARA

Several Studies on innovative nuclear reactors have been performed. It is intending to give concepts of nuclear reactors for various demands and needs for future.

1. Design study of pebble bed reactor with accumulating fuel loading scheme

Neutronic analysis were performed for the small simplified pebble bed reactors with accumulating fuel loading scheme and it was shown that the use of thorium fuel improve performance to utilize natural uranium resources effectively [1].

2. Study of space-dependent kinetic analysis method in weakly coupled systems

The new method has been developed for the space-dependent kinetic analysis in weakly coupled systems. For such systems, conventional one-point reactor kinetic analysis method cannot be applied. It was shown the new method can analyze such transient behavior in super prompt condition successfully [2].

3. Design study of small reactor for semiconductor production

A small reactor for NTD-Si was proposed in the study. In the study, conventional PWR full length fuel assemblies were used in the core. It is intended to irradiate 12 inches silicon ingots. It was shown the reactor can achieve high production rate of silicon semiconductors by using full length PWR fuel assemblies [3, 4, 5].

4. Design concept of small long life reactor for Mongolia

A small reactor using fuel element for High Temperature Gas-cooled Reactor (HTGR) was studied for electricity supply and district heating. Several parametric surveys were performed for the passive safety features and for long core life [6].

5. Study on thermal neutron filter for NTD-Si irradiation

To improve the performance in NDT-Si irradiation by research reactors, the concept of thermal filters using B_4C particles were proposed and the analysis to improve the burnup performance was performed [7].

6. Study on graphite fuel assemblies for HTGR with oxidation resistance

SiC coating on the graphite structure in HTGR is a promising method to prevent the oxidation of graphite structure in the core during accidents. Several analyses have been performed to investigate the effect on the neurotic and thermal hydraulic performances by the coating [8].

7. Study on particle type burnable poisons

In long-life prismatic HTGR, it is important to compensate excess reactivity effectively. The performance of particle type burnable poisons were analyzed. It was shown it would be effective for it by the optimization of material and designs of the particles [9].

8. Development of burnup analysis code for OTTO cycle in Pebble Bed Reactors

The development of burnup analysis code for Once Through Then Our (OTTO) refueling scheme in Pebble Bed Reactors was performed. The code is based on the Monte Carlo neutron transportation calculation method, which enable exact treatment of geometry of fuel elements and large void in the core [10].

9. Fundamental study for nuclear pumped laser system

Preliminary study for Numerical simulation of laser oscillation in nuclear pumped laser [11] and the application to inertial confinement fusion reactor [12] were studied.

REFERENCES

1. Dwi Irwanto, Toru Obara, *J. Nucl. Sci. Technol.*, **49** [2], 222-229 (2012).
2. Hiroki Takezawa and Toru, Obara, *Nucl. Sci. Eng.*, **171**, 1-12 (2012).
3. Byambajav Munkhbat, Toru Obara, *J. Nucl. Sci. Technol.*, **49** [5], 535-543 (2012).
4. Byambajav Munkhbat, Toru Obara, *J. Nucl. Sci. Technol.*, **49** [8], 845-856 (2012).
5. Byambajav Munkhbat, Toru Obara, *Trans. Am. Nucl. Soc.*, **106**, 826-829 (2012).
6. Odmaa Sambuu, Toru Obara, *Annals. Nucl. Energy*, **47**, 210-215 (2012).
7. Masao Komeda, Toru Obara, *Annals. Nucl. Energy*, **53**, 35-39 (2012).
8. Piyatida Trinuruk, Toru Obara, *Trans. Am. Nucl. Soc.*, **107**, 1262-1263 (2012).
9. Toru Obara, Taiki Onoe, *Trans. Am. Nucl. Soc.*, **107**, 1023-1024 (2012).
10. Topan Setiadipura, Toru Obara, 2012 Fall Meeting of Atomic Energy Society of Japan, C39 (2012).
11. Yosuke Isobe, Toru Obar, 2012 Annual Meeting of Atomic Energy Society of Japan, D51 (2012).
12. Takehiko Tomonari, Toru Obara, 2012 Annual Meeting of Atomic Energy Society of Japan, D50 (2012).

C.2

Start-up Analysis of CANDLE Burnup Reactors by using Accelerator Neutron Sources

Jun NISHIYAMA and Toru OBARA

1. Introduction

The CANDLE burn-up fast reactor by using accelerator neutron sources has a potential to build a system without enrichment and reprocessing plants. The CANDLE (Constant Axial shape of Neutron flux, nuclide densities and power shape During Life of Energy producing) burn-up strategy was proposed[1,2], which does not require a burnup reactivity control instrument such as a control rod, chemical control. For this burn-up strategy, distributions of fuel nuclide densities, neutron flux and power density move with the same constant speed and without any change in their shapes. When the CANDLE burnup strategy is applied to neutron rich fast reactors, only natural or depleted uranium is enough for the fresh fuel after the second cycle. However, this strategy has two problems. One is how to consist an initial core leading to equilibrium CANDLE burnup, the other is a restart problem caused by decay of ^{241}Pu during a shutdown period.

The system using accelerator neutron sources as an external source can solve these problems. As shown in Figure 1, this system is operated in early stage as a sub-critical transmutation reactor with a natural or depleted uranium initial core. During this stage, effective neutron multiplication factor is increasing. After reaching a critical, it is operated as a CANDLE burnup reactor without the external source.

The purpose of this work is to clarify the requirements and characteristics of the external source. The calculation results of the neutron flux, irradiation time and its energy dependence are reported.

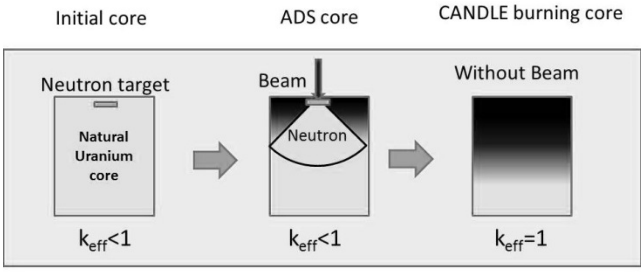

Fig. 1 Start-up of CANDLE burn-up reactor by accelerator neutron source

2. Calculation method

The calculations were carried out in the one-dimensional plane geometry for homogeneous reactor with the natural uranium metallic fuel, Lead-Bismuth coolant and constructional materials. Neutron group constants were obtained using PREPRO code[3] with JENDL-4.0[4] nuclear data library. For the burnup calculation, 4th order Runge-Kutta numerical method was used. For the flux calculation, we assumed that flux consists of external and fission neutrons as follows;

$$\begin{aligned}\phi &= \phi_s + k_s\phi_s + k_s k_f \phi_s + k_s k_f^2 \phi_s + k_s k_f^3 \phi_s + \cdots \\ &= \phi_s\left(1 + \frac{k_s}{1-k_f}\right) \qquad (1)\end{aligned}$$

where ϕ is the total flux, ϕ_s is the external flux, k_s and k_f are multiplication factor for external and fission neutrons, respectively.

3. Results

Figure 2 shows the calculated result of operation time for reaching a critical with external neutron flux $\phi_s = 10^{15}$[1/(cm^{2}s)]. In the energy range of 1-10 keV and range higher than 1 MeV, reactor reaches a critical within several hundred days. Otherwise reactor couldn't be a critical in the thermal energy region.

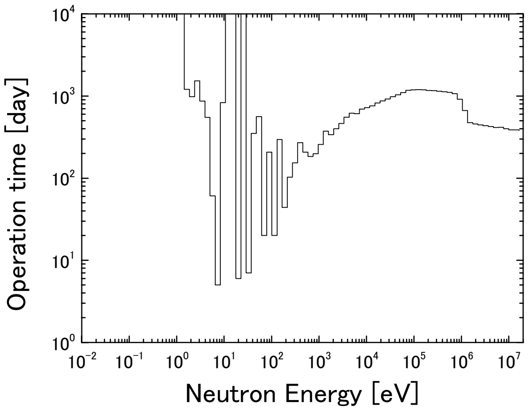

Fig. 2 Operation time for reaching a critical

4. Conclusion

For start-up analysis of the CANDLE burn-up reactor by accelerator neutron sources, characteristics of external neutron energy were simulated. Good conversion efficiency was derived in energy range of 1-10 keV and range higher than 1 MeV.

Reference

[1] H. Sekimoto, K. Ryu, Y. Yoshimura, "CANDLE: the new burnup strategy" *Nucl. Sci. Eng.*, **139**, 306-317 (2001).

[2] H. Sekimoto, "A Review of CANDLE Burn-up in Nuclear Reactors," *International Journal of Integrated Energy Systems*, **1**, 80-91 (2009).

[3] PREPRO2012,http://www-nds.iaea.or.at/ndspub/endf/prepro

[4] K. Shibata, *et al.*, JENDL-4.0: A New Library for Nuclear Science and Engineering. *J. Nucl. Sci. Technol.* **48**, 1-30 (2011).

C.3 Positional Stabilization of Torus Plasma with Simple Helical Coils

Shunji TSUJI-IIO and Hiroaki TSUTSUI

In tokamaks, elongated plasmas for good confinement suffer from so-called vertical displacement events (VDEs) during disruptions. On the other hands, it has been shown that the plasma position is robustly stable in a current-carrying stellarator, whereas that in an equivalent tokamak is unstable.1) In order to suppress VDEs, we proposed saddle shaped stellarator system, which is composed of four coils on the outside of a vacuum vessel.2) The objective of our study is to investigate the principle and to improve the configuration of the coils for vertical stability experimentally.

We designed and started constructing a small tokamak device shown in Fig. 1 ($R = 0.33$ m, $a = 0.09$ m, $B_t = 0.3$ T) which has an elongated cross section to demonstrate above mentioned effect. Firstly, we optimized the numbers and size of the toroidal field coils to reduce the toroidal field ripple. To evaluate the effect of the iron core on the magnetic fields, magnetic field analysis using the finite element method (FEM) was performed. In this device, the plasma region on the midplane is set in the range where the ripple ratio is less than 2%. Then, the shape and arrangement of the vacuum vessel with a rectangular cross-section were determined under the condition of possible confinement of plasmas with $\kappa = 1.8$. Figure 2 shows a newly manufactured vacuum vessel. We also confirmed the soundness of the coils support structure by stress analysis. A strength test on a prototype coil was performed.

Secondly, we investigated the configuration of poloidal magnetic field coils. As a result of axisymmetric MHD equilibrium calculations, we found that elongated divertor configurations up to 1.8 are feasible even with a simple combination of four PF coils (Fig. 3). In addition, we confirmed that a plasma with circular cross-section can be generated which is stable both vertically and horizontally. This result was supported by evaluation of the distribution of the magnetic field decay n-index which is an indicator of positional stability. To investigate current ramp up scenarios, we are simulating discharge evolutions with the tokamak simulation code (TSC).

Thirdly we tested a small induction generator with a flywheel for the poloidal magnetic field power supply. The voltage was demonstrated to be maintained within 10% drop even under three times the rated load during required periods for tokamak experiments (~ 20 ms).

References

1) H. Ikezi, K. F. Schwarzenegger: *Phys. Fluids,* **22**, 2009 (1979).

2) S. Hatakeyama *et. al.*, P1.046, EPS/IPCC2012, Sweden, 2012.

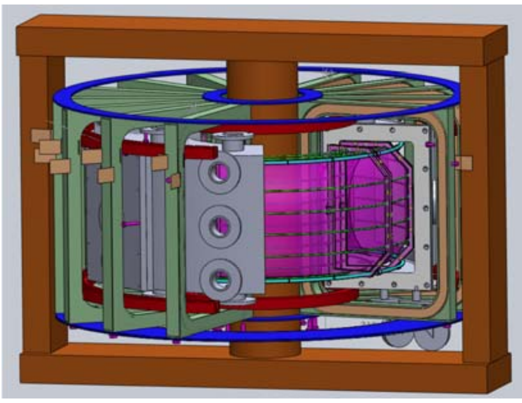

Fig. 1 Schematic illustration of the tokamak device under contruction

Fig. 2 Picture of the vacuum vessel with rectangular cross-section

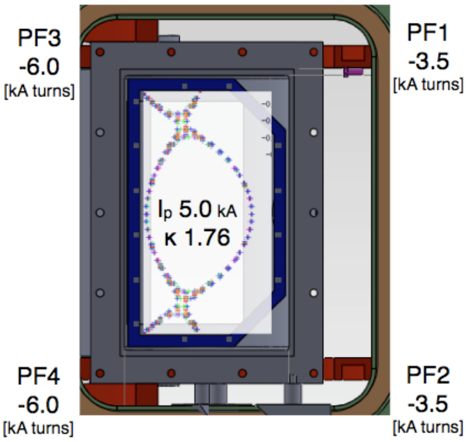

Fig. 3 An example of PF coil currents and MHD equilibrium configuration.

C.4 Nuclear Energy for Human Security

- Bridging between the peaceful use of nuclear energy and the abolition of nuclear weapon -

Tetsuo SAWADA

1. Introduction – Nuclear energy for a sustainable peace

In continuously fluctuating global circumstances, we are forced to face with a variety of disputes including terrors and wars. A sustainable peace will come following a peace building when dispute or war has come to an end. Japan is such a country. The end of the Second World War came with two atomic bomb bombardments at Hiroshima and Nagasaki. Since then, we have not gone into war for almost 70 years. It should be a good example of a sustainable peace. It is often addressed, however, a peace under the nuclear umbrella. Without a prepared troops for actions, the sea-lane defense is a good example among others that can never be protected against attacks on a tanker which transports oils from the Near and Middle East countries to Japan.

In such circumstances, it must be a crucial issue how we can position the value of the nuclear energy especially for the peaceful use. It is a point of discussion how the promotion of nuclear energy use including radiation application can be correlated with the sustainable peace. Here is a thesis that the nuclear energy use must contribute to the process of building peace as well as keeping the sustainable peace. This thesis is the essence that the nuclear energy must promote the human security.

2. Change in governance – Comprehensive global governance and human security

About four hundreds years ago, a book "Leviathan" was written by Thomas Hobbs and published in 1651. In the book, he wrote that the objective of Commonwealth, i.e., a nation, is to produce the peace and security of the people. The purpose of a commonwealth is described as follows:

> *The final cause, end, or design of men (who naturally love liberty, and dominion over others) in the introduction of that restraint upon themselves, in which we see them live in Commonwealths, is the foresight of their own preservation, and of a more contented life thereby; that is to say, of getting themselves out from that miserable condition of war which is necessarily consequent, as hath been shown, to the natural passions of men when there is no visible power to keep them in awe, and tie them by fear of punishment to the performance of their covenants....*

In a word, the objective of a nation is to secure the self-preservation and more contented life thereby. This is still true in the present global circumstances. However, here is a difficult situation that the conventional security structure has been collapsing and the global society is showing more or less anarchical aspects. We are faced with 6 categories of global threats under the circumstance:

- Wars, disputes, international terrorism,
- Corruption of nations and internal conflicts,
- Increasing death by infectious disease, such as swine flu,
- Drug,
- Environmental disruption, and
- Infringement of human rights.

Then we need multilateral measures under two conditions:

Condition 1: The global threats come over the borders, so that traditional domestic risk and security management scheme can not well cope with them. They are beyond the nation-wise capability. The reason why is a nation gives usually priority to the national interests.

Condition 2: The role of non-government organization (NGO)/non-profit organization (NPO) will be much more important and effective because they can cope flexibly with specific issue beyond national interest.

Here is a requirement. To cope with such conditions, beyond the conventional (domestic, inter-nations) governance frame, we have to shape **"Comprehensive Global Governance"** where organizations other than governments, i.e., NGO/NPO can also cooperatively join to make the frame

Various values and behavioral principles should be cultivated in the fields of environment, development, prevention of conflicts, asylum of refugees, dissolution of poverty, that can shape the new type of global governance in which **the concept of "human security" must be implemented as the most importantly *shared interest*.**

We need to advance from concentrated governance to shared governance, that is, the comprehensive governance. Thus the building the Comprehensive Global Governance can be a basis of promoting Human Security. Table 1 shows the comparison between the conventional national security and the human security.

Table 1 Comparison between national security and human security

	Subject	Object	Threat	Measure	Purpose
Conventional (National) Security	nation	Domestic people	From abroad	armaments diplomacy	Sustaining nation's sovereignty, Securing domestic people's right to life
Human Security	**nation** **NGO's** **International organizations**	Human being	**· Wars/conflicts** **· Displacement** **· Hunger/ poverty** **· Oppression on human rights** **· Environmental disruption**	**· Preemptive diplomacy** **· Humane intervene** **· Humane support** **· Social integration** **· Human development**	Securing life and dignity of human being

Complex Governance

Multi-layered subjects

Externality + Internality

Comprehensive covering of related issues/threats

If we still want to promote the peaceful use of nuclear energy, we have to cultivate the way to harmonize the nuclear energy with the human security. For this purpose it is in the first priority and prerequisite to bridge between the promotion of the peaceful use of nuclear energy and the abolition of the nuclear weapons.

3. Human Development and Components of human security

Now we can measure the degree of human security by "human development index (HDI)", that was first reported in Human Development Report by UNDP in 1994. The human development index is the normalized measure of **life expectancy, literacy, education, standard of living, and GDP per capita** for countries in the world.

It is a standard mean of measuring well-being, especially child welfare. It is used to determine and indicate whether a country is a developed, developing, or an underdeveloped country. It is also used to measure the impact of economic policies on quality of life. Here is the origin of the basic idea for the human security. What is the human security more practically? Here we show the seven componential issues of human security.

○ Issue 1: Freedom from poverty (Economic security),
○ Issue 2: Freedom from starvation (Food security),
○ Issue 3: Freedom from disease (Health care security),
○ Issue 4: Securing water and air (Environment security),
○ Issue 5: Freedom from violence and drug (Personal security),
○ Issue 6: Freedom from domestic and ethnic subordinate (Regional security), and
○ Issue 7: Securing fundamental human right (Political security).

Securing these issues are the basis of human security.

4. Is nuclear energy viable for human security?

Nuclear energy as an engine for improving the human security --- this thesis is the purpose of us who have been advocating the peaceful use of nuclear energy.

Among the above-mentioned 7 issues, nuclear energy and radiation application have substantial effects on them. The supplement of electricity can surely improve human life. The electricity produced by nuclear energy is not just for lightning daily life but enhancing people's welfare. Various kinds of radiation application contribute to improve the agricultural conditions, for instance, the improvement of species of crops. At the medical setting, the application of radiation has supported lots of practically effectiveness. Nuclear desalination can produce plenty of safe portable water, and so far we have enough actual practice and results to produce pure water by nuclear energy. Comparing to fossil fuel electricity generation systems, nuclear electricity does produce very few of air pollution materials and carbon dioxide.

Therefore, the peaceful use of nuclear energy must more or less contribute to securing the upper four issues from the seven dimensions.

As long as we insist the effective use of nuclear energy on enhancing human security, we are required to draw a picture how nuclear energy can contribute the personal, regional and political security. We are asked to respond this requirement.

5. Summary

We are going for “philanthropical dedication” to Human Security. What can we do through nuclear energy including radiation applications? We need shape it and then practice it. Based on the culture by nuclear energy, we should establish a new type of “*Global Shared Governance*” opportunity for a creative life with healing. Non-governmental and/or non-profitable activity or organization can have a helpful function for shaping the opportunity.

Our challenge is to make the viable way of nuclear energy to be dedicated to enhancing Human Security.

C.5 Effect of Neutron Moderator on Protected Plutonium Production in Fast Breeder Reactor Blanket

Hiroshi SAGARA, Chi Young HAN and Masaki SAITO

1. Introduction

In order to prevent the production of plutonium with a high purity of ^{239}Pu in the blanket of a conventional fast breeder reactor (FBR), protected plutonium production (P^3) with a high proliferation-resistance was proposed by increasing the ^{238}Pu ratio in the total plutonium through minor actinides (MAs) doping into the fresh blanket fuel **[1]**.

Loading moderator to the blanket is very effective for P^3 because principal nuclides of MAs, such as ^{237}Np and ^{241}Am in spent nuclear fuel, have large capture cross-sections in thermal to epithermal neutron energy. Moderator effect on P^3 was has been evaluated previously as showing the potential effectiveness of moderator by a simple calculation model with homogeneous material composition inside the assembly **[2]**. The recent research showed that heterogeneous moderator is potentially more effective on P^3 in blanket fuel pin because of 1) the higher resonance escape probability from ^{238}U, 2) the enhancement of neutron capture reaction of ^{237}Np and ^{241}Am with moderated neutrons **[3]**.

This paper is the summary of the paper **[4]**, to confirm the effect of neutron moderator in FBR blanket quantitatively by comparing geometrical loading pattern with 3-dimensional full-scope FBR core with precise pin-by-pin assembly model to simulate geometrical self-shielding effect correctly, and proposing a radial blanket design suitable for P^3 from the view point of MA transmutation to even-mass-number plutonium isotopes and fissile plutonium breeding.

2. Methodology

First of all, the comparison between heterogeneous and homogeneous moderator was performed. Secondly, the number and the loading pattern of moderator pins were optimized inside the radial blanket assembly. Finally, the proliferation resistance of Pu in the radial blanket was evaluated by calculating the “Attractiveness” of Pu based on its isotopic composition.

The core specifications were referred to from a sodium-cooling FBR (3.57GWth) design**[5]**. At first, CITATION, a diffusion code with fuel burnup function, was used to compare with the previous researches by the same methodology, investigating P^3 and proliferation resistance. Then, MVP and MVP-BURN, a general purpose Monte Carlo code for neutron and photon transport calculation and the function of burnup, were used for a detail and precise calculation in the radial blanket to evaluate the heterogeneous model effect **[6, 7]**. In the present paper, the results only with MVP and MVP-BURN are discussed in the next section. Figure 1 shows the calculation model of MVP. The blanket is constituted of fuel pins, composed of UO_2 (^{235}U: 0.2wt% and ^{238}U: 99.8wt%) with MA from PWR spent fuel (5%EU, 50GWd/tHM, five years cooling) pellet and SS cladding, and moderator pins, $ZrH_{1.65}$ rod with SS cladding, partly by replacing some fuel pins in the present paper. The number and position of fuel and moderator pins in the radial blanket fuel assembly were taken as parameters.

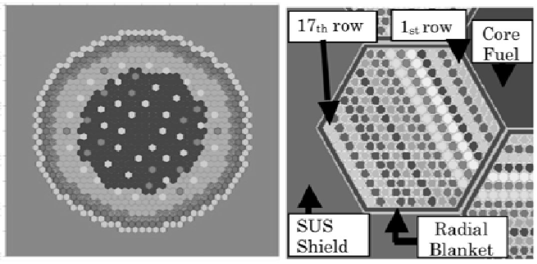

(a) Core (b) Radial Blanket

Fig.1. Calculation model of MVP

3. Results

It is noted that the heterogeneous moderator leads to more resonance escape of neutrons from ^{238}U than the homogenous one, and therefore a larger capture reaction of MAs. Figure 2 shows the transmutation ratio, defined as

$$Transmutation\ Ratio \equiv \frac{Atomic\ Density\ {}^{238}Pu\ at\ EOC\ in\ the\ radial\ blanket}{Atomic\ Density\ {}^{237}Np{+}^{241}Am\ at\ BOC\ in\ the\ radial\ blanket} \quad (1),$$

and the isotopic ratio of ^{238}Pu at EOC. The transmutation ratio is larger with the heterogeneous moderator than with the homogeneous one, and the isotopic ratio of ^{238}Pu was increased by the smaller capture reaction of ^{238}U as well as the larger transmutation ratio. It confirms the more effectiveness of heterogeneous moderator on P^3.

Figure 3 shows the transmutation ratio and fissionable Pu inventory ratio (FPIR), defined as

$$FPIR \equiv \frac{Mass\ {}^{238}Pu, {}^{239}Pu, {}^{241}Pu\ at\ given\ irradiation\ period}{Mass\ {}^{238}Pu, {}^{239}Pu, {}^{241}Pu\ at\ BOC}$$
(2),

because it is assumed that produced Pu would be recycled and utilized for incineration in Fast Reactor core and ^{238}Pu works as fissile nuclide there, this figure of merit includes ^{238}Pu, taking into account its fissile characteristics.

From the parametric investigations into the number and position of the moderator pins examples shown in Fig.4, it was revealed that the application of about 2800 moderator pins to all radial blanket assemblies satisfies both the FPIR more than 1.02, a reference value without any moderator pins, and the transmutation ratio as high as possible. In addition, it was found that the pin arrangement with a proper distance is more effective than the dense or aligned ones for higher transmutation ratio, FPIR, and ^{238}Pu uniformity.

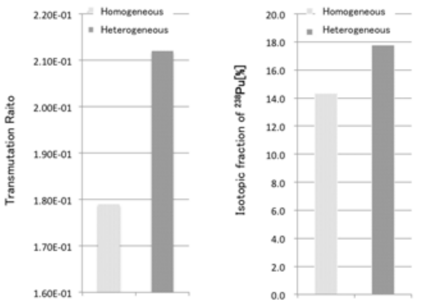

Fig. 2. Transmutation ratio, isotopic ratio of ^{238}Pu at EOC

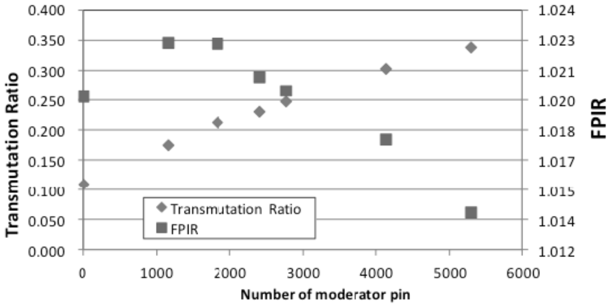

Fig.3. Transmutation ratio and FPIR with the number of moderator pins

Reference

1. M. Saito, *Int J Nucl Energy Sci Technol*, vol. **1**[2&3], pp.127-138, 2005.
2. Y. Meiliza, M. Saito and H. Sagara, *J. Nucl. Sci. Technol.*, Vol **45**, No.3, pp.230-237, 2008.
3. H. Sagara, S. Koyama, and M. Saito, *Prog. Nucl. Energy*, vol. **53**, no. 7, p. 952-957, 2011.
4. K. Matsumoto, H. Sagara, C. Y. Han, T. Ohnishi, M. Saito, I. Yamauchi, *Trans. Ame. Nucl. Soc.*, vol. **107,** no. 1, p 1018-1019 2012.
5. M. Naganuma et al. *JNC TN9400 2005-051*, (2005), [in Japanese]
6. Y. Nagaya, et al., *JAERI 1348*, (2004).
7. K. Okumura, et al., *J. Nucl. Sci. Techonol*, (2000).

C.6 Sensitivity Analysis of Low-Volatile FPs and Cm-244 Inventory in Irradiated Nuclear Fuel for Special Nuclear Material Accountancy in Fuel Debris

Hiroshi SAGARA

1. Introduction

Even in the case of severe accident such as in TMI-2 or Fukushima Dai-ichi nuclear power plant, special nuclear material (SNM) accountancy in molten core material is important and required by national/international regulatory body to assure no diversion of SNM. In TMI-2 experience, passive gamma spectroscopy of Ce-144/Pr-144, as one of the multiple technologies, was utilized to quantify SNM in fuel debris, because fission products (FPs) such as Eu, Ce, Ru have low release ratios under the condition of severe accident core melting, and co-exist inside fuel debris in oxide or metallic phases [1,2].Passive neutron measurements have also been used to quantify or verify nuclear material by coupling the measurement of spontaneous fission neutrons from Cm-244 with its ratio to Pu for quantifying SNM in spent nuclear fuel [3]. Though these passive photon/neutron measurements are conventional and robust technologies, measurement of SNM in fuel debris as a result of an accident presents different challenges than that of conventional spent fuel because some information such as irradiation profiles, release ratios of volatile FPs, and so on, would not be available. In the present paper, a sensitivity analysis of the inventory ration of low-volatile FPs and Cm-244 to SNM in conventional BWR irradiated fuel was performed numerically to determine the uncertainties of the ratio of low-volatile FPs and Cm to SNM for selected fuel irradiation parameters and calculation methodologies, in order to derive applicable indices to quantify SNM in fuel debris, by summarizing the author’s publication [4].

2. Methodology

A broad parametric survey of inventory was conducted using simple but well qualified generation/depletion calculation codes ORIGEN2.2 and ORIGEN-ARP with cross-section set, ORLIBJ40 based on JENDL4.0, A parametric survey using fuel irradiation parameters derived from the open literature [5] was performed. Finally, the inventories of FPs and Cm to Pu ratios and their uncertainties were analyzed for possible use in nuclear fuel quantification.

3. Results

For the BWR example, inventory calculations were performed assuming typical fuel assembly parameters with average enrichment of 3.01wt% UO_2 fuel with axial distribution of void fraction, power density, fuel enrichment, and relative burnup. In **Fig. 2**, the results of the Eu-154/Pu ratio are summarized. The ratio increases monotonically with burnup in each cycle fuel. While the production of Eu-154 or Pu-239 has a large variance mainly due to the axial neutron spectrum profile variance in BWR fuel, the variance is off-set by taking the ratio of Eu-154 to Pu, and the standard deviation (σ) from the approximate formula is less than 4%. Because production of both Eu-154 and Pu-239 is primarily affected by epi-thermal energy neutron absorption by precursors, Eu-153 and U-238 resonances, respectively, the sensitivity of the neutron spectrum to their production is quite similar for both nuclides. For comparison, PIE results of 3.9% EU fuel pins, discussed in **Fig. 1**, were plotted with black circles. PIE results demonstrate a good fit with the approximation formula derived from the 3.01% EU assembly analysis, and the ratio sensitivity to enrichment was shown to be small.

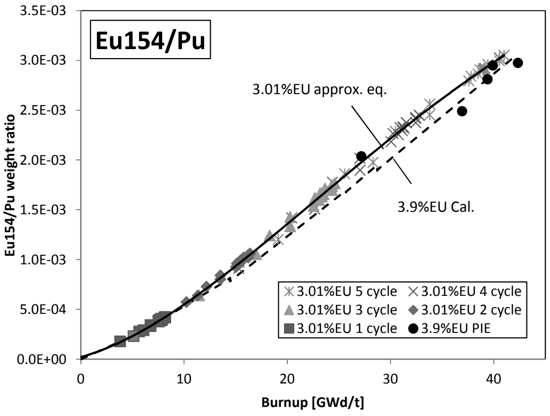

Fig. 2 Sensitivity of Eu-154/Pu ratio to initial enrichment, neutron spectrum, power density, in typical BWR fuel

Figure 3 shows the results of the axial profile of Eu-154/Cs-134 weight ratios in spent fuel for different irradiation cycles in a typical BWR fuel assembly. The ratio remains at a nearly constant value with σ <10% caused mainly by the differences in power density due to the similarity of the production mechanisms of two neutron absorptions, U-235(n,f) -> Eu-153/Cs-133(n,g) -> Eu-154/Cs-134. Compared with the PIE results of 3.9% EU, plotted as black circles, the ratio fits the results of the 3.01% EU assembly, and sensitivity to initial enrichment was low. This ratio might be utilized to estimate the release ratio of Cs from fuel debris that could be obtained by passive gamma spectrometry.

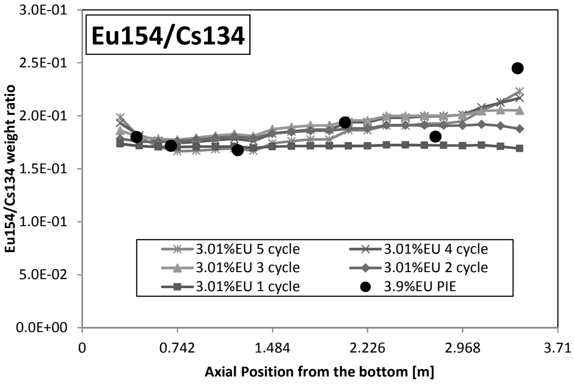

Fig. 3 Eu-154/Cs-134 ratio axial distribution in typical BWR fuel

Figure 4 shows the results of the ratio of the Cm-244/Pu weight ratio in spent fuel in a typical BWR fuel assembly for different irradiation cycles. The ratio increases exponentially with respect to burnup in each cycle. The variance was observed in Cm-244/Pu ratio with σ 10~16% in the specific burnup, mainly because of the variance of the neutron spectrum in BWR axial profile. Compared with the PIE results of 3.9% EU, plotted with black circles, it is observed that the ratio is sensitive to initial enrichment, therefore exact enrichment information would be required to use the ratio as an index to quantify the fuel material.

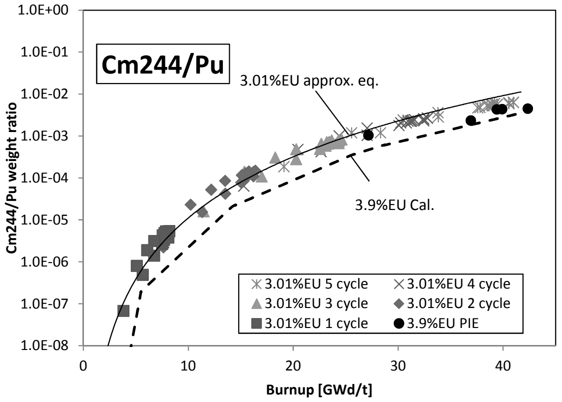

Fig. 4 Sensitivity of Cm-244/Pu ratio to initial enrichment, neutron spectrum, power density, in typical BWR fuel

SUMMARY

Sensitivity analysis of inventory ratio of low-volatile FPs and Cm-244 to SNM in conventional BWR irradiated fuel was performed numerically in order to derive applicable indices to quantify SNM in fuel debris.. Comparing with TMI-2, a PWR with 1st irradiation cycle fuels loaded, broader neutron spectrum axial profile and irradiation cycle complexity of typical BWR fuel assemblies make more variance of inventory estimation, but the better calculation predictably can be expected by significant improvement of nuclear data and codes. The Eu-154/Pu ratio has a small uncertainty ($1\sigma < 9\%$) in a specific burnup for a typical BWR fuel assembly and calculation accuracy, and it might be utilized to estimate nuclear material in fuel debris. Due to the similarity of their production mechanisms, the Eu-154/Cs-134 weight ratio maintains a nearly constant value ($1\sigma < 15\%$) for a typical BWR fuel assembly independent of cycles; therefore, it has the potential to be utilized for Cs release ratio estimation in fuel debris. The Cm-244/Pu ratio has an uncertainty (1σ 18~26%) in a specific burnup mainly because of the variance of the neutron spectrum in the BWR axial profile, the calculation and nuclear data, and it is also sensitive to initial enrichment.

REFERENCES

1. GPU NUCLEAR, *TMI-2 Defueling Completion Report* (1990).
2. M. OSBONE, et al., *Nuclear Safety*, vol. **33,** no. 3, (1992)
3. T. ONIZAWA, et al., *IAEA-CN-148* (2006).
4. H. SAGARA, H. TOMIKAWA, M. WATAHIKI and Y. KUNO, *Trans. Am. Nucl. Soc.*, vol. **107**, p. 803-804, 2012.
5. NEA, www. oecd-nea.org/sfcompo/

C.7 Evaluation of Fukushima Dai-ichi Nuclear Power Plant Accident

Kazumi KITAYAMA, Takao ISHIZUKA,
Nobuyoshi TSUZUKI and Hiroshige KIKURA

A huge earthquake, lately referred as *Higashi-Nihon Dai-Shinsa*i, occurred at approximately 100 km east off the coast of Tohoku area at 14:46 on 11th, Mar, 2011. The nuclear power plants were damaged especially in Tohoku area by the earthquake and following tsunami, and as a result, severe accidents occurred at 3 units of Fukushima Dai-ichi nuclear power station (1-F) and they released radioactive materials.

The earthquake discharged external power source from 1-F station, and the following tsunami crushed heat sink for removing residual heat. Unit #5-6 of 1-F were not severely troubled because an air-cooled diesel power generator for unit #5̃6 could keep working. However, unit #1̃4 lost all electricity and heat sink. Fuel rods of unit #4 were removed from Reactor Pressure Vessel (RPV) for refueling and core cooling for unit #4 was not necessary. Thus, the most important thing for 1-F at that time was coolant injection for cooling the reactor core of unit #1̃3.

Unit #1 of 1-F is a BWR-3 reactor. It has some core cooling facilities, those are Isolation Condenser (IC), High Pressure Coolant Injection system (HPCI), and so on. Tokyo Electric Power Company (TEPCO) decided soon after the earthquake that IC could be applied for regulation of the pressure in RPV, and that HPCI should be applied when the level of coolant water went down. Accordingly, IC was applied four times before tsunami. However, terror for tsunami left IC not working for about 2.5 hours after the first attack of tsunami. Core of unit #1 is supposed to start melting in this non-cooled time, and hydrogen which generated by the reaction between steam and zircalloy in the core exploded at 15:36 12th, Mar. The explosion also damaged fire pumps or other apparatus for other units #2̃4, and it made harder to inject the coolant water to reactor core of other units.

Unit #2 and #3 (and unit #4 and #5 also) are BWR-4 reactors. A BWR-4 type reactor has Reactor Core Isolation Cooling system (RCIC) instead of IC of BWR-3, and it has HPCI for injection at small or medium sized piping rapture as well as the case of BWR-3. After the earthquake, RCIC was started manually by operators of TEPCO at both units (#2 and #3). RCICs worked to inject cool water to reactor cores for about 20 hours at unit #3, and about 70 hours at unit #2. At unit #3, HPCI automatically followed when RCIC expired and it worked for 14 hours. Thus, RCIC and HPCI worked for 34 hours at unit #3.

However, in the case of unit #2, RCIC worked too long time. Designed working time of RCIC is usually 6-8 hours. 70 hours is extremely over the designed working time, thus, efficiency of RCIC should be decreased before it physically stopped. **Figure 1** shows pressure in RPV of unit #2 after the earthquake. From 20:00 14th, Mar., the pressure suddenly rose, thus, RCIC might become non-effective before this. The expired time was assumed around 7:30. Due to no effective core injection and delay of vent from primary containment vessel (PCV), unit #2 might be broken and it released much radioactive materials.

In the case of unit #3, HPCI worked after RCIC expiration. HPCI consumes steam about 10 times larger than that of RCIC. Accordingly, HPCI might spend all steam in short time. Pressure of RPV of unit #3 rapidly fell soon after HPCI started, and it became almost 1 MPa around 19:00, 13th, Mar. Thus, HPCI might not fully work after this time. Consequently, coolant water for core of unit #3 might not be injected from this time, and temperature of core of unit #3 might increase due to no injection. In fact, hydrogen explosion occurred at 11:01 on 14th, Mar at unit #3.

Severe accidents finally occurred at unit #1-#3 in 1-F mainly due to station black out (SBO) and loss of ultimate heat sink (LUHS). But we think the severe accident could be avoided. PCV vent can reduce not only pressure of PCV but energy in PCV existing as heated steam. Fuel rods were not damaged soon after the SBO and LUHS, thus, radioactive materials doesn't exist in the steam. Hence, early PCV vent before fuel rod damage is very effective to release the residual heat. Naturally, water injection for core cooling with another power and automatic depressurization system (ADS) must be worked with this kind of vent. And rapture disks in ventilation line must be broken for vent, though these rapture disks made difficult to vent in 1-F case in fact. However, this kind of vent doesn't require much reconstruction. The study for utilizing this vent may strengthen the safety of presenting reactors and will help for NPP's re-operation in Japan.

Reference

[1] M. Aritomi *et al.*, "What nuclear researchers and engineers can do for public right now," Baifukan (2012).

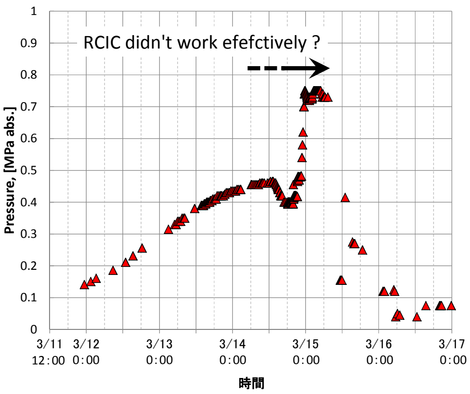

Figure 1 Pressure in RPV of unit #1, 1-F.

C.8

Numerical Analyses on Joule-Heated Glass Furnace for Disposal of High-Level Radioactive Waste

Nobuyoshi TSUZUKI and Hiroshige KIKURA

Nuclear power plants or other facilities of nuclear fuel cycle produce high-level radioactive wastes. The High-level radioactive waste is reprocessed into waste liquid, and the waste liquid is mixed into molten glass in a Joule-heated glass furnace to make vitrified waste. In the glass furnace, glass (and radioactive waste) is heated by electrical current, Joule-heated, where three kinds of field – flow field, electrical field and magnetic field – arise and interfere one another. Thus, very complicated flow behavior is produced in the Joule-heated glass furnace.

The shape of glass furnace is simulated by a cubic cavity in these calculations to simplify the various problems in glass furnace. Dimensions of the model are calculated from the public data of TVF [1], the test-type vitrification furnace. The cavity consists of two electrode plates on facing sides and constant temperature wall on the top working as a heat sink (Figure 1). Other planes are considered as adiabatic.

In order to solve the couple analysis including the three field (flow, electrical and magnetic fields), GSMAC-FEM [2] is utilized because edge finite element method (edge-FEM) can examine coupled analyses with magnetic field. Magnetic permeability of molten glass is difficult to measure due to its high temperature (≈ 1200°C) and mixed radioactive waste including platinum group metal particles. Thus, relative magnetic permeability of working fluid to vacuum (μ_r) in this study is varied from 1.0 to 2.0.

The simulation calculations show the flow behavior in this cubic cavity as follows. Joule heating induces volumetric upflow due to buoyancy. Top surface of constant temperature generates downflows by separation of cooled boundary fluid. Downflows occurred everywhere of the top surface, and unsteady flow behavior is maintained steadily, like experimental with less magnetic permeability fluid executd in the last year. We named this unstable state as 'chaotic steady state.' And simulation calculations can show magnitude change of averaged forces (buoyancy, diffusion force, Lorentz force and convection force) in the beginning of Joule heating. These results are shown in Figure 2. In the case of low magnetic permeability ($\mu_r = 1.0$, (a)), the rises of diffusion force and convection force are slow. On the other hand, in the case of high magnetic permeability ($\mu_r = 2.0$, (b)), the rises of these forces are fast. From the velocity distribution results, higher magnetic permeability induces earlier and faster volumetric upflow. Early upflow makes steady flow pattern, in which upflow in the center and downflow near the wall, and it makes the beginning time of chaotic downflow from somewhere of the top surface later. However, magnitudes of all forces after enough time passed (more than 1 hour) become almost same in both cases.

Numerical analyses suggest that magnetic field effects on the flow behavior in the beginning of Joule heating. High magnetic permeability leads early and fast chaotic downflows which occur from somewhere of the top surface. However, named 'chaotic steady state' will appear after 1-2 hours, and averaged magnitude of each forces becomes almost same in the case μ_r is 1-2. Consequently, it is concluded that the effect of magnetic permeability will become negligible after several hours passed in this system.

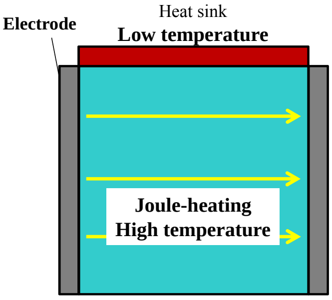

Figure 1 Schematic diagram of the cubic cavity model.

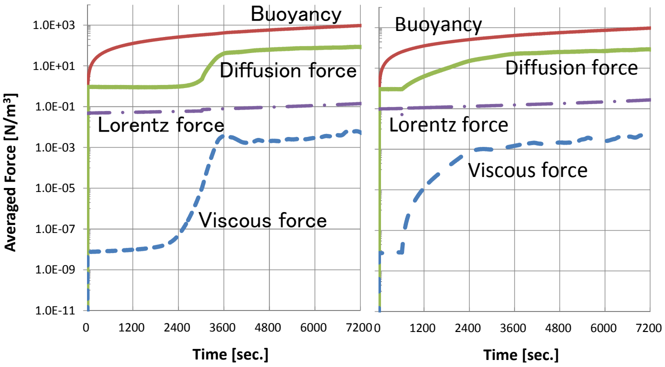

(a) $\mu_r = 1.0$ (b) $\mu_r = 2.0$

Figure 2 Time dependencies of volume averaged values of forces.

References

[1] JAEA, Thermal hydraulic analysis using experimental data of TVF cold test, JNC TN8410 98-008 (1998) [in Japanese].

[2] T. Tanahashi: GSMAC-FEM, IPC (1991) [in Japanese].

[3] K. Yang, Y. Saitoh, H. Kawai, N. Tsuzuki, H.Kikura and G. Hashimoto, Numerical Flow Analysis of Electromagnetic Fluid Using GSMAC Finite-Element Method, *Joint Symposium on Mechanical - Industrial Engineering and Robotics 2012*, Noboribetsu, Japan, 49 (2012).

[4]H. Kikura, N. Tsuzuki, T. Kawaguchi, H. Kawai, K. Minami and E. Ochi, *Flow Behavior Simulation with Model Fluid of Molten Glass by FEM*, SEAD24 in Toyama, Toyama,17B2-3 (2012-5),. [in Japanese].

[5] K. Yang, Y. Saitoh, H. Kawai, N. Tsuzuki, H.Kikura and G. Hashimoto, Numerical Flow Analysis of Electromagnetic Fluid Using GSMAC Finite-Element Method, The 20th International Conference on Nuclear Engineering (ICONE20), Anaheim, California, USA, 1-5 (2012-7), CD-ROM Paper No. ICONE20 POWER2012 54508.

C.9 A Very Low Velocity Measurement Using Ultrasonic Velocimetry

Hiroshige KIKURA

Isolation of High Level Radioactive Wastes (HLWs) from biosphere and its disposition in a deep geological repository is an urgent problem and vitrification technique of HLW has to be improved in the industrial scale. This vitrification melter is operated with internal Joule-heat generation, and the temperature of glass exceeds 1000°C. For understanding a thermal hydraulics behavior of the vitrification melter, experimental technique has to be invented. Several velocity measurement techniques such as PIV/PTV, LDA had been developed. However, because of high temperature and opaqueness, these techniques cannot to be applied for glass melts. To overcome these difficulties, we focused ourselves on UVP technique[1,2]. Realization of such a technique has difficulties in two fold; high temperature and very low velocity. We already demonstrated ultrasonic measurement technique inside glass melts employing buffer-rod. In this paper, we present a system developed to measure an extremely low velocity flow [3,4].

FFT-based Doppler method is a conventional method to obtain flow velocity profile. The Doppler-shift frequency f_{Di} and flow direction are determined by their peak value. Therefore, flow velocity V_i is calculated as Eq. (1).

$$V_i = \frac{f_{Di}}{2f_0}c \tag{1}$$

where f_0 is center frequency of transmitted signal, and c is sound speed in the fluid. Because a spectrum is calculated at discreet points, velocity values have limitations as follows:

$$V_{max} = \frac{f_{PRF}}{4f_0}c \quad (2) \qquad V_{\text{step}} = \frac{f_{PRF}}{N_j f_0}c \quad (3)$$

where f_{PRF} is a pulse repetition frequency, and N_j is a number of pulse emissions. Practically, the peak of the spectra is calculated from three point Gaussian curve fitting to improve the velocity resolution. Nevertheless, this Vstep could be equal to the lower velocity limitation. Since this technique does not require high speed ADC, it has been widely used. However, there is a trade-off relationship between temporal and velocity resolutions depending on N_j.

In order to masure very low velocity with high accuracy, we developed new data processing method, named as 'Phase Difference method.' From conjugate complex product of two successive functions, phase difference $\Delta\theta$ is obtained. Therefore, flow velocity V_{ij} is calculated as Eq. (4).

$$V_{ij} = \frac{f_{PRF}}{4\pi f_0}c \cdot \Delta\theta_{ij} \tag{4}$$

Since this technique can calculate velocity from two echoes, the temporal resolution of this method can be expressed as Eq. (5).

$$V_{ij} = \frac{f_{PRF}}{4\pi f_0}c \cdot \Delta\theta_{ij} \tag{5}$$

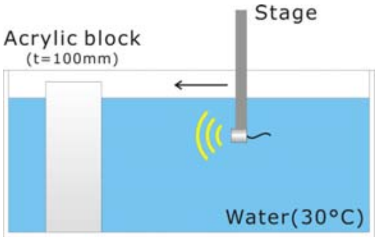

Fig. 1 Schematic diagram of experimental apparatus

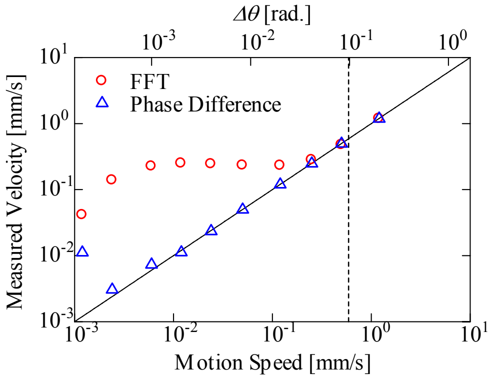

Fig. 2 Measured velocity versus motion speed for FFT method and phase difference method (f_{PRF} = 100 Hz)

As for V_{max}, it is equal to Eq. (2) because the range of $\Delta\theta$ remains between $-\pi$ and π.

Figure 1 shows a schematic illustration of verifying experimental setup. A transducer is immersed in a water of 30°C and fixed on the stage. The stage moves toward and backward the wall at a constant speed. Motion speeds can be controlled by PC from 0.0012 to 5 mm/s. The measured velocities are depicted in **Fig. 2**. With FFT-based method, measured values don't agree with real value especially when the motion speed is slower than 10^{-1} mm/s, however, measured values with Phase Difference method agree well till the motion speed is as slow as around 10^{-3} mm/s.

Reference

[1] T. Ihara, K. Tanaka, H. Kikura, Y. Takeda, E. Ochi and A. Inagaki : The Study of Velocimetry in High Temperature Flow, *The 19th International Conference on Nuclear Engineering , Osaka, Japan*, Paper No. ICONE19-43617 (2011-5).

[2] T. Ihara, H. Kikura and Y. Takeda, The Basic Study of Ultrasound Characteristics and Velocimetry in Molten Glass, *Trans. JSME, Series B*, **78**, 485-489 (2012-3) [in Japanese].

[3] T. Ihara, H. Kikura, Y. Takeda, O.Eiji and K. Minami, The Study of Measurement for a Very Slow Flow Using Phase Difference Method, *IEICE Technical Report, Ultrasonics*, **112**, 7-11 (2012-5) [in Japanese].

[4] T. Ihara H. Kikura and Y. Takeda : A Very Low Velocity Measurement Using Ultrasonic Velocimetry, *8th International Symposium on Ultrasonic Doppler Methods for Fluid Mechanics and Fluid Engineering, Dresden, Germany*, 33-36 (2012-9).

C.10

Basic study of velocity profile measurement by an air-coupled ultrasonic system

Hiroshige KIKURA

In nuclear power plants, flow measurement systems in high temperature surroundings are needed to monitor plants. However, ultrasonic measurement cannot be applied to high - temperature fluid. Piezo-electric devices in ultra-sonic transducers lose piezoelectric property over Curie temperature. Thus, ultrasonic waves have some limitations in high-temperature flow measurement. However, air is good insulater and those high temperature can be prevented by air layer. Therefore, we focused on air-coupled ultrasonic waves.

Measuring configuration for air-coupled ultrasonic flow measurement is depicted in **Figure 1**. Upstream transducer emits ultrasonic waves. asound propagates in air and passes into cylindrical pipe, then ultrasonic waves convert into guided waves which propagate along the surface of pipes and longitudinal waves which propagate in fluid flowing along pipes. Several kinds of ultrasonic waves are received by a receiving transducer. When time difference method is applied for ultrasonic flowmeters, longitudinal waves are used to measure and guided waves are regarded as noises in this system. It is necessary to isolate received signals of longitudinal waves from those of guided waves. The signals of longitudinal waves are specified experimentally by obstructing. Longtitutional waves cannot exist when obstacles exist in the center of pipe, however, the longtitutional wave can be observed when there is no obstacles.

The principle of air-coupled ultrasonic flow meter is as follows. Two tranceducers are necessary for this air-coupled ultrasonic system like shown in Figure 1. At first, upstream tranceducer emits ultrasonic wave and downstream tranceducer receives them. Next, downstream tranceducer emits waves and upstream tranceducer receives them. There is propagation time difference between two signals due to working fluid velocity though the waves traveled for the same distance. There is relationship between the propagation time difference and the fluid flow rate as,

$$V = \frac{C_w^2}{2\,D\tan\phi}\Delta t$$

where V is average flow velocity, Cw is sound speed in the fluid, D is diameter of the pipe, φ is angle between direction of ultrasound and crosssecsion plane of pipe, and Δt is propagation time difference.

Development of hardware, i. e. transducers for air-coupled measuring and external amplifier, and software to distingish longtitutional wave from noisy echo signal realised air-coupled flow measuring. Figure 2 shows the results of flow velocity using developed air-coupled ultrasonic system for vertical pipe flow. Horizontal axis shows flowrate measured by existing clamp-on ultrasonic flowmeter, and vertical axis shows flowrate measured by air-coupled ultrasonic flow measuring. Error bars shows deviations of measured velocities. The solid line is drawn by the least-squares method. The R2 value of this fitting is 0.9398. The slope of this line is 0.98. Though there is some errors, agreement between real flow rate and measured value by air-coupled flow system is confirmed by this test experimental result.

Evaluation for an air-coupled ultrasonic flowmeter was executed and the result suggests the availability of the method. In order to improve the accuracy of flowrate measurement with air-coupled ultrasonic system, application of Pulse Doppler Method will be examined.

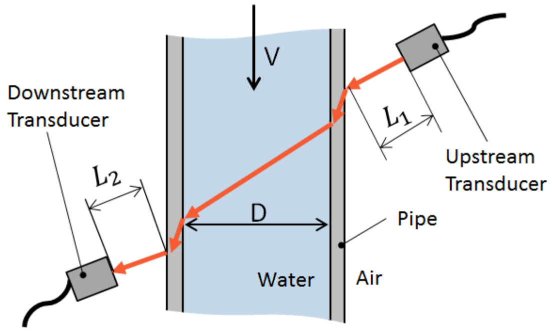

Figure 1 Measurement configuration for air-coupled ultrasonic system.

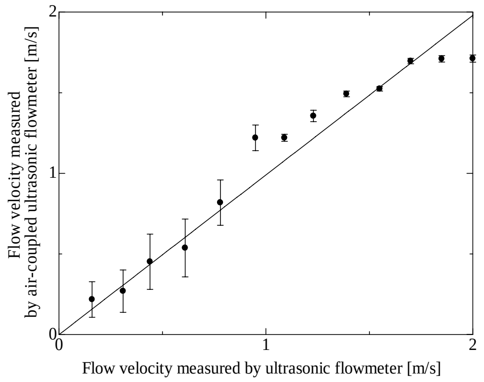

Figure 2 Measured flow velocity for a vertical pipe.

Reference

[1] K. Tsukada, T. Ihara and H. Kikura, A Study of Air-Coupled Ultrasonic Flowmeter, *The 20th International Conference on Nuclear Engineering (ICONE20)*, Anaheim, California, USA, (2012-7), CD-ROM Paper No.ICONE20 - POWER2012 - 54524.

[2] K. Tsukada, T. Ihara and H. Kikura, An Analytical Study of Air-Coupled Ultrasonic Flowmeter, *Proc of Symposium on Ultrasonic Electronics(USE2012)*, Vol.**33** , Chiba, 337-338 (2012-11).[in Japanese]

[3] K. Tsukada, T. Ihara and H. Kikura,, Study on Non-contacting Flow Rate Measurement using Air-coupled Ultrasound, *Proceedings of 49th Japan Heat Transfer Symposium,* Toyama, 125-126 (2012-5). [in Japanese]

Ⅲ. Co-operative Researches

Ⅲ.1 Co-operative Researches within Tokyo Institute of Technology

Under the generic proposition: "The Release and Utilization of Energies existing in Atoms, Molecules and Nuclei" which has been hoisted since the reorganization of RLNR, we advertise for collaborations with any department and laboratory within Tokyo Institute of Technology in order to develop researches for the improvement of energy utilization with safety, mass transmutation by nuclear reactions with high efficiency, and construction of energy system concept with high societal acceptability. The RLNR will promote these collaborations by offering the organizations, facilities, equipments and space as the research base for research project teams and research groups crossing over within Tokyo Tech. We are going to adopt unique and innovative themes which make maximum use of the activities of this research laboratory.

- Heavy-Ion Inertial Fusion and High Energy-Density Physics Driven by Heavy-Ion Beams
  Interdisciplinary Graduate School of Science and Engineering

- Development MeV Proton Microprobe Based on Glass Capillary Optics for Biological Samples
  Department of Energy Sciences, Interdisciplinary Graduate School of Science and Engineering

- Action of Bisphenol A on DNA-PK Function and DNA Double-Strand Break Repair
  Hiroshi Handa: Graduate School of Bioscience and Bioengineering, Solutions Research Laboratory

- Possible Application of Atmospheric Plasma to Cancer Therapy
  Akitoshi Okino: Interdisciplinary Graduate School of Science and Engineering

- Studies on Uranium Coordination Chemistry
  Ikeda Lab (RLNR).

- Synthesis of super ionic conductive ceramics using molten salt flux and elucidation of their electric conduction mechanism
  Internal grant for preliminary research

- Studies on Uranium Coordination Chemistry
  Ikeda Lab (RLNR).

Ⅲ.2 Co-operative Researches with Outside of Tokyo Institute of Technology

- n_TOF Collaboration, CERN

- Comprehensive study of delayed-neutron yields for accurate evaluation of kinetics of high-burn up reactors
  Technology of Japan (MEXT), with JAEA.

- Research and Development of High Performance Ceramics
  Chiba Institute of Technology, Tokai University

- Study on Novel Process of SiC/SiC Composite by Electrophoretic Deposition Method
  Japan Aerospace Exploration Agency (JAXA)

- Study on the Improvement of Irradiation Resistance of Ceramics by Their Orientation Control
  National Institute for Materials Science (NIMS)

- Evaluation of Sinterability and Properties of SiC Ceramics using Al_4SiC_4 as Sintering Additives
  National Institute for Materials Science (NIMS)

- Study on the Evaluation of Thermal Shock Fracture Behavior of Silicon Nitride Ceramics
  Tokyo Metropolitan University

- Research on formation and characterization of oxide nanopowder
  Vinca Institute , University of Belgrade, Serbia

- Fundamental Test Related with Physical Property of Glass -Advancement of Vitrification process
  Japan Nuclear Fuel Limited

- Research on Thermo-decomposition / Volume Reduction of Ferric Ferrocyanide Absorbed Cesium
  Maeda Corporation

- Research on Separation of Platinum Group Metals from Nitric Acid Solution
  Mitsubishi Materials Corporation

- Development of Functional Sheet for the Removal of Platinum Group Metals and Heat-generating Nuclides from High-level Radioactive Waste (HLW)
  Nitto Denko Corporation

- Ion Beam Analysis of Fuel-Cell Materials
  Department of Chemistry and Energy Engineering, Faculty of Engineering, Tokyo City University

- Astrobiology Experiments Based on MeV Ion Beams
  Division of Materials Science and Chemical Engineering, Faculty of Engineering, Yokohama National University

- Study on the possibility of ultra-high burnup core and fuel
  Japan Atomic Energy Agency

- Study on the possibility of CANDLE reactor
  Central Research Institute of Electric Power Industry

- Blanket Fuel with High Proliferation Resistance in Fast Breeder Reactor
  Japan Atomic Energy Agency

- Studies on Separation of Uranium Species Using Polyvinylpolypyrrolidone
  Japan Atomic Energy Agency and Tokai University

- A Study of Extraction Behavior of ReO_4^- by Using Monoamide Compounds
  Japan Atomic Energy Agency

- A Study on Partitioning of Lanthanoid and Actinoid Species
  Japan Atomic Energy Agency

- A Study on Separation of Uranyl Species Using Alginic Acid
  Prof. R.M. Hassan, Assiut University, Egypt

- A Study on Structures of Lanthanoid(III) Complexes with Monoamide Compounds in Solutions Using NMR
  Professor Z. Szabo, Royal Institute of Technology, Sweden

- Studies on Structures of Uranyl Complexes in Ionic Liquids
  Dr. C. Hennig, Forschungszentrum Rossendorf, Germany

- Cleaning Process for Semiconductor Equipment Process on Atmospheric-Pressure Non-Equilibrium DC Pulse Plasma Jet
  University of Miyazaki, King Mongkut's University of Technology Thonburi, Kagawa University, Miyakonojo National College of Technology.

- On the Possibility of Application of Plasma Technology to Geological Disposal of HLW
  University of Miyazaki

- Electric Thruster for Astronautic Application by High-Density Helicon Wave Plasma and its Diagnostics by Optical Emission Spectroscopy
  Tokyo University of Agriculture and Technology

- Chemical heat pump for waste heat recovery from iron making process Environmentally Friendly Steel Process Technology
  NEDO commissioned project, 2012.

- Study on low-carbon and carbon recycling iron-making system using ACRES
  Sumitomo Metal Ind., 2012

- Elucidation of DNA Double-Strand Break Repair and Its Possible Application to Cancer Therapy
  Tokyo Biochemical Research Foundation
  Postdoctoral Fellowships for Asian Researchers in Japan (FY2012)

- *In situ* high-resolution photoemission spectroscopic study of 1D peanut-shaped C_{60} polymers
  UVSOR Facility, Institute for Molecular Science
  Department of Materials Science, Nagoya University

- DFT study of low-dimensional peanut-shaped C_{60} polymers
  Yokohama National University

- Photodynamic properties of nanomaterials
  Department of Applied Physics, Hokkaido University

- Riemannian geometrical effects on physical properties of 1D uneven peanut-shaped C_{60} polymer
  Department of Environmental Sciences and Interdisciplinary Graduate School of Medicine and Engineering, University of Yamanashi Department of Physics, Nara Women's University

- High-resolution TEM observation of 1D uneven peanut-shaped C_{60} polymer
  UHP-TEM center, Osaka University

- A Study of Surface and Interfaces of Organic Photovoltaic Cells
  J-Power Co. Ltd

- Development of ECE imaging system by the use of 1-D horn antenna array
  National Institute for Fusion Science

- Experimenral investigation of positional stabilization of torus plasma with helical coils
  National Institute for Fusion Science

- Development of Fiber-Optic Diagnotic on Vacuum Vessel Current of QUEST
  Research Institute for Applied Mechanics, Kyushu University

- Study on Diagnostics Required for Basic Control of DEMO Fusion Reactors
  Japan Atomic Energy Agency

- Characterization of structure and physico-chemical properties of molten rare-earth metal halides
  Japan Atomic Energy Agency

- Innovative characterization of materials under severe condition Conditions Extrêmes et Matériaux Haute Température et Irradiation
  Centre National de la Recherche Scientifique

- Structure and physico-chemical properties of actinides fluorides
  Institute of Multidisciplinary Research for Advanced Materials, Tohoku University (Network Joint Research Center for Materials and Devices)

- Pyro-reprocessing of rare earth elements from Ni-MH battery
  The Fujikura Foundation

- XAFS analysis of actinide chlorides and chlorides of fission products
  Kyoto University Research Reactor Institute

- Strong Magnetic Field Generation for Laboratory X-ray Astronomy
  Institute of Laser Engineering, Osaka University

- Study on behavior of the thermal neutron inside the graphite
  National Institute of Advanced Industrial Science and Technology, National Metrology Institute of Japan (NMIJ/AIST)

- Needle-Shaped Monochromatic Brachytherapy X-ray Source for Selective Irradiation of Tumors Using X-ray Absorption Characteristics of Drugs
  Japan Society for the Promotion of Science

- Development of an atmospheric scanning positron microscope
  National Institute of Advanced Industrial Science and Technology

- Advanced study on heavy ion linac
  National Institute of Radiological Sciences

Ⅲ.3 Themes Supported by Grants-in-Aid for Scientific Research of the Ministry of Education, Culture, Sports, Science and Technology

- Recovery of Neutron-Induced Defects and Release of Helium Gas using Nano-Dilatometry Equipped with Mass Spectroscopy

- [Basic Studies for Developing Rational Treatment and Disposal System of Radioactive Wastes Generated by Fukushima Nuclear Reactor Accident as Co-researchers),

- Comprehensive study of delayed-neutron yields for accurate evaluation of kinetics of high-burn up reactors

- Comprehensive study of delayed-neutron yields for accurate evaluation of kinetics of high-burn up reactors

- Cineangiography Using Particle-Induced Dual-Wavelength Pulsed-X-rays for Minimization of Dosages of Contrast Medium and Radiation

- Needle-Shaped Monochromatic Brachytherapy X-ray Source for Selective Irradiation of Tumors Using X-ray Absorption Characteristics of Drugs

- High-Efficient Utilization of Middium-Temperature Heat by Using High-Thermal Conductivity Materials

- Load-Leveling of Renewable Energy System by Using Direct Carbon Dioxide Electrolysis

- Development of materials for chemical heat storage with metal organic framework (MOF) as host matrix

- Strategic Design of Radiosensitizer Based on the Molecular Mechanisms of the Recognition and Repair of DNA Double-Strand Breaks

- Sterically Independent Regulation of Coordination Number around Metal Ions –Effective Use of Ionic Liquid as Exotic Reaction Field−

IV. List of Publications

A. Kimura, T. Fujii, S. Fukutani, K. Furutaka, S. Goko, K. Y. Hara, H. Harada, K. Hirose, J. Hori, M. Igashira, T. Kamiyama, T. Katabuchi, T. Kin, K. Kino, F. Kitatani, Y. Kiyanagi, M. Koizumi, M. Mizumoto, S. Nakamura, M. Ohta, M. Oshima, K. Takamiya, Y. Toh: Neutron-capture cross-sections of Cm-244 and Cm-246 measured with an array of large germanium detectors in the ANNRI at J-PARC/MLF; *Journal of Nuclear Science and Technology*, Vol. **49**, No. 11, pp. 708-718, (2012).

K. Hirose, M. Oshima, F. Kitatani, A. Kimura, M. Koizumi, Y. Toh, S. Nakamura, K. Hara, H. Harada, K. Furutaka, M. Igashira, T. Katabuchi, K. Terada, T. M., M. Mizumoto, T. Kamiyama, K. Kino, Y. Kiyanagi, J. Hori: Cross section measurement of Sn-119(n,γ) using ANNRI-NaI(Tl) detector at J-PARC; *2012 Fall Meeting of the Atomic Energy Society of Japan*, Higashi Hiroshima, September 19-21, 2012, I04.

H. Harada, M. Ohta, A. Kimura, K. Hirose, K. Hara, M. Oshima, F. Kitatani, T. Kin, M. Koizumi, S. Goko, Yosuke Toh, S. Nakamura, K. Furutaka, M. Igashira, T. Katabuchi, M. Mizumoto, Y. Kiyanagi, K. Kino, K. Takamiya, S. Fukutani, T. Fujii, J. Hori: Measurement of Neutron-Capture Cross Section of Am-241 using ANNRI; *2012 Fall Meeting of the Atomic Energy Society of Japan*, Higashi Hiroshima, September 19-21, 2012, I03.

T. Katabuchi, M. Mizumoto, M. Igashira, K. Hirose, Atsushi Kimura, S. Nakamura, Yosuke Toh, K. Furutaka, M. Koizumi, M. Oshima, H. Harada, J. Hori, K. Kino, T. Kamiyama, Y. Kiyanagi: Measurement of neutron capture cross section of Tc-99 using an NaI(Tl) spectrometer at J-PARC/MLF ANNRI; *2012 Fall Meeting of the Atomic Energy Society of Japan*, Higashi Hiroshima, September 19-21, 2012, I05.

K. Terada, M. Igashira, T. Katabuchi, T. Matsuhashi: Measurements of keV-Neutron Capture Cross Sections and Capture Gamma-Ray Spectra of 110Pd; *2012 Fall Meeting of the Atomic Energy Society of Japan*, Higashi Hiroshima, September 19-21, 2012, I07.

Z. Khan, T. Katabuchi, K. Miyazaki, T. Kobayashi, N. Hayashizaki, K. Terada, T. Matsuhashi, M. Igashira, K. Ogawa: Feasibility Study on Pinhole Camera for Online Dosimetry in Boron Neutron Capture Therapy; *2012 Fall Meeting of the Atomic Energy Society of Japan*, Higashi Hiroshima, September 19-21, 2012, I39.

S. Nakamura, Atsushi Kimura, F. Kitatani, T. Kin, M. Koizumi, Yosuke Toh, K. Hara, K. Hirose, K. Furutaka, H. Harada, M. Oshima, T. Katabuchi, M. Mizumoto, M. Igashira, K. Kino, F. Hiraga, T. Kamiyama, Y. Kiyanagi, J. Hori, H. Yashima: Measurement of Neutron-Capture Cross Section of Pd-108 using ANNRI; *2012 Fall Meeting of the Atomic Energy Society of Japan*, Higashi Hiroshima, September 19-21, 2012, I02.

M. Igashira, Hiroyuki Tsuda, K. Terada, T. Katabuchi: Measurements of keV-Neutron Capture Cross Sections and Capture Gamma-Ray Spectra of Nb-93, Rh-103 and In-115; *2012 Annual Meeting of Atomic Energy Society of Japan*, Fukui, March 30-35, 2012, O06.

T. Katabuchi, K. Miyazaki, B. Hales, M. Igashira, N. Hayashizaki, T. Kobayashi: Feasibility Study of Pinhole Camera for Online Dosimetry Imaging in Boron Neutron Capture Therapy; *2012 Annual Meeting of Atomic Energy Society of Japan*, Fukui, March 30-35, 2012, O44.

K. Terada, M. Igashira, T. Katabuchi, T. Matsuhashi: Measurements of keV-Neutron Capture Cross Sections and Capture Gamma-Ray Spectra of 106,108Pd; *2012 Annual Meeting of Atomic Energy Society of Japan*, Fukui, March 30-35, 2012, O05.

K. Kino, T. Kamiyama, Y. Kiyanagi, F. Hiraga, M. Furusaka, Masayuki Ohta, M. Oshima, F. Kitatani, Atsushi Kimura, T. Kin, M. Koizumi, S. Goko, Yosuke Toh, S. Nakamura, K. Hara, H. Harada, K. Hirose, K. Furutaka, M. Igashira, T. Katabuchi, M. Mizumoto, J. Hori, K. Takamiya, S. Fukutani, T. Fujii: Measurement of Neutron-Capture Cross Section of Tc-99 using ANNRI; *2012 Annual Meeting of Atomic Energy Society of Japan*, Fukui, March 30-35, 2012, C33.

B. Hales, T. Katabuchi, K. Terada, M. Igashira, N. Hayashizaki, T. Kobayashi: Feasibility Study of SPECT System for Online Dosimetry Imaging in Boron Neutron Capture Therapy; *2012 Annual Meeting of Atomic Energy Society of Japan*, Fukui, March 30-35, 2012, O40.

H. Koura and S. Chiba: Single-Particle Levels of Spherical Nuclei in the Super heavy and Extremely Super heavy Mass Region; *Journal of the Physical Society of Japan* **82**, 014201 (2012).

M.-K. Cheoun, E. Ha, T. Hayakawa, S. Chiba, K. Nakamura, T. Kajino and G.J. Mathews: Neutrino induced reactions forv-process nucleosynthesis of ^{92}Nb and ^{98}Tc; *Phys. Rev. C* **85**, 065807-1 (2012).

Y. Aritomo, K. Hagino, K. Nishio, S. Chiba: Dynamical approach to heavy-ion induced fission using actinide target nuclei at energies around the Coulomb barrier; *Phys. Rev. C* **85**, 044614 (2012).

T. Maruyama, G. Watanabe and S. Chiba: Molecular Dynamics for Dense Matter; *Prog. Theor. Exp. Phys.* **01A201**-1 (2012).

D. Ichinkhorloo, Y. Hirabayashi, K. Kato, M. Aikawa, T. Matsumoto, and S. Chiba: Analysis of ^{7}Li(n,n')^{7}Li* reactions using the continuum-discretized coupled-channels method; *Phys. Rev. C* **86**, 064604-1(2012).

Y. Aritomo, K. Hagino, S. Chiba and K. Nishio: Dynamical approach to heavy-ion induced fusion using actinide target; *AIP Conf. Proc.* 1491, 303 (2012).

Y. Aritomo, D.J. Hinde, A. Wakhle, R.du Rietz, M. Dasgupta, K. Hagino, S. Chiba and K. Nishio: Dynamical approach to fusion-fission process in superheavy mass region; *EPJ Web of Conference* 35, 05001(2012).

S. Chiba: Research in Surrogate Reacions at JAEA/Tokyo Tech.; *International Conference on Nuclear Data for Science and Technology*, ND2013, 4-8 March, 2013, Sherataon Hotels and Towers New York, U.S.A.

R. Capote, E.Sh. Soukhovitskii, J.M. Quesada and S. Chiba: Rotational-Vibrational Description of Nucleon Scattering on Actinide Nuclei Using a Dispersive Coupled-Channel OMP; *International Conference on Nuclear Data for Science and Technology*, ND2013, 4-8 March, 2013, Sherataon Hotels and Towers New York, U.S.A.

J. Quesada, E.Sh. Soukhovitski, R. Capote and S. Chiba: A Lane consistent optical model potential for nucleon induced reactions on 238U and 232Th nuclei with full coupling: *Wonder 2012, 3rd International Workshop on Nuclear Data Evaluaiton for Reactor Apolications,* CEA/NEA, 25-28 September, 2012, Aix-en Provence, France.

T. Sato, K. Niita, N. Matsuda, S. Hashimoto, Y. Iwamoto, S. Noda, H. Iwase, H. Nakashima, T. Fukahori, S. Chiba and L. Sihver: Overview of the PHITS Code and its Application to Medical Physics; *Workshop on Computational Medical Physics,* Nara prefectural new public hall, 2 Sept. 2012, Nara, Japan.

S. Chiba: Future development of nuclear technology and its relation with basic science; *YITP-oriented research meeting on nuclear energy, biology and physics;* Yukawa Institute for Theoretical Physics, Kyoto University , 8-10 August, 2012. Soryushironkenkyuu Vol13, http://www2.yukawa.kyoto-u.ac.jp/~sokened/sokendenshi/vol13/nbp2012/8-8-A1-SC-S.pdf}.

Y. Aritomo, D.J. Hinde, A. Wakhle, R. du Rietz, M. Dasgupta, K. Hagino, S. Chiba, K. Nishio: Dynamical calculation for heavy-ion induced fission; *Heavy Ion Accelerator Symposium*, 11-13 April, 2012, The Australian National University, Canberra, Australia.

Y. Aritomo, K. Hagino, K. Nishio, S. Chiba: Dynamical approach to heavy-ion induced fission using actinide target; *Nuclear Structure and Dynamics II*, 9-13, July, 2012, Opatija, Croatia.

Katsumi Yoshida, Hajime Katsumata, Masamitsu Imai, Toyohiko Yano: Effect of BN Particle Size on Sinterability, Mechanical Properties and Machinability of SiC/BN Composites with Oxide Additives; *J. Soc. Inorg. Mater., Japan (Muki-Materiaru)*, Vol.**19**, No.356, pp.23-29 (2012).

Branko Matovic, Dusan Bucevac, Noppasint Jiraborvornpongsa, Katsumi Yoshida, Toyohiko Yano: Synthesis and Characterization of Nanometric Strontium-Doped Ceria Solid Solutions via Glycine-Nitrate Procedure; *J. Ceram. Soc. Japan*, Vol.**120**, No.2, pp.69-73 (2012).

Rikako Miyamoto, Kenta Ohashi, Katsumi Yoshida, Naoyuki Matsumoto, Hirobumi Shibata, Takashi Meguro, Shigeo Fukuyama, Kazuaki Hashimoto: Effect of Vanadium Ion Addition on Sintering of β-Tricalcium Phosphate by Hot Pressing; *Phosphorous Research Bulletin*, Vol.**26**, pp.4-5 (2012).

Katsumi Yoshida, Yuji Aoyagi, Hiroyuki Akimoto, Toyohiko Yano, Masaki Kotani, Toshio Ogasawara: Interfacial Control of Uni-Directional SiC_f/SiC Composites Based on Electrophoretic Deposition and Their Mechanical Properties; *Compos. Sci. Technol.*, Vol.**72,** No.14, pp.1665-1670 (2012).

Branko Matovic, Dusan Bucevac, Marija Prekajski, Vesna Maksimovic, Devendraprakash Gautam, Katsumi Yoshida, Toyohiko Yano: Synthesis and Characterization of Nanometric Yttrium-Doped Hafnia Solid Solutions; *J. Euro. Ceram. Soc.*, Vol.**32**, pp.1971-1976 (2012).

Yoshikazu Suzuki, Tohru S. Suzuki, Yutaka Shinoda, Katsumi Yoshida: Uniformly Porous $MgTi_2O_5$ with Narrow Pore-Size Distribution: XAFS Study, Improved In Situ Synthesis, and New In Situ Surface Coating; *Adv. Eng. Mater.*, Vol.**14**, No.12, pp.1134-1138(2012).

Go Kametani, Takenobu Sakai, Shuichi Wakayama, Katsumi Yoshida: AE Evaluation of Thermal Shock Fracture Process in Silicon Nitride with Controlled Grain Size; The Japanese Society for Non-Destructive Inspection, Progress in Acoustic Emission XVI, *Proceedings of The 21st International Acoustic Emission Symposium (IAES21-OKINAWA)*, pp.217-222 (2012).

Masafumi Akiyoshi, Hidetsugu Tsuchida, Ikuji Takagi, Toshimasa Yoshiie, Xu Qiu, Koichi Sato and Toyohiko Yano: Irradiation effects on thermal diffusivity and positron annihilation lifetime in ceramics induced by neutron and 30 MeV electron; *J. Nucl. Sci. Technol.*, Vol.**49**, 595-601 (2012).

Toyohiko Yano: Message from the Editorial Board for Reconstruction from the Higashi-Nippon Disaster; *Bulletin of the Ceram. Soc. Jpn.*, **47**[11], 876-878, (2012) Katsumi Yoshida, Chin-Chet See, Toyohiko Yano, Satoshi Yokoyama: Microstructure of Porous Silicon Carbide Ceramics Based on In-Situ Grain Growth; *10th International Symposium on Ceramic Materials and Components for Energy and Environmental Applications*, May 21, 2012, Dresden, Germany, p.38.

Toshio Ogasawara, Takuya Aoki, Masaki Kotani, Katsumi Yoshida, Yosuke Okubo, Toyohiko Yano: Processing and Properties of Silicon Alloy Infiltrated SiC fiber/SiC Matrix Composites; *10th International Symposium on Ceramic Materials and Components for Energy and Environmental Applications*, May 23, 2012, Dresden, Germany, p.113.

Katsumi Yoshida, Hiroyuki Akimoto, Yuji Aoyagi, Masaki Kotani, Toshio Ogasawara, Toyohiko Yano: Interfacial Control of Uni-Directional SiC_f/SiC Composites Based on Electrophoretic Deposition Method; *10th International Symposium on Ceramic Materials and Components for Energy and Environmental Applications*, May 23, 2012, Dresden, Germany, p.115.

Katsumi Yoshida, Yuji Aoyagi, Hiroyuki Akimoto, Toyohiko Yano, Masaki Kotani, Toshio Ogasawara: Application of Electrophoretic Deposition For Interfacial Control of SiC_f/SiC Composites; *Workshop on The Design of Ceramic-Fiber Based Composites for Service Above 1400 Centigrade*, June 11, 2012, Boulder, Colorado, USA.

Katsumi Yoshida, Hiroyuki Akimoto, Akihiro Yamauchi, Toyohiko Yano, Masaki Kotani, Toshio Ogasawara: Application of Electrophoretic Deposition for Interfacial Control of SiC_f/SiC Composites; *The 6th International Conference on the Science and Technology for Advanced Ceramics (STAC-6)*, June 26, 2012, Yokohama, Japan, 1P-P-O2.

Areerak Rueanngoen, Masamitsu Imai, Katsumi Yoshida, Toyohiko Yano: Annealing Behavior of SiAlON Ceramics Neutron-Irradiated in JMTR up to a Fluence of $8.5x10^{24}$ n/m^2; *The 6th International Conference on the Science and Technology for Advanced Ceramics (STAC-6)*, June 26, 2012, Yokohama, Japan, 1P-CH-P8.

Katsumi Yoshida, Yutaka Shinoda, Yoshikazu Suzuki: Sintering of Silicon Carbide Ceramics with Al_2O_3-TiO_2 Additives by Hot-Pressing; *The 6th International Conference on the Science and Technology for Advanced Ceramics (STAC-6)*, June 26, 2012, Yokohama, Japan, 1P-S-P51.

Tomohiro Kobayashi, Katsumi Yoshida, Toyohiko Yano: Synthesis and Sintering of Tructured Octahedral Boron Carbide Powder; *The 6th International Conference on the Science and Technology for Advanced Ceramics (STAC-6)*, June 26, 2012, Yokohama, Japan, 1P-S-P52.

Yoshikazu Suzuki, Tohru S. Suzuki, Yutaka Shinoda, Katsumi Yoshida: Uniformly Porous $MgTi_2O_5$ with Narrow Pore-Size Distribution: XAFS Study, Improved In-Situ Synthesis, and New In-Situ Surface Coating; *The 6th International Conference on the Science and Technology for Advanced Ceramics (STAC-6)*, June 27, 2012, Yokohama, Japan, 2A-EE-O5.

Noppasint Jiraborvornpongsa, Masamitsu Imai, Katsumi Yoshida, Toyohiko Yano: Thermal Conductivity Enhancement of Alumina Containing SiC Nanowires; *The 6th International Conference on the Science and Technology for Advanced Ceramics (STAC-6)*, June 27, 2012, Yokohama, Japan, 2A-S-O2.

Yutaka Shinoda, Yoshikazu Suzuki, Katsumi Yoshida: Silicon Carbide Ceramics with in-situ Mullite Dispersion by Using Al_2O_3-SiO_2 Additives; *The 6th International Conference on the Science and Technology for Advanced Ceramics (STAC-6)*, June 27, 2012, Yokohama, Japan, 2A-S-O4.

Toyohiko Yano, Katsumi Yoshida: Processing and Property of Continuous Fiber-Reinforced SiC Matrix Composites; *International Conference on Traditional and Advanced Ceramics 2012 (ICTA2012)*, August 24, 2012, Bangkok, Thailand, INA-09, p.26.

Katsumi Yoshida, Hiroyuki Akimoto, Akihiro Yamauchi, Toyohiko Yano, Masaki Kotani, Toshio Ogasawara: Fabrication of High Performance SiC_f/SiC Composites Based on Electrophoretic Deposition Method; *International Conference on Traditional and Advanced Ceramics 2012 (ICTA2012)*, August 23, 2012, Bangkok, Thailand, AO-047, p.65.

Noppasint Jiraborvornpongsa, Masamitsu Imai, Katsumi Yoshida, Toyohiko Yano: SiC Nanowires Synthesized and Effects of Their Addition on the Thermal Conductivity of Alumina Matrix Composites; *International Conference on Traditional and Advanced Ceramics 2012 (ICTA2012)*, August 23-24, 2012, Bangkok, Thailand, AP-041, p.132.

Katsumi Yoshida, Chin-Chet See, Satoshi Yokoyama, Toyohiko Yano: Fabrication of Porous SiC Ceramics Based on In-Situ Grain Growth and Their Microstructures; *International Conference on Traditional and Advanced Ceramics 2012 (ICTA2012)*, August 23-24, 2012, Bangkok, Thailand, AP-049, p.135.

Areerak Rueanngoen, Masamitsu Imai, Katsumi Yoshida, Toyohiko Yano: Recovery of Neutron Irradiated SiAlON Ceramics by Thermal Annealing up to 1200°C; *The Nuclear Materials Conference 2012 (NuMat 2012)*, October 23, 2012, Osaka, Japan, P1.42.

Tomohiro Kobayashi, Katsumi Yoshida, Toyohiko Yano: Fabrication of Carbon Nanotubes/Boron Carbide Composites with an Aluminium Additive; *The Nuclear Materials Conference 2012 (NuMat 2012)*, October 24, 2012, Osaka, Japan, P2.26.

Katsumi Yoshida, Satoshi Kajikawa, Toyohiko Yano: Microstructure Design and Control for Improvement of Thermal Conductivity of SiC_f/SiC Composites; *The Nuclear Materials Conference 2012 (NuMat 2012)*, October 24, 2012, Osaka, Japan, P2.35.

Toyohiko Yano, Yusuke Futamura, Masamitsu Imai, Katsumi Yoshida: Recovery Behavior of Neutron-Induced Damage of AlN Irradiated at Higher Temperatures by Thermal Annealing; *The Nuclear Materials Conference 2012 (NuMat 2012)*, October 24, 2012, Osaka, Japan, O84.

Go Kametani, Takenobu Sakai, Shuichi Wakayama, Katsumi Yoshida: AE Evaluation of Thermal Shock Fracture Process in Silicon Nitride with Controlled Grain Size; *The Japanese Society for Non-Destructive Inspection, The 21st International Acoustic Emission Symposium (IAES21-OKINAWA)*, November 30, 2012, Okinawa, Japan.

Tomohiro Kobayashi, Katsumi Yoshida, Toyohiko Yano: Effects of B_4C Addition on Yield and Morphology of B_4C powder Synthesized from B_2O_3-C-B_4C Mixtures; *The 50th Anniversary Symposium on Basic Science of Ceramics*, Tokyo, January 12, 2012, 1P01, p.126.

Noppasint Jiraborvornpongsa, Masamitsu Imai, Katsumi Yoshida, Wasana Khongwong, Toyohiko Yano: Mechanical and Thermal Properties of SiC Nanowires-Reinforced Alumina Matrix Composite; *The 50th Anniversary Symposium on Basic Science of Ceramics*, Tokyo, January 12, 2012, 1P02, p.127.

Katsumi Yoshida, Yoshiori Akiyama, Masamitsu Imai, Toyohiko Yano: Sinterability and Microstructure of Mullite Ceramics with Iron Oxide Addition; *The 50th Anniversary Symposium on Basic Science of Ceramics*, Tokyo, January 13, 2012, 2H06, p.278.

Areerak Rueanngoen, Komei Kanazawa, Masamitsu Imai, Katsumi Yoshida, Toyohiko Yano: Swelling and Microstructure of Neutron-Irradiated SiAlON Ceramics; *5th Student Meeting of the Kanto-Koetsu Division of the Atomic Energy Society of Japan*, Kanagawa, March 9, 2012, 2B11, p.26.

Katsumi Yoshida, Yutaka Shinoda, Yoshikazu Suzuki: Sinterability of Hot-Pressed Silicon Carbide using Alumina and Titania as Sintering Additives; *Annual Meeting of The Ceramic Society of Japan, 2012*, Kyoto, March 19, 2012, 1E32, p.22.

Katsumi Yoshida, Satoshi Yokoyama, Chin-Chet See, Toyohiko Yano: Effect of SiC Particle Size on the Microstructure of Porous SiC Ceramics Based on In-Situ Grain Growth; *25th Fall Meeting of The Ceramic Society of Japan*, Nagoya, September 19, 2012, 1E23.

Toyohiko Yano, Katsumi Yoshida: Processing and Mechanical Properties of SiC Continuous Fiber Reinforced SiC Matrix Composites; *25th Fall Meeting of The Ceramic Society of Japan*, Nagoya, September 20, 2012, 2E17.

Yosuke Okubo, Katsumi Yoshida, Toyohiko Yano, Toshio Ogasawara, Takuya Aoki: Fabrication of SiC_f/SiC Composite Fabricated by Advanced Melt Infiltration Method; *25th Fall Meeting of The Ceramic Society of Japan*, Nagoya, September 20, 2012, 2E19.

Noppasint Jiraborvornpongsa, Masamitsu Imai, Katsumi Yoshida, Toyohiko Yano: Effect of Synthesis Temperature and Gas Flow Rate on the SiC Nanowires Formation by Thermal Evaporation Method; *25th Fall Meeting of The Ceramic Society of Japan*, Nagoya, September 20, 2012, 2PE01.

Tomohiro Kobayashi, Katsumi Yoshida, Toyohiko Yano: Fabrication and Microstructure of Carbon Nanotubes/Boron Carbide Composites; *25th Fall Meeting of The Ceramic Society of Japan*, Nagoya, September 20, 2012, 2PE02.

Areerak Rueanngoen, Masamitsu Imai, Katsumi Yoshida, Toyohiko Yano: Irradiation Effects and Thermal Annealing Behavior on Polymorphs of SiAlON Ceramics; *25th Fall Meeting of The Ceramic Society of Japan*, Nagoya, September 20, 2012, 2PE03.

Go Kametani, Takenobu Sakai, Shuichi Wakayama, Katsumi Yoshida: Evaluation of Thermal Shock Fracture Process in Silicon Nitride with Controlled Grain Size by Disc-on Rod Test; *25th Fall Meeting of The Ceramic Society of Japan*, Nagoya, September 21, 2012, 3D15.

W. Watanabe, T. Maekawa, Y. Miyazaki, T. Kida, K. Takeshita, A. Mori: Quadruple Click: A Facile Pathway leading to Tetrakis(4-(1,2,3-triazolyl)methyl)-ethylenediamine Derivatives as a New Class of Extracting Agents for Soft Metal Ions ; *Chem.Asian J.*, Vol.**7**, Iss.7, pp.1679-1683 (2012).

M. Nakase, K. Takeshita: Scale-up Effect of Oil-water Countercurrent Centrifugal Extractor on Extraction Performance; *TRANSACTIONS- AMERICAN NUCLEAR SOCIETY*, Vol. **107** (2012).

M. Nakase, K. Takeshita: Numerical and Experimental Study on Oil-water Dispersion in New Countercurrent Centrifugal Extractor; *Procedia Chemistry*, Vol. **7**, pp. 288-294 (2012).

S. Koyama, M. Suto, H. Ohbayashi, K. Takeshita, T. Ogata, H. Oaki, Y. Inaba: Recovery of Minor Actinides from Spent Fuel via an Extraction Chromatographic Technique using TPPEN-Immobilized Gels; *Separation Science and Technology*, Vol. **47**, Iss.14-15, pp. 2024-2028 (2012).

K. Watanabe, T. Yano, K. Takeshita, K. Minami, E. Ochi: X-ray CT Imaging of the Vitrified Glasses Containing Pseudo-Radioactive Wastes - Structure and chemical reactions of glass beads and wastes in Cold Cap - ; *Glass Technology : European Journal of Glass Science and Technology Part A*, Vol.**53**, No.6, pp.273-278 (2012).

M. Nakase, K. Takeshita: Relation between oil-water flow and extraction performance in liquid-liquid countercurrent centrifugal extractors with Taylor vortices; *Journal of Nuclear Science and Technology*, Vol. **50**, ISS.3, pp. 287-295 (2013).

M. Nakase, K. Takeshita: Continuous Separation of Eu/Sm by Oil-water countercurrent centrifuge extractor with Taylor vortexes; *8th International Conference on f-Elements (ICFE8)*, Udine, Italy, August 26-31, 2012.

M. Nakase, K. Takeshita: Numerical and Experimental Study on Oil-water Dispersion in New Countercurrent Centrifugal Extractor; *ATALANTE 2012 Nuclear chemistry for sustainable fuel cycles*, Montpellier, France, September 2-7, 2012,.

K. Takeshita: Extraction Chromatographic Separation of Am(III) and Eu(III) by Functional Polymer Gels with TPEN Analogs; *BIT's 2nd New Energy Forum2012*, Guangzhou, China, October 19-21, 2012.

M. Nakase, K. Takeshita: Scale-up Effect of Oil-water Countercurrent Centrifuge Extractor on Extraction Performance; *ANS Winter Meeting and Nuclear Technology Expo*, San Diego, US, November 11-15, 2012.

K. Takashita, H. Takahashi, K. Mogami, A. Ishido: Recovery of Cesium from Agricultural Soil by Combined Process with Hydrothermal Decomposition and Coagulation Settling; *The 1st Meeting of the Society for Remediation of Radioactive Contamination in Environment*, Fukushima, May 19-21, 2012, S5-2.

K. Kanazawa, T. Fukuda, H. Takahashi, Y. Inaba, T. Ogata: The study on Separation and Removal Techniques of Cesium from Plant using Hydrothermal Decomposition; *The 1st Meeting of the Society for Remediation of Radioactive Contamination in Environment*, Fukushima, May 19-21, 2012.

H. Takahashi, C. Iguchi, K. Takeshita, Y. Inaba, K. Kanazawa, T. Fukuda, K. Mogami, A. Ishido: Development of Cesium Recovery Process from Soil and Plant using Hydrothermal Decomposition and Coagulation Settling; *The 8th Seminar of Atomic Energy Society of Japan, Reprocessing and Recycle Technology Division*, August 8, Tokyo, 2012.

Y. Inaba, R. Hasu, A. Mori, K. Takeshita: Heavy Metal Separation by Alkyl-chain-introduced into Hydrophobized Multidentate Ligand containing Nitrogen; *The 44th Autumn Meeting of the Society of Chemical Engineers, Japan*, Sendai, September 19-21, 2012, R119.

K. Takeshita, H. Takahashi, Y. Inaba, T. Ogata: Application of Ion Exchange Technique to Decontamination of Polluted Sludge and Soil generated by Fukushima Nuclear Disaster; *2012 Fall Meeting of the Atomic Energy Society of Japan*, Hiroshima, September 19-21, 2012, C32.

M. Nakase, K. Takeshita: Scale up effect of liquid-liquid countercurrent centrifugal extractor for multiple theoretical stages; *2012 Fall Meeting of the Atomic Energy Society of Japan*, Hiroshima, September 19-21, 2012, E24.

O. Higashijima, Y. Nakano, K. Takeshita: Thermal Decomposition Analysis of Nitrade and Glass Beads Mixture in Fuel Reprocessing Waste; *2012 Fall Meeting of the Atomic Energy Society of Japan*, Hiroshima, September 19-21, 2012, E47.

K. Takeshita: Restoration Technology of Water Environment Contaminated by Radioactive Cesium; *2012 Annual Meeting of the Japan Society of Nuclear and Radiochemical Sciences*; Tokyo, October 3-5, 2012.

Y. Inaba, A. Mori, K. Takeshita: Synthesis of Hydrophobized TPEN Derivative for Extraction Separation of MA/Ln; *2012 Annual Meeting of the Japan Society of Nuclear and Radiochemical Sciences*; Tokyo, October 3-5, 2012.

K. Watanabe, N. Ikeji, R. Nakata, T. Amagasa, T. Yano, K. Takeshita, K. Minami, E. Ochi: High temperature X-ray CT analysis for in-situ observation of glass melting reaction process; *53th Colloquium on Glass and Photonics Materials*, Sapporo, October 25-26, 2012.

K. Takeshita: Development of Decontamination Technology of Water, Soil and Sewage Sludge polluted by Fukushima Daiichi NPP Accident; *The 31th Colloquium on Solvent Extraction of Japan Association of Solvent Extraction*, Kanazawa, November 16-17, 2012.

N. Umemoto, Y. Inaba, A. Mori, K. Takeshita: Heavy metal separation by new polymer gels cross-linked by TPEN derivative with multidentate nitrogen-donor ligands; *The 31th Colloquium on Solvent Extraction of Japan Association of Solvent Extraction*, Kanazawa, November 16-17, 2012.

T. Sugano, H. Inazuka, T. Ogata, Y. Inaba, K. Takeshita: Development of Precious Metal Recovery Process by Photoresponsive Solvent Extraction Method; *The 31th Colloquium on Solvent Extraction of Japan Association of Solvent Extraction*, Kanazawa, November 16-17, 2012.

K. Ootake, T. Ogata, Y. Inaba, K. Takeshita: Development of Heavy Metal Extraction Process by Controlling of

Complexation between Metal and Dithiocarbamate using Ultrasound; *The 31th Colloquium on Solvent Extraction of Japan Association of Solvent Extraction*, Kanazawa, November 16-17, 2012.

K. Watanabe, R. Nakata, T. Kishi, S. Shibata, T. Yano, K. Takeshita, K. Minami, E. Ochi: High-Temperature X-ray CT imaging of Vitrification Process of Glass Beads and Pseudo-Radioactive Waste; *The 29th International Korea-Japan Seminar on Ceramics*, Daegu, Korea, November 21-24.

Y. Inaba, N. Umemoto, A. Mori, K. Takeshita: Heavy metal separation by polymer gels cross-linked by TPEN derivative with multidentate nitrogen-donor ligands; *The 78th Annual Meeting of the Society of Chemical Engineers*, Toyonaka, March 17-19, 2013, R104.

K. Watanabe, N. Ikeji, R. Nakata, T. Amagasa, T. Yano, K. Takeshita, K. Minami, E. Ochi: Formation and analysis of vitrification of glass beads with pseudo-radioactive wastes; *2013 Annual Meeting of the Ceramic Society of Japan*, Tokyo, March 17-19, 2013.

T. Amagasa, K. Watanabe, N. Ikeji, R. Nakata, T. Kishi, S. Shibata, T. Yano, K. Takeshita, K. Minami, E. Ochi: High-temperature X-ray CT imaging of vitrification process of glass beads and pseudo-radioactive wastes; *2013 Annual Meeting of the Ceramic Society of Japan*, Tokyo, March 17-19, 2013.

M. Nakase, K. Takeshita: Feasibility Study on Extraction, Separation and Back Extraction Process with Liquid-liquid Countercurrent Centrifugal Extractor; *2013 Annual Meeting of the Atomic Energy Society of Japan*, Higashi-Oosaka, March 26-28, 2013, F14.

Y. Nakano, O. Higashijima, K. Takeshita, T. Fukuda, K. Minami, E. Ochi: Thermal Decomposition of Simulated High-level Liquid Wastes in Temperature Rising Process; *2013 Annual Meeting of the Atomic Energy Society of Japan*, Higashi-Oosaka, March 26-28, 2013, F05.

S. Suzuki, T. Yaita, T. Kobayashi, H. Shiwaku, H. Oaki, K. Takeshita, A. Mori: Separation of MA and Ln by Extraction Chromatography using Functional Gel copolymerized with Mmultidentate Inclusion Ligands (1)Structure Optimization of Functional Gel Copolymerized with Mmultidentate Inclusion Ligands by XAFS; *2013 Annual Meeting of the Atomic Energy Society of Japan*, Higashi-Oosaka, March 26-28, 2013, F19.

H. Oaki, K. Takeshita, T. Yaita, S. Suzuki, S. Koyama, A. Mori: Separation of MA and Ln by Extraction Chromatography using Functional Gel copolymerized with Multidentate Inclusion Ligands (2) Thin-film Coating of Gel into Porous Silica and Column Separation Tests; *2013 Annual Meeting of the Atomic Energy Society of Japan*, Higashi-Oosaka, March 26-28, 2013, F20.

M. Suto, H. Ohbayashi, S. Koyama, K. Sekioka, K. Takeshita, Y. Inaba, T. Ogata, H. Oaki: Separation of MA and Ln by Extraction Chromatography using Functional Gel copolymerized with Multidentate Inclusion Ligands. (3) Recovery of Minor Actinide from the Spent Fuel; *2013 Annual Meeting of the Atomic Energy Society of Japan*, Higashi-Oosaka, March 26-28, 2013, F21.

K. Takeshita, T. Yaita, S. Suzuki, S. Koyama, A. Mori: Separation of MA and Ln by Extraction Chromatography using Functional Gel copolymerized with Multidentate Inclusion Ligands (4) MA Separation Process; *2013 Annual Meeting of the Atomic Energy Society of Japan*, Higashi-Oosaka, March 26-28, 2013, F22.

Y. Oguri, K. Kondo, J. Hasegawa: Numerical Study of Heavy-Ion Stopping in Foam Targets with One-Dimensional Subcell-Scale Hydrodynamic Motions; *Nucl. Instrum. Methods Phys. Res., Sect. A*, in press.

J. Hasegawa, K. Kondo, Y. Oguri, K. Horioka: Ion Beam Focusing with Cone Optics for WDM Experiments; *Nucl. Instrum. Methods Phys. Res., Sect. A*, in press.

Y. Oguri, Y. Hu, K. Kondo, H. Fukuda, J. Hasegawa: Digital Subtraction Cineangiography Using Proton-Induced Quasi-Monochromatic Pulsed X-rays; *Int. J. PIXE*, to be published.

K. Ploykrachang, J. Hasegawa, H. Fukuda, K. Kondo, Y. Oguri: Production of Quasi-Monochromatic X-Ray Microbeams Using MeV-Protons and a Polycapillary X-ray Half Lens; *Int. J. PIXE*, to be published.

J. Hasegawa, K. Kondo, Y. Oguri, K. Horioka: Ion Beam Focusing with Cone Optics for WDM Experiments; *19th International Symposium on Heavy Ion Inertial Fusion (HIF2012),* August 12-17, 2012, Berkeley, California, USA, ID 69.

K. Horioka, M. Nakajima, T. Kawamura, J. Hasegawa, S. Ikeda, Y. Sakai, Y. Oguri, K. Kondo, S. Kawata, T. Kikuchi, T. Sasaki, M. Murakami, K. Takahashi, M. Okamura, K. Takayama: Japanese Program Overview on HIF and Related Research Activities; *19th International Symposium on Heavy Ion Inertial Fusion (HIF2012),* August 12-17, 2012, Berkeley, California, USA, ID 83.

Y. Oguri, K. Kondo, J. Hasegawa: Numerical Study of Heavy-Ion Stopping in Foam Targets with One-Dimensional Subcell-Scale Hydrodynamic Motions; *19th International Symposium on Heavy Ion Inertial Fusion (HIF2012),* August 12-17, 2012, Berkeley, California, USA, ID 103.

Y. Oguri, Y. Hu, K. Kondo, H. Fukuda, J. Hasegawa: Proton-Induced Dual-Energy X-ray Cineangiography for Reducing Doses of Radiation and Contrast Media; *2012 Fall Meeting of Atomic Energy Society of Japan*, September 19-21, 2012, Hiroshima, K09.

Y. Oguri, Y. Hu, K. Kondo, H. Fukuda, J. Hasegawa: Digital Subtraction Cineangiography Using Proton-Induced Quasi-Monochromatic Pulsed X-rays; 28th *Symposium on PIXE in Japan*, November 7-9, 2012, Tokyo, Japan, 5-1.

K. Ploykrachang, J. Hasegawa, H. Fukuda, K. Kondo, Y. Oguri: Production of Quasi-Monochromatic X-Ray Microbeams Using MeV-Protons and a Polycapillary X-ray Half Lens; 28th *Symposium on PIXE in Japan*, November 7-9, 2012, Tokyo, Japan, 2-1.

Masao Komeda, Toru Obara: Study on the burn-up charactierisitics of a thermal neutron filter containing B_4C particles for NTD-Si irradiation; *Annlas of Nuclear Energy*, Vol.**53**, 35-39 (2012).

Byambajav Munkhbat, Toru Obara: Design simplification of a small nuclear reactor for large-diameter neutron transmutation doping silicon using control rods; *Journal of Nuclear Science and Technology*, Vol.**49** [8] , pp. 845-856, (2012).

Odmaa Sambuu, Toru Obara: Conceptual design for a small modular district heating reactor for Mongolia; *Annlas of Nuclear Energy*, **47**, 210-215 (2012).

Byambajav Munkhbat, Toru Obara: Design Concept of a Small Nuclear Reactor for Large-Diameter NTD-Si using a Conventional PWR Full-Length Fuel Assembly; *Journal of Nuclear Science and Technology*, Vol.**49** [5], pp. 535-543, (2012).

Hiroki Takezawa and Toru Obara: New Approach to Space-Dependet Kinetic Analysis by the Integral Kinetic Model; *Nuclear Science and Engineering*, Vol.**171**, pp.1-12 (2012).

Dwi Irwanto, Toru Obara: Burnup Characteristics and Fuel Cycle Economics of Mixed Uranium-Thorium Fuel in a Simplified Small Pebble Bed Reactor; *Journal of Nuclear Science and Technology*, Vol.**49** [2] , pp 222-229, (2012).

Toru Obara, Taiki Onoe: Effect of Particle Type Burnable Poisons in HTGR; *Transactions of the American Nuclear Society*, Vol.**107**, 1023-1024 (2012).

Piyatida Trinuruk, Toru Obara: Effect of SiC Coating over Graphite Structure in HTGR; *Transactions of the American Nuclear Society*, Vol.**107**, 1262-1263 (2012).

Toru Obara, Dwi Irwanto: Burnup Performance of Small Pebble Bed Reactor with Accumlative Fuel Loading Scheme; *Proceedings of 6th International Topical Meeting on High Temperature Reactor Technology HTR2012*, October 28- *November 1, 2012, Tokyo, Japan*, HTR2012-5-019 (2012).

Byambajav Munkhbat, Toru Obara: Conceptual design of a small nuclear reactor for NTD-Si using short PWR fuel assemblies; *Transactions of the American Nuclear Society*, Vol.**106**, 826-829 (2012).

Toru Obara, Hiroki Takezawa: Possibility of nuclear pumped laser experiment using low enriched uranium; AIP Conference Proceedings Volume 1448, *The 3rd Internetional Conference on Advances in Nuclear Science and Engineering 2011 ICANSE2011*, pp. 25-29 (2012).

Toru Obara: Concept of Small Pebble Bed Reactor with Accumulative Fuel Loading Scheme; *Third International Ulaanbaatar Conference on Nuclear Physics and Applications UBC2012*, 17-20 September 2012, Ulaanbaatar, Mongolia (2012).

Byambajav Munkhbat, Toru Obara: Design Concept of a Small Nuclear Reactor for Large-Diameter NTD-Si using Short PWR Fuel Assemblies; *2012 Fall Meeting of Atomic Energy Society of Japan*, September 19-21, 2012, Hiroshima, Japan, P40 (2012).

Piyatida Trinuruk, Toru Obara: Prismatic HTGR with Silicon Carbide Coated Graphite Block Core (1) Effects on Thermal-Hydraulic Behavior under the Normal Operation; *2012 Fall Meeting of Atomic Energy Society of Japan*, P41 (2012).

Jun Nishiyama, Toru Obara: Study on start-up of a CANDLE burn-up reactor by using accelerator neutron sources; *2012 Fall Meeting of Atomic Energy Society of Japan*, September 19-21, 2012, Hiroshima, Japan, P35 (2012).

Dwi Irwanto, Toru Obara: Design Study of Innovative Simplified Small Pebble Bed Reactor; （５）Passive Safety Analysis for Decay Heat Removal without Forced Cooling; *2012 Fall Meeting of Atomic Energy Society of Japan*, September 19-21, 2012, Hiroshima, Japan, C38 (2012).

Topan Setiadipura, Toru Obara: Validation of Depletion Module of Equilibrium Burnup Analysis Code for OTTO Cycle in Pebble Bed Reactor; *2012 Fall Meeting of Atomic Energy Society of Japan*, September 19-21, 2012, Hiroshima, Japan, C39 (2012).

Byambajav Munkhbat, Toru Obara: Design study on a small reactor for silicon semiconductor production using LWR fuel；(4) Uniformity of doping; *2012 Fall Meeting of Atomic Energy Society of Japan*, September 19-21, 2012, Hiroshima, Japan, D06 (2012).

Taiki Onoe, Toru Obara: Study on improvement of burn-up performance in HTGR by burnable poison particle; *2012 Annual Meeting of Atomic Energy Society of Japan*, March 19-21, 2012, Fukui, Japan, D08 (2012).

Piyatida Trinuruk, Toru Obara: Neutronic Analysis of Prismatic HTGR with Silicon Carbide Coated Graphite Block Core; *2012 Annual Meeting of Atomic Energy Society of Japan*, March 19-21, 2012, Fukui, Japan, D09 (2012).

Takehiko Tomonari, Toru Obara: Design study on Reactor Pumped Laser for Inertial Confinement Fusion Reactor; *2012 Annual Meeting of Atomic Energy Society of Japan*, March 19-21, 2012, Fukui, Japan, D50 (2012).

Yosuke Isobe, Toru Obara: Study on simulation of nuclear pumped laser oscillation in a reactor core; *2012 Annual Meeting of Atomic Energy Society of Japan*, March 19-21, 2012, Fukui, Japan, D51 (2012).

Yoshiki KIMURA, Masaki SAITO and Hiroshi SAGARA: Improvement of Evaluation Methodology of Plutonium for Intrinsic Feature of Proliferation Resistance Based on Its Isotopic Barrier; *Ann. Nucl. Energy*, Vol. **40**, Issue 1, pp.130-140, 2012.

Takashi OHNISHI, Shin-ichi KOYAMA, Tomooki SHIBA, Hiroshi SAGARA and Masaki SAITO: Protected Plutonium Production at fast breeder reactor blanket –chemical analysis of uranium-238 samples irradiated in experimental fast reactor JOYO; *Prog. Nucl. Energy*, Vol. **57**, Issue 1, pp.125-129, 2012.

E. Hamase, M. Saito, H. Sagara and C. Y. Han: Long-life Fast Breeder Reactor with Highly Protected Pu Breeding by Introducing Axial Inner Blanket and Doping Minor Actinides; *Ann. Nucl. Energy*, Vol. **44**, Issue 1, pp.87-102, 2012.

Yoshiki KIMURA, Masaki SAITO, Hiroshi SAGARA and Chi Young Han: Evaluation of proliferation resistance of plutonium based on spontaneous fission neutron emission rate; *Ann. Nucl. Energy*, Vol. **46**, pp.152-159, 2012.

M. Nakamura, M. Saito and H. Sagara: Neutronics analysis of americium-based fuel for long-life core; *Ann. Nucl. Energy*, vol. **43**, p. 77-82, 2012.

Sidik Permana, Mitsutoshi Suzuki, Masaki Saito, Novitrian, Abdul Waris, Zaki Suud: Study on material attractiveness aspect of spent nuclear fuel of LWR and FBR cycles based on isotopic plutonium production; *Energy conversion and Management*, Vol. **72**, pp.19-26, 2013.

Erina Hamase, Frederic Damian, Cristine Poinot-salanon, Masaki Saito, Hiroshi Sagara and Chi Young Han: A feasibility study on long-life reduced-moderation water reactor with highly protected Pu breeding by doping with minor actinides; *Ann. Nucl. Energy*, Vol. **54**, pp.76-84, 2013.

Tomooki Shiba, Hiroshi Sagara, Takashi Ohnishi, Shin-ichi Koyama, Shigetaka Maeda, Chi Young Han, Masaki Saito: Effect of radial zoning of 241Am content on homogenization of denatured Pu with broad range of neutron energy based on U irradiation test in the experimental fast reactor Joyo; *Ann. Nucl. Energy*, Vol. **51**, pp.74-80, 2013.

H. Sagara, H. Tomikawa, M. Watahiki, Y. Kuno: Sensitivity Analysis of Low-Volatile FPs and Cm-244 Inventory in Irradiated Nuclear Fuel for Special Nuclear Material Quantification in Fuel Debris; *Trans. Am. Nucl. Soc.*, vol. **107**, no. 1, p 803-804, 2012.

K. Matsumoto, H. Sagara, C. Y. Han, T. Ohnishi, M. Saito, I. Yamauchi: Effect of Neutron Moderator on Protected Plutonium Production in Fast Breeder Reactor Blanket; *Trans. Ame. Nucl. Soc.,* vol. **107**, no. 1, p 1018-1019, 2012.

H. Sagara, H. Tomikawa, M. Watahiki, Y. Kuno: Feasibility Study of Gamma Spectroscopy of Low-Volatile FPs for Special Nuclear Material Accountancy in Molten Core Material; *Proc. Inst. Nucl. Mat. Manage. 53rd annual mtg.*, Orland, July 14-18, 2012.

Hiroshi SAGARA, Hirofumi TOMIKAWA, Masaru WATAHIKI, Yusuke KUNO: Applicability of accompanying FP passive gamma measurement to nuclear material quantification in fuel debris; *Proc. Int. Nucl. Mat. Manage. Japan 33rd Annual Mtg.*, Tokyo, Oct. 25-26, 2012.

Yoshimasa Shuzui, Masaki Saito: Study on low-moderated long-life core with miner-actinide loading fuel; *2013 Annual Mtg. Atomic Energy Society Japan*, Osaka, March 26-28, 2013, G03.

Ippei Yamauchi, Hiroshi Sagara, Masaki Saito, Takashi Onishi: Optimal study of moderator design in fast reactor blanket fuel for protected Pu production; *2013 Annual Mtg. Atomic Energy Society Japan*, Osaka, March 26-28, 2013, G05.

Yoshinori TANI, Chi Young HAN, Hiroshi SAGARA, Masaki SAITO: Study on Advanced Nuclear Fuel with High Proliferation Resistance by Doping Radioactive Lanthanides; *2013 Annual Mtg. Atomic Energy Society Japan*, Osaka, March 26-28, 2013, G06.

Taku Hashimoto and Masaki Saito: Study on accelerator driven system for space nuclear fuel supply; *2013 Annual Mtg. Atomic Energy Society Japan*, Osaka, March 26-28, 2013, G19.

N. Miyamoto, T. Tsukahara, Y. Kachi, M. Harada, Y. Kayaki, T. Ikariya, Y. Ikeda: Studies on Solubility of Uranyl Complexes in Supercritical Carbon Dioxide and Its Controlling Factors Using UV-visible and ^{17}O- and

^{19}F-NMR Spectroscopy; *J. Nucl. Sci. Technol.*, **49**, 37-46 (2012).

T.J. Bell, Y. Ikeda: Efficient Extraction of Rh(III) from Nitric Acid Medium Using a Hydrophobic Ionic Liquid; *Dalton Trans.*, **41**, 4303-4305 (2012).

M. C. Ali, T. Suzuki, Y. Tachibana, Y. Sasaki, Y. Ikeda: Selective extraction of perrehnate anion in nitric acid solution using 2,2’-(methylimino)bis(*N,N’*-diethylacetamide) as an extractant; *Sep. Purif. Technol.*, **92**, 77-82 (2012).

N. Miyamoto, T. Tsukahara, Y. Ikeda: NMR Spectroscopic Evidences of Lewis Acid-Lewis Base Complex Formation of Perfluoroborane with Uranyl β-Diketonato Complexes; *Chem. Lett.*, **41**, 513-515 (2012).

B. Machura, M. Wolff, D. Tabak, Y. Ikeda, K. Hasegawa: Novel *trans*-dioxorhenium complex with imidazo[1,2a]pyridine ligand – Synthesis, spectroscopic and electrochemical characterization, X-ray crystal structure and DFT calculations; *Polyhedron*, **39**, 76-84 (2012).

T. Ogura, K. Sasaki, K. Takao, T. Arai, Y. Ikeda: Electrochemical Behavior of $[UO_2Cl_4]^{2-}$ in 1-Ethyl-3-methylimidazolium Based Ionic Liquids; *Sci. China Chem.*, **55**, 1699-1704 (2012).

M. Nogami, Y. Sugiyama, T. Kawasaki, M. Harada, Y. Kawata, Y. Morita, T. Kikuchi, Y. Ikeda: Stability of Pyrrolidone Precipitants against γ-Ray Irradiation; *Sci. China Chem.*, **55**, 1739-1745 (2012).

T. Suzuki, T. Kawasaki, K. Takao, M. Harada, M. Nogami, Y. Ikeda: A Study on Selective Precipitation Ability of Cyclic Urea to U(VI) for Developing Reprocessing System Based on Precipitation Method; *J. Nucl. Sci. Technol.*, **49**, 1010-1017 (2012).

Y. Tachibana, M. Nogami, Y. Sugiyama, Y. Ikeda: Effect of Pd(II) Species on Decomposition Reactions of Pyrrolidone Derivatives by Ozone; *Ozone Sci. Engin.,* **34**, 359-369 (2012).

T. Suzuki, T. Kawasaki, K. Takao, M. Harada, M. Nogami, Y. Ikeda: A study on Selective Separation of U(VI) Based on Precipitation Method Using Cyclic Urea Derivatives with Low Hydrophobicity; *Atalante 2012*, September 3 - 7, 2012, France, Montpellier.

S. Okumura, Z. Szabo, and Y. Ikeda: Structural Studies on Lanthanide Species Extracted by Using Diamide Compounds as Extractant for Actinide/Lanthanide Separation; *Actinide and Fission Product Partitioning and Transmutation 12th Information Exchange Meeting*, September 24-27, 2012, Prague, Czech Republic.

T. Watanabe, Y. Ikeda: A Study on Identification of Uranyl Comprexes in Aqueous Solution Containing Carbonate ion and Hydrogen Peroxide; *Asian Nuclear Prospect*ｓ *2012（ANUP2012）*, October 16-19, 2012, China, Beijing.

Y. Ohasi, N. Asanuma, M. Harada, Y. Ikeda: A Study on Treatment Method of Uranium Wastes Using Selective Adsorbent to Uranium; *56th symposium of Japan Society of Nuclear and Radiochemical Sciences*, Tokyo, October 3-5, 2012.

T. Kawasaki, Y. Ikeda: Structural Studies on Complexes in Solvent Extraction of Lanthaniod and Actinoid Species Using Diamide Extracting Reagents; *56th symposium of Japan Society of Nuclear and Radiochemical Sciences*, Tokyo, October 3-5, 2012.

Y. Sato, Y. Ikeda, T. Arai: Studies of Structures oand Reactivity of Uranyl(VI) Nitrate Complexes with Pyrrolidone Derivatives in Non-aqueous Solvent; *56th symposium of Japan Society of Nuclear and Radiochemical Sciences*, Tokyo, October 3-5, 2012.

K. Sasaki, M. Harada, Y. Ikeda, T. Arai: A Study on Extraction Behavior of Uranyl(VI) Species Using Task-specific Ionic Liquids; *28th Meeting of Japan Society of Ion Ion Exchange*, Tokyo, October 18-19, 2012.

K. Sasaki, T. Suzuki, M. Harada, Y. Ikeda, T. Arai: Extraction Properties of Uranyl(VI) Species Using Ionic Liquids with High Solubility to Metal Oxides; *3rd Meeting of Ionic Liquids*, Okinawa, December 7-8, 2012.

S. Okumura, T. Kawasaki, T. Tsukahara, Y. Ikeda: Structural Studies on Lanthanoid(III) Complexes with DGA Compounds in Non-aqueous Solvent Using NMR; *35th Symposium on Solution Chemistry of Japan*, Tokyo, November 12-14, 2012.

Y. Ikeda: Chemistry of Uranium Complexes in Ionic Liquids and Its Application; *180th Committee Molten Salt Chemistry*, Chiba, January 24, 2013.

M. Shimokawa, H. Kokubo, N. Asanuma, Y. Ikeda: Extraction of La(III) and Nd(III) into Imidazolium Based Ionic Liquids – Effect of Hydrophobicity and HNO_3 Concentrations on Extraction -; *8th Seminar on Reprocessing and Recycle Technology*, Tokyo, August 24, 2012.

T. Suzuki, T. Kawasaki, M. Harada, Y. Ikeda, K. Takao: Basic Studies on Reprocessing Based on Precipitation Using Urea Derivatives as Precipitants with High Precipitation Ability to Uranul(VI); *8th Seminar on Reprocessing and Recycle Technology*, Tokyo, August 24, 2012.

D. Hwang, T. Tsukahara, Y. Ikeda, K. Tanaka, M. Ohsaka: Analyses of Mechanism of Synthetic Ractions of Lantanoid Oxides Using Hydrothermal Crystallization in Supercritical Water; *8th Seminar on Reprocessing and Recycle Technology*, Tokyo, August 24, 2012.

Y. Tachibana, T. Suzuki, M. Nogami, Y. Sugiyama, Y. Ikeda: A Study on Effect of Fission Products on Decomposition of Pyrrolidone Derivatives Using Ozone; *The Fall Meeting of the Atomic Energy Society of Japan* , Hiroshima, 2012.

T. Kawasaki, S. Okumura, Y. Ikeda, Y. Sasaki: Mutual Separation of MA Using Hydrophilic and Hydrophobic Diamide Compounds (9) - Crystal Structures of Lanthanoid(III) Complexes with Diamide Compounds-; *The Fall Meeting of the Atomic Energy Society of Japan* , Hiroshima, 2012.

M. Harada, Y. Ikeda, Y. Ohashi, N. Asanuma: Development of Uranium Waste Treatment Processes Using Adsorbent with High Adsorptivity to Uranium; *The Fall Meeting of the Atomic Energy Society of Japan* , Hiroshima, 2012.

T. Suzuki, T. Kawasaki, M. Harada, Y. Ikeda, K. Takao, M. Nogami: Basic Studies on Reprocessing Based on Precipitation Using Cyclic Urea Derivatives as Precipitants with High Precipitation Ability to Uranul(VI); *The Annual Meeting of the Atomic Energy Society of Japan* , Osaka, 2013.

HAN Chi Young, OZAWA Masaki, SAITO Masaki: Resourceability on Nuclear Fuel Cycle by Transmutation Approach; *SCIENCE CHINA Chemistry(SPECIAL TOPIC: Nuclear Fuel Cycle Chemistry),* Vol.**55** No.9, pp.1746-1751, September 2012.

Shin-ichi Koyama, Tatsuya Suzuki, Masaki Ozawa, Kiyoko Kurosawa, Reiko Fujita, Hitoshi Mimura, Ken Okada, Yasuji Morita and Yasuhiko Fujii: Advanced-ORIENT Cycle Project: Summary of Phase I Fundamental Studies; Procedia Chemistry, **7** (2012) 222-230.

Masaki Ozawa: From Radioactive Waste to Resource, a New Transmutation Strategy; *4th International Congress on Ceramics including 3rd Ceramic Leader ship Summit Track Shaping the Future of Ceramics, Environments, Energy and Transportation: Energy Production and Storage II, ICC-049-2012,* **Invited Lecture**, Abstracts pp.80,95、July 15-19, 2012 Sheraton Chicago Hotel& Towers Chicago, Illinois, USA.

Masaki Ozawa: New Element Strategy on Nuclear Fuel Cycle - Creation of New Rare Earth by Transmutation -; *8th International Conference on f-Elements (ICFE8),* August 26-31, 2012 UDINE, ITALY.

Masaki Ozawa: Turning Wastes into Resources, by Neutron Capture Transmutation of Radioactive Wastes; *BIT's 2nd Low Carbon Earth Summit-2012, 2nd New Energy Forum 2012 (NEF-2012)* , Booklet pp222, Oct. 19-21, 2012, Guangzhou, China.

M.Ozawa, C.Y.Han, Y.Sakata, M.Saito: Neutronic Feasibility of La Production from Ba in Nuclear Reactors; *RARE EARTHS* No.60, pp.22-23, ISSN0910-2205 Kidorui CODEN:KIDOEP, The Rare Earth Society of Japan, 2012.5.

Masaki Ozawa: Fuel Cycle's Element Strategy ～ Consideration and Suggestion on Present and Future Direction of Nuclear Fuel Cycle～; *Extraordinary Special Board for General Energy Policy at The Liberal Democratic Party – The 7th PT of Historical Investigation of Nuclear Fuel Cycle and Radioactive Wastes,* Head Quarter of The Liberal Democratic Party, 2012.5.25.

Y.Sakata, C.Y.Han, M.Ozawa, M.Saito: *RARE EARTHS* No.60, pp.24-25, ISSN0910-2205Kidorui CODEN: KIDOEP, The Rare Earth Society of Japan, 2012.5.

Masaki Ozawa: New Element / Resource Strategy in Nuclear Fuel Cycle – A Scenario by Creation of Elements by Transmutation; Atomic Energy Society of Japan, *The 5th Committee Meeting of P&T of Radioactive Wastes*, 2013.1.25

Masaki Ozawa, Chi Young Han, Toshitaka Kaneshiki, Masao Nomura: Element Strategy on Nuclear Fuel Cycle (α)Separation and Transmutation of Radioactive Barium to Rare Earth Elements; *Annual Meeting of Atomic Energy Society of Japan,* G-22, Oosaka, March 27,2013.

H. Akatsuka: Optical Emission Spectroscopy Measurement of Plasmas and their Atomic and Molecular Processes — Application to Nitrogen Plasma; *The 51st Summer School of Plasma Science for Younger Generations*, *the Japan Society of Plasma Science and Fusion Engineering*, Vol. **51**, pp. 13-24, 2012.

Hiroo Numata, Hiroshi Akatsuka and Haruaki Matsuura: Optimization of a Molten Salt Electrolytic Bath Geometry for Rare Earth Metal Recovery using a Finite Element Method; *Z. Naturforsch*, Vol. **68a**, (2013) pp. 48 - 58.

Hiroshi Akatsuka: Dissociation Degree of Nitrogen Molecule in Low-pressure Microwave-discharge Nitrogen Plasma with Various Gas Admixtures; *The 7th Asia-Pacific International Symposium on the Basics and Applications of Plasma Technology (APSPT7)*, p. 68, April 14 – 16, 2012, Taipei Medical University, Taipei, Taiwan.

Hiroshi Akatsuka, Kei Kuwano, Koichi Naoi, Atsushi Nezu and Haruaki Matsuura: Differences in Rotational Temperatures between Neutral Molecules and Molecular

Ions of N_2/O_2 Low-Pressure Plasmas; *The 7th Asia-Pacific International Symposium on the Basics and Applications of Plasma Technology (APSPT7)*, p. 166, April 14 – 16, 2012, Taipei Medical University, Taipei, Taiwan.

Takeshi Nakahagi, Atsushi Nezu, Haruaki Matsuura, Hiroshi Akatsuka: Particle-Based Simulation of Weakly-Ionized Arc-Jet Flowing along Open Magnetic-Field Line; *Proc. Symp. Astronautic Transportation 2011*, Sagamihara, ISAS-JAXA, 2012, STEP-2011-003, IS6000003083 (http://repository.tksc.jaxa.jp/pl/dr/IS6000003083).

Yoh Nagahara, Hiroki Ichii, Kazuyuki Yoshida, Atsushi Nezu, Hiroshi Akatsuka: Effect of Neutral Particle-Collision on the Subsonic Transition of Supersonic Plasma Flow; *Proc. Symp. Astronautic Transportation 2011*, Sagamihara, ISAS-JAXA, 2012, STEP-2011-002, IS6000003082 (http://repository.tksc.jaxa.jp/pl/dr/IS6000003082).

Takeshi Nakahagi, Atsushi Nezu, Haruaki Matsuura, Hiroshi Akatsuka: Particle Simulation of Weakly-Ionized Arc-Jet Expanding along Open-Field-Line as Rarefied Gas Dynamics; *The Papers of Technical Meeting on Plasma Science and Terchnology and Pulsed Power Technology, IEE Japan*, pp 77 – 81, Morioka, August 8 – 10, 2012, PST-12, PPT-12.

Takeshi Nakahagi , Atsushi Nezu , Haruaki Matsuura, Hiroshi Akatsuka: DSMC Simulation of Arc-Jet Flow with Low Ionization Degree along Open-Field-Line; *Extended Abstracts of the 73rd Autumn Meeting 2012*; The Japan Society of Applied Physics, Matsuyama, September 11 – 14, 2012, 08-016.

Takeshi Nakahagi, Atsushi Nezu, Haruaki Matsuura, Hiroshi Akatsuka: DSMC Simulation of Neutral Particles and Ions in an Expanding Arc-Jet Plasma with Low-Ionization Degree; *Proc. 2012 Annual Conference of Fundamentals and Materials Society, IEE Japan*, Akita, September 20 – 21, 2012, p. 357.

Hiroshi Akatsuka: Recent Development of Spectroscopic Measurement Method of Nitrogen Plasma with Low Discharge Pressure; *Proc. 28th Kyushu-Yamaguchi Meeting of Plasma Research Group*, Yufuin, November 10 – 11, 2012, pp. 22-25.

Hirokazu Kawano, Atsushi Nezu, Haruaki Matsuura and Hiroshi Akatsuka: Difference in Rotational Temperature between Neutral Molecules and Molecular Ions in N_2/O_2 Plasmas; *Proc. 29th JSPF Annual Meeting*, Kasuga, November 27 – 30, 2012, 29pC01.

Takeshi Nakahagi, Atsushi Nezu, Haruaki Matsuura and Hiroshi Akatsuka: DSMC Simulation of Flowing Characteristics of Rarefied Weakly-Ionized Arc-Jet Expanding along Open-Field-Line; *Proc. 29th JSPF Annual Meeting*, Kasuga, November 27 – 30, 2012, 28D03P.

Keisuke Tajima, Atsushi Nezu, Haruaki Matsuura, Hiroshi Akatsuka: Experimental Study on Steady-State Plasma Flow Injected into Curved Magnetic Field; *The Papers of Technical Meeting on Plasma Science and Terchnology and Pulsed Power Technology, IEE Japan*, Tokyo, December 10 – 12, 2012, PST-12-88, PPT-12-111.

Yoshihiro Shimizu, Atsushi Nezu, Haruaki Matsuura and Hiroshi Akatsuka: OES Measurement of Rotational Temperature of Hydrogen Molecule and Estimation of Gas Temperature of Low-Pressure Microwave Discharge Hydrogen Plasma; *30th Symposium on Plasma Processing (SPP30)*, Hamamatsu, January 21 – 23, 2013, pp. 131-132.

Junya Konno, Atsushi Nezu, Haruaki Matsuura and Hiroshi Akatsuka: A Study on Excitation Kinetics of Low-Pressure Discharge Oxygen Plasma; *30th Symposium on Plasma Processing (SPP30)*, Hamamatsu, January 21 – 23, 2013, pp. 151-152.

Masahiko Hatcho, Sou Watanabe, Haruaki Matsuura, Hiroshi Akatsuka: Optical Emission Spectroscopic Characteristics of Expanding Nitrogen Arc-Jet Plasma; *The Papers on Technical Meeting on "Plasma Science and Technology", IEE Japan*, Hitachi, pp. 13-18, Mar. 2013, PST-13-12.

Hiroshi Akatsuka, Yoshihiro Shimizu, Atsushi Nezu, Haruaki Matsuura: OES Measurement of Molecular Rotational Temperature and Estimation of Gas Temperature of a Low-Pressure Microwave Discharge Hydrogen Plasma; *2013 Annual Meeting Record, IEE Japan*, Nagoya, March 20– 22, 2013, Vol. 1, p. 208.

Hiroshi Akatsuka, Masahiko Hatcho and Haruaki Matsuura: Dominance of Atomic N Lines in Comparison with Molecular N_2 Band Spectra of Expanding Nitrogen Arc-Jet Plasma; *Extended Abstracts of The 60th JSAP Spring Meeting*, Atsugi, March 27 – 30, 2013, p. 08-050.

Hiroshi Akatsuka: Optical Emission Spectroscopic Measurement of Low-Pressure Discharge Nitrogen Plasma - Recent Development of Temperature and Dissociation Degree Measurement; *The 132nd regular research meeting of Sputtering and Plasma Process Sub-Division, the Vacuum Society of Japan, Sputtering & Plasma Prosesses*, Tokyo, March 14, 2013, Vol. **28**, No. 1, pp. 11-20.

Masatoshi Kondo, Minoru Takahashi, Teruya Tanaka, Valentyn Tsisar, Takeo Muroga: Compatibility of Reduced Activation Ferritic Martensitic Steel JLF-1 with Liquid Metals Li and Pb–17Li; *Fusion Engineering and Design*, Vol. **87**, pp.1777-1787 (2012).

Minoru Takahashi, Tooru Kobayashi, Mingguang Zhang, Michael Mák, Jiří Štefanica, Václav Dostál, Wei Zhao: Study on High Speed Lithium Jet for Neutron Source of Boron Neutron Capture Therapy (BNCT); *Journal of Power and Energy Systems*, Vol.**6**, No.2, pp.324-338 (2012).

Rongyuan Sa, Minoru Takahashi: Experimental Study on Thermal Interaction of Ethanol Jets in High Temperature Fluorinert; *Journal of Power and Energy Systems*, Vol.**6**, No.2, pp.314-323 (2012).

Minoru Takahashi, Rongyuan Sa, Asril Pramutadi, Eriko Yamaki-Irisawa: Overview of Recent Studies Related to Lead-Alloy-Cooled Fast Reactors; *American Institute of Physics (AIP) Conference Proceeding Series*, 1448, pp.39-49 (2012).

Minoru Takahashi: LMFR Development Status and Perspectives in Japan; *International Work Shop on Innovative Nuclear Reactors Cooled by Heavy Liquid Metals; Status and Perspectives*, Pisa, April 17-20, 2012.

Minoru Takahashi: National Status on LFR Development: Japan; Seminar:Activities for Lead-cooled Fast Reactors (LFR) in Generation IV; *International Forum (GIF),* Tamachi Campus, Tokyo Institute of Technology,Tokyo, November 9, 2012.

Teddy Ardiansyah, Minoru Takahashi: Numerical Calculation of Cavitation Bubble for the Simulation of Noise Spectrum; *2012 Annual Meeting of Atomic Energy Society of Japan*, Fukui, March 19-21, 2012, G01.

Minoru Takahashi, Mingguang Zhang: Development of Liquid Lithium Target for Neutron Capture Therapy Using Accelerator (3) Droplet Entrainment from Plane Jet; *2012 Annual Meeting of Atomic Energy Society of Japan*, Fukui, March 19-21, 2012, G11.

H. Ishitobi, J. Ryu, Y. Kato: Evaluation of Heat Output Capacities of Lithium Chloride-modified Magnesium Hydroxide at Various Mixing Ratios,Temperatures, and Vapor Pressures for Thermochemical Energy Storages; *Ind. Eng. Chem. Res.*, **52**, pp. 5321-5325 (2013).

Yukitaka KATO, Kanta INOUE, Michito URASAKI, Satoshi TANAKA, Hiroaki NINOMIYA, Tomoya MINAGAWA, Azusa SAKURAI and Junichi Ryu: Develpoment of Composite Hydrogen Permeation Membrane Using A Reverse Build-Up Method; *Heat Transfer Eng.*, **34** (11-12), pp. 1-8 (2013).

Hirokazu Ishitobi, Keirei Uruma, Masato Takeuchi, Junichi Ryu and Yukitaka Kato: Dehydration and hydration behavior of metal-salt-modified materials for chemical heat pumps; *Applied Thermal Eng.*, **50**, pp. 1639-1644 (2013).

Seon Tae KIM, Junichi RYU, Yukitaka KATO: The optimized mixing ratio of expanded graphite mixture for packed bed reactor of chemical heat pump; *Applied Thermal Engineering*, **50**, pp. 485-490 (2013).

Hiroyuki Sato, Xing L. Yan, Yukio Tachibana, Yukitaka Kato: Assessment of Load-following Capability of VHTR Cogeneration Systems; *Annals of Nuclear Energy*, **49**, pp. 33-40 (2012).

Hiroyuki Sato, Xing L. Yan, Yukio Tachibana, Yukitaka Kato: Load-following Operations of VHTR Gas-turbine Cogeneration System for Developing Countries; *International Journal of Gas Turbine, Propulsion and Power Systems*, **4** (3), pp. 17-24 (2012).

A. Shkatulov, J Ryu, Y. Kato, Y. Aristov: Composite Material "$Mg(OH)_2$/Vermiculite": A Promising New Candidate for Storage of Middle Temperature Heat; *Energy*, **44**, pp. 1028-1034 (2012).

Odtsetseg Myagmarjav, Junichi Ryu, Yukitaka Kato: Effect of Lithium Bromide on Chemical Heat Storage Material with Expanded Graphite; *Heat Powered Cycles Conference 2012* (HPC2012), HPC330, The Netherlands, 9 (9-12) September 2012.

Yukitaka Kato, Arnoldus L. Dipu, Junichi Ryu: Scale Evaluation of Carbon Recycling Iron Making System; *Proc. of Scanmet IV*, Luleå, Sweden, 12(11-13) July, 2012.

Y. Kato: Feasibility of vehicle thermal energy storage (VTES); *Proceedings of the 12th International Conference on Energy Storage (Innostock 2012)*, INNO-S-19 (Oral), 16 (15-18) May, 2012, Lleida, Spain.

Seon Tae KIM, Junichi RYU, Yukitaka KATO: Reactivity Enhance of Packed Bed Chemical Material Using Expanded Graphite for Chemical Heat Pump; *Proceedings of the 12th International Conference on Energy Storage (Innostock 2012)*, INNO-ST-04 (Poster), 16 (15-18) May, 2012, Lleida, Spain.

Yukitaka Kato: Possibility of Active Carbon Recycling Energy System (ACRES); *Kagaku-kogaku*, **77** (3), pp. 185-187 (2013).

Yukitaka Kato: Development of thermochemical energy storage for middle temperature; *OHM*, **66** (6) (2012).

Yukitaka Kato: [Invited lecture] Activity of committee of future energy and society systems; *78th SCEJ Annual Meeting*, A201, Osaka,18 March, 2013.

Yukitaka Kato: Development of iACRES; *CAMP-ISIJ* Vol.**26** (2013)-228.

A. L. Dipu, Y. Kato: Investigation of Carbon Dioxide Reduction in Tubular Solid Oxide Electrolysis Cell for a

Carbon Recycling Iron-making System; *CAMP-ISIJ* Vol.**26** (2013)-230.

Zamengo Massimiliano,Ryu Junichi, Kato Yukitaka: Investigations on a composite block for a magnesium oxide / water chemical heat pump; *78th SCEJ Annual Meeting*, B305, Osaka,19 March, 2013.

Dipu A. L., Fujii G., Ryu J., Kato Y.: Carbon Dioxide Electrolysis under Various CO2 Concentrations Using Tubular Solid Oxide Electrolysis Cell; *78th SCEJ Annual Meeting*, M116, Osaka,17 March, 2013.

Yukitaka Kato: Carbon recycling methodologies for iACRES; *164th ISIJ Autumn Meeting, Matusyama*, 19 September, 2012.

J. Ryu, Y. Sato, T. Mizuno, H. Ishitobi, Y. Kato: Durability of repetitive operation for metal hydroxide composites; *44th SCEJ Autumn Meeting*, M104, Sendai, 12 September, 2012.

H. Ishitobi, J. Ryu, Y. Kato: Measurement of dehydration heats of rare-earth hydroxides; *44th SCEJ Autumn Meeting*, M105, Sendai, 12 September, 2012.

J. Kariya, Kim Seon Tae, J. Ryu, Y. Kato: Calcium oxide/water chemical heat pump using expanded graphite; *44th SCEJ Autumn Meeting*, M107, Sendai, 12 September, 2012.

Zamengo Massimiliano, Kim Seon Tae, Ryu Junichi, Kato Yukitaka: The effects of density on $Mg(OH)_2$ - expanded graphite pellets for a chemical heat pump; *44th SCEJ Autumn Meeting*, M108, Sendai, 12 September, 2012.

Zamengo Massimiliano, Ryu Junichi, Kato Yukitaka: Thermal conductivity enhancement of a packed bed reactor in a magnesium oxide/water chemical heat pump; *49th HTSJ Meeting*, E333, Toyama, 1 June, 2012.

K. Tani, K. Shinohara, T. Oikawa, H. Tsutsui, S. Miyamoto, Y. Kusama, T. Sugie: Effects of ELM mitigation coils on energetic particle connement in ITER steady-state operation; *Nucl. Fusion*, **52**, 013012 (2013).

S. Maeyama, A. Ishizawa, T.-H. Watanabe, N. Nakajima, S. Tsuji-Iio, H. Tsutsui: Numerical techniques for parallel dynamics in electromagnetic gyrokinetic Vlasov simulations; *Computer Physics Communications,* **184**, 2462-2473 (2013).

Y. Urushihara, J. Kobayashi, Y. Matsumoto, K. Komatsu, S. Oda, H. Mitani: DNA-PK inhibition causes a low level of H2AX phosphorylation and homologous recombination repair in Medaka (Oryzias latipes) cells; *Biochemical and Biophysical Research Communications*, Vol. **429**, pp.131-136, (2012).

Y. Ito, T. Ito, S. Karasawa, T. Enomoto, A. Nashimoto, Y. Hase, S. Sakamoto, T. Ito, T. Mimori, Y. Matsumoto, Y. Yamaguchi, H. Handa: Identification of DNA-dependent protein kinase catalytic subunit (DNA-PKcs) as a novel target of Bisphenol A; *PLos ONE*, Vol. **7**, No.12, (2012) e50481.

M. Someya, K. Sakata, Y. Matsumoto, H. Tauchi, M. Kai, M. Hareyama, M. Fukushima: Effects of depletion of dihidropyrimidine dehydrogenase on focus formation and RPA phosphorylation; *Journal of Radiation Research*, Vol **53**, pp.250-256 (2012).

K. Miura, K. Sakata, M. Someya, Y. Matsumoto, H. Matsumoto, A. Takahashi, M. Hareyama: The combination of olaparib and camptothecin for effective radiosensitization; *Radiation Oncology,* Vol. **96**, pp.259-266 (2012).

M. Takagi, K. Sakata, M. Someya, Y. Matsumoto, H. Tauchi, M. Hareyama, M. Fukushima: The combination of hyperthermia or chemotherapy with gimeracil for effective radiosensitization; *Strahlentherapie und Onkologie,* Vol. **188**, pp.256-261 (2012).

J. Hayashi, K. Sakata, M. Someya, Y. Matsumoto, M. Satoh, K. Kataya, M. Hori, M. Takagi, M. Hareyama: Analysis of Ku and XRCC4 expressions of hypopharyngeal cancer tissues and results treated with chemoradiotherapy; *Oncology Letters*, Vo. **4**, pp.151-155 (2012).

Y. Matsumoto: Fukushima Daiichi Nuclear Power Plant Accident from the Aspect of Radiation Biologist; *International Conference of Radiation Biology 2012*, 22-24 November 2012, Navi Mumbai, India, Inaugural Session.

Y. Matsumoto: Fukushima Daiichi Nuclear Power Plant Accident from the Aspect of Radiation Biologist; *International Conference on Radiation, Cancer and Society*, 26-28 November 2012, Allahabad, India, Symposium Talk.

Y. Matsumoto: Fukushima Daiichi Nuclear Power Plant Accident from the Aspect of Radiation Biologist II Countermeasures and Social Responsibilities; *International Conference on Radiation, Cancer and Society*, 26-28 November 2012, Allahabad, India, Symposium Talk.

M.K. Sharma, Y. Matsumoto: Regulation of non-homologous end joining repair mechanism of DNA double-strand break by kinase activity of DNA-PK; *28th RBC-NIRS International Symposium*, 29-30 November 2012, Kyoto.

S. Liu, R.P. Kamdar, N. Adachi, Y. Matsumoto: Role of BRCT domains of DNA Ligase IV in its chromatin binding and recruitment of XRCC4. *28th RBC-NIRS International Symposium*, 29-30 November 2012, Kyoto.

M. Tomita, J. Kobayashi, K. Iwabuchi, Y. Matsumoto, N. Adachi, M. Takata, K. Otsuka, K. Sakai, H. Utsumi: Molecular mechanisms involved in the repair of DNA double-strand breaks in cells exposed to low-dose-rate γ-radiation; *3rd International Symposium of RIRBM, Hiroshima University -Biological Effects of Low Dose Radiation-*, 12-13 February 2013, Hiroshima.

M.K. Sharma, R. Wanotayan, M. Fukuchi, S. Imamichi, Y. Matsumoto: Analysis of XRCC4 phosphorylation in vitro and in cellulo by DNA-PK; *Japan Society for Radiation Research 56th Annual Meeting*, 6-8 September 2012, Sendai.

S. Imamichi, Y. Matsumoto: The fidelity of the repair of DNA damage by neutron irradiation and its dependence on XRCC4 status; *Japan Society for Radiation Research 56th Annual Meeting*, 6-8 September 2012, Sendai.

S. Liu, R.P. Kamdar, N. Adachi, Y. Matsumoto: Chromatin binding of XRCC4-DNA ligase IV complex revealed by biochemical fractionation analysis; *Japan Society for Radiation Research 56th Annual Meeting,* 6-8 September 2012, Sendai.

M.K. Sharma, Y. Matsumoto: Importance of DNA-PK phosphorylation in NHEJ repair and cancer radiotherapy; *15th Symposia of International Association for Sensitization of Cancer Therapy*, 9-10 February, Nara.

R. Wanotayan, M.K. Sharma, Y. Matsumoto: Functional analyses of systematic series of XRCC4 mutants in DNA double-strand break repair; *15th Symposia of International Association for Sensitization of Cancer Therapy*, 9-10 February, Nara.

Y. Sunatani, R.P. Kamdar, M.K. Sharma, O. Matsui, M. Hashimoto, Y. Matsumoto, K. Iwabuchi: Mechanism of apoptosis induction via regulation of ASAP complex by XRCC4; *35th Annual Meeting of Molecular Biology Society of Japan*, 11-14 December 2012, Fukuoka.

J. Onoe, T. Ito, S. Kimura, H. Shima, Y. Toda, and H. Yoshioka: One-dimensional uneven peanut-shaped C_{60} polymer: a quantum electronic system on Riemannian space; (invited paper), *Fullerene, Nanotubes, and Carbon Nanostructures* **20**, 1-16 (2012).

J. Onoe, A. Takashima, S. Ono, H. Shima, and T. Nishii: Anomalous enhancement in the infrared phonon intensity of one-dimensional uneven peanut-shaped C_{60} polymer; *J. Phys.*: *Condens. Matter* **24**, 175405 (2012).

J. Onoe, T. Ito, H. Shima, H. Yoshioka and S. Kimura: Observation of Riemannian geometrical effects on electronic state; *Europhys. Lett.* **98**, 27001 (2012).

A. Takashima, T. Nishii, and J. Onoe: Formation process and electron incident energy dependence of one-dimensional uneven peanut-shaped C_{60} polymer studied using *in situ* high-resolution infrared spectroscopy and first-principles density-functional calculations; *J. Phys. D*: *Appl. Phys.* **45**, 485302 (2012).

S. Ryuzaki and J. Onoe: *In situ* impedance spectroscopic study of the built-in potentials in the vicinity of the donor/acceptor interface of organic thin film solar cells under illumination (in Japanese); *J. Surf. Sci. Soc.* **33**, 93–99 (2012).

S. Ryuzaki and J. Onoe: Correlation between molecular crystallinity/orientation and external quantum efficiency for organic solar cells (in Japanese); *Bull. Soc. Nanosci. Technol.* **10**, 57–62 (2012).

S. Ryuzaki and J. Onoe: Photo-generated carrier dynamics in the vicinity of the donor/acceptor interface of organic solar cells; *IEEJ Trans. C* **132**, 1291–1296 (2012).

M. Kurihara and J. Onoe: Relativistic Density-Functional Study of Nuclear Fuels; *Advances in Nuclear Fuel* (S.T. Revanker ed.), InTech-Open Access Publisher, Chap. 4, pp. 73–94 (2012).

J. Onoe: Quantum Chemistry (textbook); *Kindai Kagakusha* (2012).

J. Onoe ed.: Nanocarbon (textbook); *Kindai Kagakusha* (2012).

J. Onoe: Prediction and observation of Riemannian geometrical effects on electronic states (Invited lecture); Department of Physics, University of “Babes-Bolyai”, Cluj-Napoca, Romania, Sept. 7 (2012).

J. Onoe: One-dimensional exotic-nanocarbons: Electronic and electric properties (Invited lecture); Advanced Technology Institute, University of Surrey, Guildford, UK, Sept. 21 (2012).

J. Onoe: Relativistic density-functional study of the solid solution of nuclear fuel alloys (Invited talk); *J-Power workshop on the computational methods for the life time of Advanced Heat-Resistance Materials*, Tokyo, June (2012).

J. Onoe: Impedance spectroscopic study of organic solar cells under photo-illumination: the open-circuit voltage and built-in potential (Invited talk); *the 147th Committee Meeting on Amorphous and Nano Materials*, Japan Society for the Promotion of Science, October (2012).

J. Onoe: Non-destructive impedance spectroscopy of organic solar cells under illumination: on the origins of the open-circuit voltage (Invited Talk); *The workshop on new surface science for device applications*, The Chubu

Branch, Jpn. Surf. Sci. Soc., November (2012).

J. Onoe, S. Ryuzaki, M. Nishiyama, and T. Nishii: Electron-transport properties of air-exposed one-dimensional uneven peanut-shaped C_{60} polymer films; *International Conference on Diamond and Carbon Materials*, Granada (Spain), Sept. 3-6 (2012).

S. Ryuzaki and J. Onoe: *In situ* non-destructive impedance spectroscopic study of Zn-porphyrin/C_{60} hetero-junction solar cells; *25th International Microprocesses and Nanotechnology Conference*, Kobe (Japan), Oct. 30 - Nov. 2 (2012).

J. Onoe, S. Ryuzaki, M. Nishiyama, and T. Nishii: Electron conductivities of one-dimensional uneven peanut-shaped C_{60} polymer film; *7th ACCMS-VO (Asian Consortium on Computational Materials Science-Virtual Organization)*, Sendai (Japan), Nov. 23-25 (2012).

J. Onoe, T. Ito, S. Ryuzaki, H. Shima, H. Yoshioka, and S. Kimura: Electronic and electric properties of one-dimensional exotic-nanocarbon; *Third International Conference on Multifunctional, Hybrid and Nanomaterials (Hybrid Materials 2013)*, Sorrento, Italy, March 3-7 (2013).

K. Fukuda, M. Kobayashi, J. Onoe, and R. Umemiya: The mechanical properties of pristine C_{60} films (2); *Extended Abstract of 19th Kanto Branch at Jpn. Soc. for Mechanical Eng.*, pp.207–208 (2012).

S. Ryuzaki, M. Nishiyama, and J. Onoe: Electronic conduction mechanism of one-dimensional conductive fullerene polymer films; *10th Annual Meeting of the Society of Nano Science and Technology*, Osaka, June 14-16 (2012).

A. Takashima, T. Nishii, and J. Onoe: The dependence of electron-beam incident energy on the formation of one-dimensional exotic-nanocarbon; *10th Annual Meeting of the Society of Nano Science and Technology*, Osaka, June 14-16 (2012).

J. Onoe, T. Ito, H. Shima, H. Yoshioka, and S. Kimura: Prediction and Evidence of the geometric curvature effects on electronic properties; *25th Annual Meeting of the Society of DV-Xα*, Fukuoka, Aug. 6–8 (2012).

T. Ogura, K. Sasaki, K. Takao, T. Arai, Y. Ikeda: Electrochemical Behavior of $[UO_2Cl_4]^{2-}$ in 1-Ethyl-3-methylimidazolium Based Ionic Liquids; *Sci.ChinaChem.*, Vol.**55**, pp. 1699-1704 (2012).

K. Takao, T. Tsubomura: Weakly-Basic Anion Exchange Resin Scavenges Impurities in Ionic Liquid Synthesized from Trialkyloxonium Salt; *J. Chem. Eng. Data*, Vol.**55**, pp. 2497-2502 (2012).

T. Suzuki, T. Kawasaki, K. Takao, M. Harada, M. Nogami, Y. Ikeda: A Study on Selective Precipitation Ability of Cyclic Urea to U(VI) for Developing Reprocessing System Based on Precipitation Method; *J. Nucl. Sci. Technol.*, Vol.**49**, pp. 1010-1017 (2012).

C. Hennig, S. Takao, K. Takao, S. Weiss, W. Kraus, F. Emmerling, A. C. Scheinost: Structure and Stability Range of a Hexanuclear Th(IV)-Glycine Complex; *Dalton Trans.*, Vol.**41**, pp. 12818-12823 (2012).

K. Takao, T. J. Bell, Y. Ikeda: Actinide Chemistry in Ionic Liquids; *Inorg. Chem.*, Vol.**52**, pp. 3459-3472 (2013).

K. Takao, T. Ogura, T. Tsubomura, Y. Ikeda: Location of Unpaired Electron in Uranyl(VI) Complex after One-electron Reduction; *The 62nd Conference of Japan Society of Coordination Chemistry*, Toyama, September 21-23, 2012, 2Ba-04.

A. Mase, N. Ito, M. Oda, Y. Komada, D. Nagae, D. Zhang, Y. Kogi, S. Tobimatsu, T. Maruyama, H. Shimazu, E. Sakata,bF. Sakai, D. Kuwahara, T. Yoshinaga, T. Tokuzawa, Y. Nagayama, K. Kawahata, S. Yamaguchi, S. Tsuji-Iio, C.W. Domier, N.C. Luhmann Jr., H.K. Park, .G Yun, W. Lee, S. Padhi and K.W. Kim: Reflectometric measurement of plasma imaging and applications; *J. Instrum.* **7**, Jan. 2012 JINST 7 C01089. 1-20 (2012).

S. Maeyama, A. Ishizawa, T.-H. Watanabe, N. Nakajima, S. Tsuji-Iio and H. Tsutsui: Hybrid method of semi-Lagrangian and additive semi-implicit Runge-Kutta schemes for gyrokinetic Vlasov simulations; *Comput. Phys. Commun*. **183**, 1986-1992 (2012).

Y. Nagayama, D. Kuwahara, T. Yoshinaga, Y. Hamada, Y. Kogi, A. Mase, H. Tsuchiya, S. Tsuji-Iio, S. Yamaguchi: Development of 3D microwave imaging reflectometry in LHD; *Rev. Sci. Instrum.*, **83**, 10E305-1-6 (2012).

Hatakeyama, Y. Shibata, S. Kawakami, H. Tsutsui, S. Tsuji-Iio, R. Shimada, N. Ohno, T. Akiyama, Y. Suzuki, K.Y. Watanabe: Preliminary Experiments on the Vertical Stability with Helical Coils in a Small Tokamak, HYBTOK-II; *39th EPS Conference on Plasma Physics,* July 2-6 2012, Stockholm, P1.046 (2012).

T. Miyaura, H. Tsutsui, S. Tsuji-Iio, R. Shimada, K. Watanebe, Y. Suzuki: Magnetic Field Reconstruction of LHD Plasma by the Use of Surface Current Potential; *29th Annual Meeting of the Japan Soc. of Plasma Sci. and Nucl. Fusion Res.*, 27D25P, Nov. 27-30, Kasuga, Fukuoka, (2012).

S. Hatakeyama, H. Tsutsui, S. Tsuji-Iio, R. Shimada, K. Shibata, T. Ohno, T. Akiyama, Y. Suzuki, K.Y. Watanabe: Design and Construction of VDE-free Small Tokamak; *29th Annual Meeting of the Japan Soc. of Plasma Sci. and Nucl. Fusion Res.*, 27D33P, Nov. 27-30, Kasuga, Fukuoka, (2012).

D. Kuwahara, Y. Nagayama, H. Tsuchiya, S, Tsuji-Iio, T, Yoshinaga, S. Yamaguchi, Y. Kogi, A. Mase: Development of Variable Frequency Microwave Imaging Rreflectometer; *29th Annual Meeting of the Japan Soc. of Plasma Sci. and Nucl. Fusion Res.*, 29D07P, Nov. 27-30, Kasuga, Fukuoka, (2012).

Haruaki Matsuura, Atsushi Nezu, Hideaki Shiwaku, Tsuyoshi Yaita, Hajimu Yamana, Toshiyuki Fujii, Kazuhito Fukasawa, Takeshi Uda, Akihiro Uehara: Local structural analysis of neodymium cation in molten chlorides; *The 79th annual conference of the electrochemistry society of Japan*, March 29-31, Hamamatsu, Japan, 1M21, 332, 2012.

Kazuhiro Fujita , Atsushi Nezu, Hiroshi Akatsuka and Haruaki Matsuura: The effect of fluoride addition on the electrochemical behavior of neodymium in molten chloride; *The 79th annual conference of the electrochemistry society of Japan*, March 29-31, Hamamatsu, Japan, 3M24, 350, 2012.

Haruaki Matsuura, Masahiko Numakura, Kazuhiro Fujita, Atsushi Nezu, Hiroshi Akatsuka, Catherine Bessada, Nobuaki Sato: Structure and Physico - chemical Properties of Molten Thorium Fluoride Mixtures - Synthesis of Thorium - lithium Fluoride Mixtures; *Proceedings of the 4th Asian Conference on Molten Salt Chemistry and Technology and the 44th Symposium on Molten Salt Chemistry,* September, 23-27 Matsushima, Japan, G27, 249-256, 2012.

Kazuhiro Fujita , Atsushi Nezu, Hiroshi Akatsuka and Haruaki Matsuura: Effect of Fluoride Addition on Electrochemical Behavior and Local Structure of Neodymium Cation in Molten Lithium - Potassium Chloride; *Proceedings of the 4th Asian Conference on Molten Salt Chemistry and Technology and the 44th Symposium on Molten Salt Chemistry,* September, 23-27 Matsushima, Japan,G29, 264-270, 2012.

K. Kondo, T. Moriyama, J. Hasegawa, K. Horioka, Y. Oguri: Electro-magnetically driven shock and dissociated hydrogen target for stopping power measurement; *Nucl. Instrum. Methods Phys. Res., Sect. A*, in press.

K. Kondo, T. Moriyama, J. Hasegawa, K. Horioka, Y. Oguri: Production of dissociated hydrogen gas by electro-magetically driven shock; *Research Report NIFS Proceedings*, **93**, (2013), pp. 6-9.

K. Kondo, T. Moriyama, J. Hasegawa, K. Horioka, Y. Oguri: Dissociated hydrogen gas production experiment by electro-magetically driven shock tube; *The papers of Technical meeting on "Pulsed Power Technology" IEE Japan,* PPT-13-2, (2013), pp. 7-10.

K. Kondo, T. Moriyama, J. Hasegawa, K. Horioka, Y. Oguri: Electro-magnetically driven shock and dissociated hydrogen target for stopping power measurement; *19th International Symposium on Heavy Ion Inertial Fusion (HIF2012),* August 12-17, 2012, Berkeley, California, USA, ID 107.

K. Kondo, T. Moriyama, J. Hasegawa, K. Horioka, Y. Oguri: Production of dissociated hydrogen gas by electro-magetically driven shock; *FY2012 symposium for Pulsed-power-driven high energy density plasma*, January 10-11, 2013, Gifu.

T. Moriyama, K. Kondo, J. Hasegawa, K. Horioka, Y. Oguri: Study of a shock-driven lond-duration dissociated hydrogen target for heavy-ion interaction experiment; *68th Annual Meeting of Physical Society of Japan*, March 26-29, 2013, Hiroshima

Jun Nishiyama, Hideki Harano, Tetsuro. Matsumoto, Yasushi Sato, Akira Uritani, Katsuhisa Kudo: Absolute measurement for activity of ^{198}Au foil using $4\pi\beta-\gamma$ coincidence counting method and corrections by Monte Carlo simulation; *Radiation Protection Dosimetry*, Vol. **148**, No. 2, pp.237-241 (2012).

Akihiko Masuda, Tetsuro Matsumoto, Hideki Harano, Jun Nishiyama, Yosuke Iwamoto, Masayuki Hagiwara, Daiki Satoh, Hiroshi Iwase, Hiroshi Yashima, Takashi Nakamura, Tatsuhiko Sato, Toshiro Itoga, Yoshihiro Nakane, Hiroshi Nakashima, Yukio Sakamoto, Christian Theis, Eduard Feldbaumer, Lukas Jaegerhofer, Christian Pioch, Vladimir Mares, Atsushi Tamii, Kichiji Hatanaka: Response Measurement of a Bonner Sphere Spectrometer for High-Energy Neutrons; *IEEE Transactions on Nuclear Science*, Vol. **59**, No. 1, pp.161-166 (2012).

Vladimir Mares, Christian Pioch, Werner Ruhm, Hiroshi Iwase, Yosuke Iwamoto, Masayuki Hagiwara, Daiki Satoh, Hiroshi Yashima, Toshiro Itoga, Tatsuhiko Sato, Yoshihiro Nakane, Hiroshi Nakashima, Yukio Sakamoto, Tetsuro Matsumoto, Akihiko Masuda, Hideki Harano, Jun Nishiyama, Christian Theis, Eduard Feldbaumer, Lukas Jaegerhofer, Atsushi Tamii, Kichiji Hatanaka, and Takashi Nakamura: Neutron Dosimetry in Quasi-Monoenergetic Fields of 244 and 387 MeV; *IEEE Transactions on Nuclear Science*, Vol. **60**, No. 1, pp.299-304 (2013).

Jun Nishiyama, Toru Obara: Study on start-up of a CANDLE burn-up reactor by using accelerator neutron sources; *2012 Atomic Energy Society of Japan Autumn Meeting*, Hiroshima, September 19-21, 2012, P35.

T. Ogura, K. Sasaki, K. Takao, T. Arai, Y. Ikeda: Electrochemical Behavior of $[UO_2Cl_4]^{2-}$ in 1-Ethyl-3-methylimidazolium Based Ionic Liquids; *Sci.ChinaChem.*, Vol.**55**, pp. 1699-1704 (2012).

K. Takao, T. Tsubomura: Weakly-Basic Anion Exchange Resin Scavenges Impurities in Ionic Liquid Synthesized from Trialkyloxonium Salt; *J. Chem. Eng. Data*, Vol.**55**, pp. 2497-2502 (2012).

T. Suzuki, T. Kawasaki, K. Takao, M. Harada, M. Nogami, Y. Ikeda: A Study on Selective Precipitation Ability of Cyclic Urea to U(VI) for Developing Reprocessing System Based on Precipitation Method; *J. Nucl. Sci. Technol.*, Vol.**49**, pp. 1010-1017 (2012).

C. Hennig, S. Takao, K. Takao, S. Weiss, W. Kraus, F. Emmerling, A. C. Scheinost: Structure and Stability Range of a Hexanuclear Th(IV)-Glycine Complex; *Dalton Trans.*, Vol.**41**, pp. 12818-12823 (2012).

K. Takao, T. J. Bell, Y. Ikeda: Actinide Chemistry in Ionic Liquids; *Inorg. Chem.*, Vol.**52**, pp. 3459-3472 (2013).

K. Takao, T. Ogura, T. Tsubomura, Y. Ikeda: Location of Unpaired Electron in Uranyl(VI) Complex after One-electron Reduction; *The 62nd Conference of Japan Society of Coordination Chemistry*, Toyama, September 21-23, 2012, 2Ba-04.

Yasushi TAKEDA, Hiroshige KIKURA, et al.,: Ultrasonic Doppler Velocity Profiler for Fluid Flow; *Fluid Mechanics and its Application*, Springer, (2012), pp.107-200.

Masanori ARITOMI, Hiroshige KIKURA, Kazumi KITAYAMA, Takao ISHIZUKA, Nobuyoshi TSUZUKI and Yukihisa YABUSHITA: Now what can be done by Nuclear schloars and engineers?; *Baifukan*, (2012). in Japanese.

Sanehiro WADA, Kenichi TEZUKA, Weerachon TREENUSON, Nobuyoshi TSUZUKI and Hiroshige KIKURA: Study on the optimal number of transducers for pipe flow rate measurement downstream of a single elbow using the Ultrasonic Velocity Profile method; *Science and Technology of Nuclear Installations*, Vol. **2012**, Article ID 464313, (2012), pp.1-12.

Tomonori IHARA, Hiroshige KIKURA and Yasushi TAKEDA: The basic study of ultrasound characteristics and velocimetry in molten glass; *Transaction of the Japan Society of Mechanical Engineers series B*, Vol. **78**, No. 787, (2012), pp. 485-489.

Tomonori IHARA, Hiroshige KIKURA, Yasushi TAKEDA, Eiji OCHI and Kazuhiro MINAMI: Study on flow measurement of very low velocity using Phase Difference Method; *IEICE Technical Report, 'Ultrasonics'*, Vol. **112**, No. 68 (2012), pp.7-11. in Japanese.

Kun YANG, Yoshitaka SAITOH, Hideki KAWAI, Nobuyoshi TSUZUKI, Hiroshige KIKURA and Gaku HASHIMOTO: Numerical Flow Analysis of Electromagnetic Fluid Using GSMAC Finite-Element Method; *Joint Symposium on Mechanical - Industrial Engineering and Robotics 2012*, Noboribetsu, Japan (2012), p.49.

Makaki SAITO and Hiroshige KIKURA: Nuclear Human Resource Development in Tokyo Institute of Technology; *The 4th ENEN Special Event "Fukushima accident and its potential influence on nuclear E&T"*, Saclay, France (2012).

Hiroshige KIKURA: Trace the accident of Fukushima Dai-ichi NPP –Time estimation of core uncovering-; *Workshop "What happened in Fukushima? Fact and Future,* Okayama (2012). in Japanese.

Keisuke TSUKADA, Tomonori IHARA and Hiroshige KIKURA: Study on Non-contacting Flow Rate Measurement using Air-coupled Ultrasound; *Proceedings of 49th Japan Heat Transfer Symposium*, Toyama (2012-5), SP28. in Japanese.

Hiroshige KIKURA, Nobuyoshi TSUZUKI, Tatsuya KAWAGUCHI, Hideki KAWAI, Kazuhiro MINAMI and Eiji OCHI: Flow Behavior Simulation with Model Fluid of Molten Glass by FEM; *SEAD*24 in Toyama, Toyama (2012-5), 17B2-3. in Japanese.

Keisuke TSUKADA, Tomonori IHARA and Hiroshige KIKURA: Study on Non-contacting Flow Rate Measurement using Air-coupled Ultrasound; *Proceedings of 49th Japan Heat Transfer Symposium*, Toyama (2012-5), pp. 125-126. in Japanese.

Weerachon TREENUSON, Nobuyoshi TSUZUKI and Hiroshige KIKURA: Development of Flow Rate Measurement in the Bent Pipe using Ultrasonic Velocity Profile method; *Proceedings of 17th Power and Energy Symposium*, Fukuoka (2012-6), pp. 291-294.

Hiroshige KIKURA, Thang Tat NGUYEN and Ari HAMDANI: Two Phase Flow Measurement on Taylor Vortex Flow by using UVP and WMT; *2012 Japan-U.S. seminar on Two-Phase flow Dynamics*, Tokyo, Japan (2012-6), Paper No.T20, pp.1-6.

Tat Thang NGUYEN, Hideharu TAKAHASHI, Nobuyoshi TSUZUKI, Hiroshige KIKURA and Hideki MURAKAWA: Visualization Measurement of Gas-liquid Two-phase Taylor-Couette flow using Multi-wave Ultrasonic Velocity Profiler Method; *40th Symposium on Visualization 2012*, Tokyo, (2012-7), C217.

Ari HAMDANI, Tat Thang NGUYEN, Nobuyoshi TSUZUKI, Hiroshige KIKURA and Daisuke ITO: Visualization Measurement of Gas-liquid Two-phase Taylor-Couette flow using Wire Mesh Tomography Method; *40th Symposium on Visualization 2012*, Tokyo, (2012-7), D106.

Keisuke TSUKADA, Tomonori IHARA and Hiroshige KIKURA: A Study of Air-Coupled Ultrasonic Flowmeter; *The 20th International Conference on Nuclear Engineering (ICONE20),* Anaheim, California, USA, (2012-7), CD-ROM Paper No.ICONE20 POWER2012 54524, pp.1-6.

Kun YANG, Yoshitaka SAITOH, Hideki KAWAI, Nobuyoshi TSUZUKI, Hiroshige KIKURA and Gaku HASHIMOTO: Numerical Flow Analysis of Electromagnetic Fluid Using GSMAC Finite-Element Method; *The 20th International Conference on Nuclear Engineering (ICONE20)*, Anaheim, California, USA, (2012-7), CD-ROM Paper No. ICONE20 POWER2012 54508, pp.1-5

Makaki SAITO and Hiroshige KIKURA: Nuclear Human Resource Development in Tokyo Institute of Technology; *The 20th International Conference on Nuclear Engineering (ICONE20),* Anaheim, California, USA, (2012-7)

Weerachon TREENUSON, Nobuyoshi TSUZUKI and Hiroshige KIKURA: Verification of Flow Rate Measurement at Bent Pipe Comparing between Experiment and Numerical Calculation; *Proceedings of the 31st Annual Meeting of JSMF Symposium on Multiphase Flow 2012*, Kashiwa (2012-8), pp. 76-77.

Ari HAMDANI, Tat Thang NGUYEN, Daisuke ITO, Hiroshige KIKURA and Nobuyoshi TSUZUKI: Observation of Bubble Behavior in Taylor-Couette Flow using Wire-Mesh Sensor; *Proceedings of the 31st Annual Meeting of JSMF Symposium on Multiphase Flow 2012*, Kashiwa (2012-8), pp. 98-99.

Hiroshige KIKURA: Velocity Profile Measurement using pulsed ultrasound and application for Phased Array measurement; *Phased array ultrasonic testing committee,* Tokyo (2012-8), in Japanese.

Weerachon TREENUSON, Nobuyoshi TSUZUKI, Hiroshige KIKURA, Masanori ARITOMI, Sanehiro WADA and Kenichi TEZUKA: Development of Flow Rate Measurement in the Bent Pipe using Ultrasonic Velocity Profile method; *The 9th International Topical Meeting on Nuclear Thermal-Hydraulics*, Operation and Safety (NUTHOS-9), Kaohsiung, Taiwan, (2012-9), Paper No. N9P0293, pp.1-15.

Hiroshige KIKUIRA, Thang Tat NGUYEN, Hideki MURAKAWA and Masanori ARITOMI: Development of ultrasonic velocity profile method for two-phase flow measurement; *6th Japanese – European Two-Phase Flow Group Meeting*, Kumamoto City, Japan (2012-9), USB, Paper No. S11-2, pp.1-10.

Keisuke TSUKADA, Tomonori IHARA and Hiroshige KIKURA: Study on non-contacting flowmeter using air-coupled ultrasound; *AESJ Autumn meetings 2012*, Hiroshima, (2012-9), poster session. in Japanese.

Tomonori IHARA, Hiroshige KIKURA and Yasushi TAKEDA: A Very Low Velocity Measurement using Ultrasonic Velocimetry; *8th International Symposium on Ultrasonic Doppler Methods for Fluid Mechanics and Fluid Engineering(ISUD8)*, Dresden, Germany(2012-9), pp.33-36.

Weerachon TREENUSON, Nobuyoshi TSUZUKI, Hiroshige KIKURA, Masanori ARITOMI, Sanehiro WADA and Kenichi TEZUKA: Development of Flow Rate Measurement at Bent Pipe using Comparison between Ultrasonic Velocity Profile (UVP) Method and Computational Fluid Dynamics (CFD); *Proceedings of the 3rd International Forum on Heat Transfer(IFHT2012)*, Nagasaki, Japan (2012-11), Paper No.82, pp.1-6.

Weerachon TREENUSON, Nobuyoshi TSUZUKI, Hiroshige KIKURA, Masanori ARITOMI, Morihiro WADA and Kenichi TEZUKA: High Accurate Flow Measurement at the Bent Pipe by using Ultrasonic Velocity Profile Method; *The 11th AESJ Kanto-Koetsu office Workshop for Young Researchers,* Tokyo (2012-11), S3-9, p. 9.

Keisuke TSUKADA, Tomonori IHARA and Hiroshige KIKURA: An Analytical Study of Air-Coupled Ultrasonic Flowmeter; *The 33rd Symposium on Ultrasonic Electronics (USE2012), Proceedings of Symposium on Ultrasonic Electronics*, Vol.**33** , Chiba, (2012-11), pp.337-338.

Takuya FUKUMOTO, Keisuke TSUKADA, Tomonori IHARA, Nobuyoshi TSUZUKI, Hiroshige KIKURA: The Basic Study for Flow Velocity Profile Measurement using Phased Array Technique; *Proceedings of 6th Study report presentations*, AESJ Kanto-Koetsu office, Tokyo, (2013-3), A04, p. 4. in Japanese.

Ari HAMDANI, Daisuke ITO, Nobuyoshi TSUZUKI and Hiroshige KIKURA: Two-Phase Observation of Taylor-Couette Flow using Wire-Mesh Sensor; *Proceedings of 6th Study report presentations*, AESJ Kanto-Koetsu office, Tokyo, (2013-3), A07, p. 7.

Antonin POVOLNY, Nobuyoshi TSUZUKI and Hiroshige KIKURA: Thermo-Hydraulic Instabilities in Boiling-driven Natural Circulation Loop; *Proceedings of 6th Study report presentations*, AESJ Kanto-Koetsu office, Tokyo, (2013-3), A08, p. 8.

Masaaki TACHI, Hiroshige KIKURA and Kazumi KITAYAMA: Study on Enforced Severe Accident Management of BWR; *Proceedings of 6th Study report presentations*, AESJ Kanto-Koetsu office, Tokyo, (2013-3), **B16**, p. 35.

M. Sekine, K. Kondo, M. Okamura, and N. Hayashizaki: A study of H^+ production using metal hydride and other compounds by means of laser ion source; *Review of Scientific Instruments*, Vol. **83,** (2012) pp.02B318-1/3.

Wei Zhou, Zhe Chen, Nagayasu Oshima, Kenji Ito, Brian E. O'Rourke, Ryunosuke Kuroda, Ryoichi Suzuki, Hiroshi Yanagishita, Takuro Tsutsui, Akira Uedono, and Noriyosu Hayashizaki: In-situ characterization of free-volume holes in polymer thin films under controlled humidity conditions with an atmospheric positron probe microanalyzer; *Applied physics letters*, Vol. **101**, (2012) pp.014102-1/3.

Liang Lu, Toshiyuki Hattori, Noriyosu Hayashizaki: Design and simulation of C^{6+} hybrid single cavity linac for cancer therapy with direct plasma injection scheme; *Nuclear Instruments and Methods in Physics Research A*, Vol. **668**, (2012) pp.11-21.

Noriyosu Hayashizaki, Koichi Saito, Mitsuhiro Yoshida, Nobukazu Toge, Naohito Saito, Tsutomu Mibe: Study on Linear Accelerator for Low Energy Muon; *2014 Annual Meeting of Physical Society of Japan*, Hyogo, March 24-27, 2012, 24aGB-2.

Naoki YAMANO, Noriyosu HAYASHIZAKI, Yoshihisa MATSUMOTO, Nakahiro YASUDA: A Study on Nuclear Consensus Building (IV) - Risk Communication for Influence on Low Doses of Ionizing Radiation -; *2012 Fall Meeting of Atomic Energy Society of Japan*, Hiroshima, September 19-21, 2012, H13.

Daisuke Satoh, Noriyosu Hayashizaki, Mitsuhiro Yoshida: Development of long-lived high quantum efficiency IrCe photocathode for SuperKEKB injectorfor; *2012 Fall Meeting of Atomic Energy Society of Japan*, Hiroshima, September 19-21, 2012, K24.

Takashi Kaneko, Noriyosu Hayashizaki: Development of induction cavity of beam pulsing system for positron annihilation spectroscopy; *2012 Fall Meeting of Atomic Energy Society of Japan*, Hiroshima, September 19-21, 2012, K26.

Koichi SAITO, Noriyosu HAYASHIZAKI, Mitsuhiro YOSHIDA, Naohito SAITO, Tsutomu MIBE: Study on Linear Accelerator for Low-Energy Muon; *2012 Fall Meeting of Atomic Energy Society of Japan*, Hiroshima, September 19-21, 2012, K27.

Yoshiaki HIRATA, Noriyosu HAYASHIZAKI, Tsuguhiro MIYASHITA, Shigehiko Kuribayashi: Dose Evaluation of Iridium-192 Brachytherapy using PHITS, *2012 Fall Meeting of Atomic Energy Society of Japan*, Hiroshima, September 19-21, 2012, P42.

BULLETIN OF THE RESEARCH LABORATORY
FOR NUCLEAR REACTORS

(Formerly, REPORT OF THE RESEARCH LABORATORY
FOR NUCLEAR REACTORS, BULLETIN OF
THE TOKYO INSTITUTE OF TECHNOLOGY)

Abbreviation of the ”**BULLETIN OF THE RESEARCH LABORATORY FOR NUCLEAR REACTORS**” is BULL. RES. LAB. NUCL. REACTOR.

All communications should be addressed to the editor, Research Laboratory for Nuclear Reactors, Tokyo Institute of Technology (Tokyo Kogyo Daigaku),
2-12-1-N1-16, O-okayama, Meguro-ku, Tokyo 152-8550, Japan.

TEL. +81-3-5734-3054, FAX. +81-3-5734-2959
http://www.nr.titech.ac.jp/